Department of Exploration Geophysics

Investigations of Elastic Properties of Isotropic and Anisotropic Rocks at Seismic Frequencies Using Forced-Oscillation Experiments

Vassili Timofeevitch Mikhaltsevitch

This thesis is presented for the Degree of
Doctor of Philosophy
of
Curtin University

August 2017

Declaration

To the best knowledge and belief this thesis contains no material previously published by any other person except where due acknowledgement has been made.

This thesis contains no material which has been accepted for the award of any other degree or diploma in any university.

Signature: 

Date: 18 August 2017

This thesis is dedicated to my family

ABSTRACT

A study of the fluid effects on the elastic properties of sedimentary rocks is important for the interpretation of seismic data obtained for reservoirs containing various fluids, as well as for monitoring the fluid movement during hydrocarbon extraction in producing fields or during injection of supercritical CO_2 into depleted natural gas reservoirs. The analysis of the petrophysical properties of the reservoirs is associated with a number of challenges. Some of these challenges stem from physicochemical interactions between the rock and pore fluids, which can affect mechanical properties of the rock. Hence, the study of the pore fluid effects on the elastic properties of rocks is important for understanding the changes of the reservoir properties caused by fluid movements.

In this project, we employ the experimental forced-oscillation method for seismic-frequency laboratory investigations of the impact of fluid-rock interactions on the elastic and anelastic properties of sedimentary rocks.

First, we constructed a new forced-oscillation laboratory setup based on the strain-stress relationship, which operates at seismic frequencies and measures the complex Young's moduli and Poisson ratio of rock samples at confining pressures of up to 70 MPa. Using this setup, we investigated the elastic properties of water-saturated sandstones with low intrinsic permeability. The conducted experiments revealed a strong extensional attenuation and dispersion of the bulk and Young's moduli within the seismic bandwidth, which, according to our analysis, can be caused by squirt flow.

We also developed a procedure based on the Kramers-Kronig relationship for verification of the data obtained in forced-oscillation experiments. The procedure was successfully tested on a viscoelastic polymethyl methacrylate sample and on two water- and one glycerol-saturated sandstones.

In the next step, we investigated the effects of supercritical CO_2 injection on the elastic moduli of Donnybrook sandstone. It was found that the moduli of the sandstone flooded with supercritical CO_2 are close to the dry moduli. We also demonstrated that the moduli of the sandstone comprising supercritical CO_2 can be adequetely predicted by Gassmann's equations.

Then, we studied the effect of n-decane and water saturation on the elastic moduli of Savonnieres limestone at seismic and ultrasonic frequencies. It was shown that the bulk and shear moduli of the n-decane saturated Savonnieres limestone are consistent with Gassmann's model, while a change of the sample state from dry to water saturated increases the bulk modulus of the limestone in agreement with Gassmann's predictions, but decreases the shear and Young's moduli. In the experiments carried out on partially water-saturated limestone, we observed a decrease in all elastic moduli with increasing saturation.

Finally, we elaborated an experimental technique to determine elastic anisotropy parameters in shales, which was successfully applied to characterise the anisotropy in Wellington and Mancos shales.

ACKNOWLEDGEMENTS

Without the help of a number of people this thesis would not have been possible. Firstly, I am very grateful for the inspiration which I received from my supervisor Associate Professor Maxim Lebedev. I would not have gotten far without his guidance, endless enthusiasm, encouragement and support. His thoughtful ideas and invaluable contributions set this work on a firm basis. I could not have asked for a better supervisor.

Importantly I wish to thank my associate supervisor, Professor Boris Gurevich, for useful discussions and technical input. I am also grateful to Dr Marina Pervukhina for helping me with shale measurements and contributing to this research. Much of the work contained in the thesis was carried out in collaboration with other researchers whose contributions are highly appreciated.

I have found that interaction with my fellow colleagues at Curtin has been one of the distinct pleasures during my research project. The collegiate spirit which exists in the Department of Exploration Geophysics is a major strength. My thanks to all for providing a challenging multicultural and intellectual environment and keeping my spirits alive.

My special thanks go to Ms Deirdre Hollingsworth for her administrative help and to Mr Robert Verstandig for the IT support.

I must also acknowledge the sponsors of the Curtin Reservoir Geophysics Consortium (CRGC) and CSIRO Earth Sciences and Resource Engineering.

Finally, I would like to thank my wife Dr Nicky Howe for her unconditional love, patience and support.

TABLE OF CONTENTS

LIST OF FIGURES

LIST OF TABLES

Introduction

1 Research background

In terms of rock physics, a reservoir rock is in general a complex three-component substance consisting of solid, liquid and gaseous phases. The physical properties of the rocks are determined primarily by the properties of the phases themselves, their quantitative ratio in the rock and the interactions between the solid and fluid phases. The study of the elastic and anelastic behaviour of fluid-saturated reservoir rocks is a subject of steadily growing interest among researchers inasmuch as the analysis of the aspects of this behaviour yields detailed information about hydraulic properties of reservoir rocks (Müller et al., 2010) and provides a physical basis for seismic interpretation (Wang, 1997). In general, the elastic moduli and attenuation in fluid-saturated rocks are frequency dependent (Müller et al. 2010) which presents a significant challenge to the quantitative interpretation of the field data obtained at seismic frequencies using the results of the most common laboratory techniques, such as ultrasonic and resonant, operating at kHz - MHz frequencies. Therefore, the development of the forced-oscillation (also called subresonant) laboratory systems operating at seismic (1 Hz – 100 Hz) and/or teleseismic (less than 1 Hz) frequencies gives a unique experimental capability for characterizing the mechanical properties and pore fluid contents of reservoir rocks.

1.1 Forced-oscillation laboratory setups

In the past decades, a variety of forced-oscillation (FO) methods have been employed to measure the mechanical properties of rocks, in which dissipated energy is characterised by a phase lag between stress and strain. The upper frequency of the LF methods, generally covering the frequency range from 10^{-5} to 100 Hz, is limited by spurious acoustic resonances in the tested sample or in the mechanical parts of the instrument (Lakes, 2004; D'Anna and Benoit, 1990).

The first FO measurements of the intrinsic attenuation and elastic parameters of rocks were performed by Bruckshaw and Mahanta (1961), Peselnick and Outerbridge (1961), and Usher (1962). Bruckshaw, Mahanta and Usher developed a forced vibration method where the Young's modulus of a specimen is estimated by measuring the magnitude of vibration for an exciting sinusoidal force at a frequency much less than the resonant frequency of the measurement system, and the attenuation is determined as the phase shift (loss angle) between the specimen vibrations and the applied force. Peselnick and Outerbridge (1961) designed a torsion pendulum, where a tested specimen is submitted to a harmonic torque at frequencies of 1 to 10 Hz, that enables measurements of attenuation and shear moduli of coherent rocks. Bruckshaw and Mahanta (1961) observed an increase of 2 % in the Young's modulus of various dry rocks at frequencies between 40 and 120 Hz. A similar result for dry sedimentary and igneous rocks was obtained by Usher (1962) at the frequency range from 2 to 40 Hz. Usher also observed a decrease in the Young's modulus of the rocks containing moisture, accompanied by a large increase in attenuation with frequency. Peselnick and Outerbridge (1961) combined attenuation data for dry Solenhofen limestone obtained using the torsional pendulum (4 - 10 Hz) and a bar resonance setting (10 kHz) with the results of the ultrasonic attenuation measurements (10 MHz) of Peselnick and Zietz (1959) conducted on the same sample. They found that the shear internal friction in the dry limestone increases fivefold with an increase of frequency from 4 Hz to 10 MHz, while the shear modulus remains constant.

In all first FO experiments the amplitude of strains in rocks was not controlled. Later in a number of studies (Gordon and Davis, 1968; Winkler et al., 1979; Mavko, 1979), it has been reported that frictional attenuation in rocks depends on strain amplitude but it becomes strain-independent for amplitudes $<10^{-6}$, which more

adequately represent seismic-wave strains in real fields. Therefore, to meet the reservoir conditions, laboratory measurements should be performed with strains below 10^{-6}.

Another requirement, which should be taken into account when constructing a low-frequency (LF) device, is related to the boundary conditions. As was shown by Dunn (1986) and White (1986) in their analysis of the experiments carried out by Spencer (1981), the attenuation in a fluid-saturated rock sample with open boundaries can stem from radial fluid flow due to the pressure difference between the central and peripherical parts of the sample (the Biot-Gardner effect). Hence, to avoid the distortion of the attenuation associated with intrinsic absorption mechanisms by the Biot-Gardner effect, the boundaries of the tested samples have to be closed by the confining pressure which has to be equal to the static axial pressure applied to the sample.

The LF laboratory apparatuses, which are capable of measuring the complete set of elastic moduli, such as Young's, bulk and shear moduli, and also satisfy the strain-amplitude and boundary conditions, were designed by Spencer et al. (1994), Batzle et al. (1999), Mikhaltsevitch et al. (2011a, 2011b), Pimienta et al. (2015), and Szewczyk et al. (2016).

In the devices proposed by Spencer et al. (1994) and Batzle et al. (1999) the hydrostatic confining pressure is exerted by pressurized nitrogen gas. An axial periodical dynamic force is applied to the sample by an electromechanical shaker at a frequency of 0.2 Hz to 155 Hz (Spencer et al., 1994) or 5 Hz to 2 kHz (Batzle et al., 1999). Since the shaker is unable to operate under high load, the entire device, including the jacketed rock sample with two strain gauges (Batzle et al., 1999) or capacitive displacement transducers (Spencer et al., 1994) to measure axial and radial strains, is mounted inside a gas pressure vessel. This design creates significant limitations on the dimensions of mechanical assembly of the device. The insufficient mass of the mechanical assembly is a source of spurious resonances (Batzle et al., 2006).

Another LF laboratory apparatus with the longitudinal type of the forced oscillations and hydraulic oil as a confining-pressure medium was built in the Rock Physics Laboratory at the Department of Exploration Geophysics of Curtin University (Mikhaltsevitch et al., 2011a, 2011b). The apparatus operates in the frequency range from 0.01 Hz to 100 Hz and measures Poisson ratio and Young

modulus by comparing the strains in a rock and in a standard with well-known parameters. The dynamic strains generated in the rock by a piezoelectric actuator do not exceed 10^{-6}. The extensional attenuation is measured as a phase lag between the phases of the applied stress and strain in the sample.

Recently, two laboratory setups enabled to investigate elastic parameters of rocks at seismic frequencies were reported by Pimienta et al. (2015) and Szewczyk et al. (2015). Both setups are conceptually similar in design to the devices presented by Spencer et al. (1994) and Batzle et al. (1999). A few modifications in the instrument proposed by Pimienta et al. (2015) and Szewczyk et al. (2016) include the replacement of the medium for confining pressure by hydraulic oil and using a piezoelectric actuator instead of an electromechanical shaker. The setup described by Pimienta et al. (2015) is built on the basis of the apparatus presented earlier by Adelinet et al. (2010) and allows to measure bulk modulus using oscillations of the confining pressure at teleseismic frequencies (0.01 Hz – 0.1 Hz).

1.2 Measurements of the elastic properties of rocks using forced-oscillation experiments

Literature on the laboratory LF measurements of the elastic properties of rocks which satisfy the strain-amplitude and boundary conditions is relatively sparse.

Most of the measurements presented in the literature are conducted on sandstones and carbonates (Spencer et al., 1994; Spencer, 2013; Spencer and Shine, 2016; Batzle et al., 1999, 2006; Adam et al., 2006, 2009; Adam and Batzle, 2008; Pimienta et al., 2015, 2016). Spencer et al. (1994) investigated the elastic moduli of the empty grain framework in unconsolidated and consolidated sandstones. They found that the correlation between the frame and mineral Poisson's ratios is strong in consolidated sandstones and weak for unconsolidated sands. In the research conducted on bitumen sand, Spencer (2013) showed the reduction in the bulk and shear moduli with temperature. Later, Spencer and Shine (2016) demonstrated that the bulk and shear moduli of fluid-saturated sandstones gradually diverge from the moduli predicted by Gassmann’s theory with increasing frequency and viscosity of the pore fluid. Batzle et al. (1999, 2006) demonstrated that fluid-saturated reservoir rocks with low fluid mobility (the ratio of rock permeability to fluid viscosity) can be

strongly dispersive in the seismic frequency range. Adam et al. (2006) and Adam and Batzle (2008) evaluated the effect of saturation on elastic properties of carbonate rocks at seismic frequencies. They observed the weakening of shear modulus with saturation in some carbonate samples and found that the behaviors of shear and bulk moduli are not correlated for brine-saturated carbonates. Behura et al. (2007) carried out the laboratory measurements on heavy-oil-saturated carbonate at frequencies of 0.01 Hz to 80 Hz. Their results for shear modulus behavior are similar to the results reported by Spencer (2013) for bitumen sand. Pimienta et al. (2015, 2016) evaluated the dispersion of the elastic moduli of glycerine- and water-saturated sandstones at frequencies of 0.01 Hz to 100 Hz. They found that the moduli and Poisson ratio experience strong variations at the frequencies associated with the drained/undrained and relaxed/unrelaxed transitions.

The measurements of the elastic properties of shales were presented by Sarker and Batzle (2010) and Szewczyk et al. (2016). Sarker and Batzle (2010) tested three samples cut at 0°, 45° and 90° angles with respect to the bedding plane and found no dispersion between low (0.2 – 1000 Hz) and ultrasonic (800 kHz) frequencies for room-dry and n-decane saturated Mancos shale. Significant P-wave anisotropy was observed, in particular, for the dry sample. They also observed a significant reduction of P-wave anisotropy after saturation. Szewczyk et al. (2016) investigated partially water-saturated Mancos and Pierre shales at seismic (1 Hz – 155 Hz) and ultrasonic (0.5 MHz) frequencies and found that the Young's modulus of both shales is growing with increasing water saturation.

The low-frequency experiments with basalt were performed by Adelinet et al. (2010) and Adam and Otheim (2013). Adelinet et al. (2010) studied dry and 100%-water-saturated basalt at teleseismic (0.01 Hz – 0.1 Hz) and ultrasonic (1 MHz) frequencies. They observed no significant change in dry bulk modulus between low and high frequencies, however, under saturated conditions, the undrained bulk modulus at low frequencies was less than the saturated modulus at the ultrasonic frequency which was attributed to the squirt-flow effect. Adelinet et al. (2010) also found that drained and dry bulk moduli measured at low frequencies are not equal at confining pressures < 50 MPa, which was accounted for the physico-chemical interactions between water and rock. Adam and Otheim (2013) examined the elastic properties of basalt under dry, liquid CO_2- and water-saturated conditions at seismic (2 Hz – 300 Hz) and ultrasonic (800 kHz) frequencies. They found no frequency

dispersion in the elastic moduli of dry and liquid CO_2- saturated basalt, while the bulk and shear moduli of water-saturated basalt were frequency dependent. The behavior of the water-saturated moduli was explained by the impact of the squirt-flow mechanisms.

Let us also note, that a comprehensive review of the literature on attenuation measurements in reservoir rocks at seismic frequencies using the forced oscillation approach was given by Subramaniyan et al. (2014).

2 Aim of the research

The overall objectives of this project are to develop and validate an experimental approach based on a stress-strain technique which could be used for low-frequency laboratory investigations of the elastic and anelastic properties of the main sedimentary rocks such as sandstones, carbonates and shales. Eventually, being able to adequately quantify elastic and anelastic parameters of sedimentary rocks, this approach can help improving the efficiency of the seismic data interpretation and reservoir characterization. To achieve this objective, the research carried out in this project is focused on the following topics.

- At the first stage of the project, we develop a new forced-oscillation laboratory apparatus based on the strain-stress relationship which operates at seismic (1 – 100 Hz) and teseismic (<1 Hz) frequencies and measures the complex Young's moduli and Poisson ratio of rock samples at confining or uniaxial pressures from 0 to 70 MPa. One of the major requirements to the construction of the device is that the mechanical assembly of the apparatus has to be designed to completely eliminate spurious acoustic resonances in its parts.

- The reliability of the low-frequency tests can be significantly enhanced by introducing a procedure of verification of the experimental data based on the Kramers-Kronig relation. We develop a simple procedure concerning the application of the local approximation of the Kramers-Kronig relationship to validate the experimental data obtained for solid specimens at seismic frequencies.

- In most sedimentary rocks with low intrinsic permeability and, as a

consequence, with low fluid mobility, the relative motion between the pore fluid and the rock skeleton has a significant effect on the acoustic wave propagation even at seismic frequencies. Therefore, in many cases the experiments conducted only at seismic frequencies are not sufficient to validate commonly used theoretic models of elastic moduli dispersion and attenuation. One of the goals of this research is to fill the gap in the experimental study of the elastic and anelastic properties of low-permeability water-saturated rocks at seismic frequencies.

- Since the influence of CO_2 saturation on the acoustic properties of reservoir rocks became a subject of intensive study in recent years, one of the goals of this project is to investigate the effects of supercritical CO_2 injection on the elastic and anelastic properties of sandstone at seismic frequencies and compare the obtained data with the results of ultrasonic measurements.

- The study of the pore fluid effects on the elastic properties of carbonates is important for understanding a change of the field-performance properties of a carbonate reservoir. In this research, we investigate the applicability of Gassmann's model for predictions of the elastic moduli of fully water- and hydrocarbon-saturated limestone and the influence of partial water saturation on elastic and anelastic properties of the rock at seismic frequencies.

- The anisotropic behavior of shales is usually associated with the properties of a transversely isotropic medium, which are determined by five elastic constants such as five independent components of the compliance or stiffness matrix. We develop a methodology based on stress-strain relationship to measure five independent compliance components and estimate Thomsen's anisotropy parameters. The methodology is tested on Wellington and Mancos shale.

3 Overview of the thesis

This thesis comprises seven chapters. The content of each chapter is briefly summarized below.

Chapter 1. This chapter describes a low-frequency laboratory apparatus based on the strain-stress technique with the longitudinal type of the forced oscillations designed and constructed in the Rock Physics Laboratory at the Department of Exploration Geophysics of Curtin University University (Mikhaltsevitch et al., 2011a, 2011b, 2012; Lebedev et al., 2012). The performance of the apparatus is experimentally tested using dry Berea sandstone, Eagle Ford shale and polymethyl methacrylate (PMMA).

Chapter 2. In this chapter, we present the results of the laboratory measurements of elastic and anelastic parameters of dry and water saturated sandstones with low (~0.7 and 1.1 mD) and high (~425 mD) permeability conducted at seismic (0.1-120 Hz) frequencies. The measurements, carried out on the saturated low-permeability sandstones, revealed prominent peaks of extensional attenuation and a considerable dispersion of bulk moduli, while the attenuation and dispersion in the saturated high-permeability sandstone were below the measurement error. Replacing water with brine (45,000 ppm NaCl) as a pore fluid in one of the low-permeability specimens did not affect any of the measured parameters. The dispersion of the elastic moduli of all sandstones in dry condition was within the experimental error. Our analysis shows that the attenuation and dispersion found in both low-permeability sandstones cannot result from the global flow mechanism or from the mesoscopic heterogeneities of the rocks, but are qualitatively consistent with the mechanism of local (squirt) flow between compliant grain contacts and stiff inter-granular pores. The results of our experiments demonstrate that for low-permeability rocks the low-frequency limit of acoustic wave dispersion can correspond to seismic frequencies.

Chapter 3. This chapter presents a simple procedure based on the Kramers-Kronig relation for the validation of the laboratory tests carried out on the solid specimens at seismic frequencies. The local approximation of the Kramers-Kronig relationship was applied to verify the seismic-frequency measurements conducted on four specimens: a viscoelastic PMMA sample, two water- and one glycerol-saturated

sandstone samples. The experimental tests were performed at various axial (PMMA sample) and confining (sandstone samples) pressures. Our analysis shows that the quantitative relationship between the extensional attenuation and the Young's modulus is consistent with the causality principle presented by the Kramers-Kronig relationship. No particular physical models implying any constraints on the physical properties of the samples are required for this validation.

Chapter 4. The aim of this chapter is to investigate the effects of supercritical CO_2 ($scCO_2$) injection on the elastic and anelastic properties of sandstone at seismic and ultrasonic frequencies. The chapter presents the results of the low-frequency and ultrasonic experiments conducted on water saturated sandstone (Donnybrook, Western Australia) flooded with $scCO_2$. During the experiments with $scCO_2$ the low-frequency and ultrasonic systems, and the pump dispensing $scCO_2$ were held at a temperature of 42º C. The elastic parameters obtained for the sandstone with $scCO_2$ at seismic (0.1 – 100 Hz) and ultrasonic (~0.5 MHz) frequencies are very close to those for the dry rock. The extensional attenuation is also measured at seismic frequencies for the dry, water saturated and $scCO_2$-injected sandstone. The applicability of Gassmann's fluid substitution theory to obtained results is also tested during the experiments.

Chapter 5. In this chapter, we study the applicability of Gassmann's model for predictions of the elastic moduli of water- and hydrocarbon-saturated Savonnieres limestone and the influence of partial water saturation on elastic and anelastic properties of the rock. We present the results of two sets of laboratory experiments on the Savonnieres oolitic limestone where we (i) evaluate the effect of full water and n-decane saturation on elastic moduli and attenuation at seismic (0.1 Hz – 120 Hz) and ultrasonic (0.5 MHz) frequencies, and (ii) quantify the dependence of elastic moduli and extensional attenuation on water saturation at two seismic frequencies of 1 Hz and 10 Hz. We demonstrate that the change in the bulk modulus of the limestone fully saturated either with n-decane or water is in agreement with Gassmann's fluid substitution theory, while the shear modulus of the limestone in water-saturated state is noticeably reduced. The measurements with partial saturation show that the bulk modulus decreases with increasing water saturation to a lesser extent than the Young's and shear moduli. Our results show that extensional

attenuation in the samples with closed boundaries is insignificant under dry and fully saturated conditions, but influenced greatly by the liquid content when saturation is between 0 and 20% or 95% and 100%.

Chapter 6. The anisotropic behavior of shales is usually associated with the properties of a transversely isotropic medium, which are determined by five elastic constants such as five independent components of the compliance or stiffness matrix. The focus of Chapter 6 is centered on the development of the laboratory low-frequency technique to measure five independent compliance components and estimate Thomsen's anisotropy parameters. The technique is tested using three fully water-saturated shale samples from the Wellington formation cored along the horizontal, vertical and 45°-inclination directions with respect to the bedding plane at seismic frequencies between 0.1 Hz and 100 Hz. The conducted tests confirm that the low-frequency measurements can be successfully used for characterization of the elastic anisotropy of shales. The technique was also applied to estimate the influence of water saturation on the stiffness tensor components c_{11} and c_{33}, and on the P-wave anisotropy of Mancos shale at seismic frequencies using two samples cored in the vertical and horizontal directions with respect to the bedding plane.

Chapter 7. This chapter summarizes the main outcomes of this research project.

The author's publications related to chapters 1-6

Chapter 1

Patent:

Lebedev M., V. Mikhaltsevitch, M. Lwin, and B. Gurevich, 2012, An apparatus for and a method of characterising mechanical properties of a sample. Patent AU2011318229 granted in Australia on 22 January 2015.

Conference proceedings:

Mikhaltsevitch, V., M. Lebedev, and B. Gurevich, 2011a, A low-frequency apparatus for characterizing the mechanical properties of rocks, 73rd EAGE Conference and Exhibition Incorporating SPE EUROPEC 2011: EAGE, P155.

Mikhaltsevitch, V., M. Lebedev, and B. Gurevich, 2011b, A low-frequency laboratory apparatus for measuring elastic and anelastic properties of rocks, SEG Technical Program Expanded Abstracts 2011, 2256-2260.

Mikhaltsevitch V., M. Lebedev, and B. Gurevich, 2011, A low-frequency laboratory apparatus for characterizing mechanical properties of rocks, International Union of Geodesy and Geophysics (IUGG) XXV General Assembly, Melbourne, Australia, # 5665.

Mikhaltsevitch, V., M. Lebedev, and B. Gurevich, 2015, A laboratory study of the elastic and anelastic properties of the Eagle Ford shale, Third International Workshop on Rock Physics, Perth, Australia.

Mikhaltsevitch, V., M. Lebedev, and B. Gurevich, 2015, A laboratory study of the elastic and anelastic properties of the Eagle Ford shale, 77th EAGE Conference and Exhibition, Extended Abstracts, We P8 04.

Mikhaltsevitch, V., M. Lebedev, and B. Gurevich, 2015, A laboratory study of the "barrel shape" effect in a viscoelastic cylindrical sample at seismic frequencies, ASEG-PESA 24th International Geophysical Conference and Exhibition, ASEG Extended Abstracts, 1-2.

Chapter 2

Journal paper:

Mikhaltsevitch, V., M. Lebedev, and B. Gurevich, 2014, A laboratory study of low-frequency wave dispersion and attenuation in water-saturated sandstones: The Leading Edge, **33**, 616 -622.

Refereed Conference Paper:

Mikhaltsevitch, V., M. Lebedev, and B. Gurevich, 2013, An experimental study of low-frequency wave dispersion and attenuation in water saturated sandstones, Poromechanics V: Proceedings of the Fifth Biot Conference on Poromechanics, 135-144.

Conference proceedings:

Mikhaltsevitch, V., M. Lebedev, and B. Gurevich, 2011, An experimental study of low-frequency wave dispersion and attenuation in water saturated sandstone, First International Workshop on Rock Physics, Golden, USA.

Mikhaltsevitch, V., M. Lebedev, and B. Gurevich, Low-frequency measurements of the mechanical parameters of sandstone with low permeability, ASEG Extended Abstracts 2012: 22nd Geophysical Conference, 1-4.

Mikhaltsevitch, V., M. Lebedev, and B. Gurevich, 2012, An experimental study of modulus dispersion and attenuation in sandstones at seismic frequencies, Second International Workshop on Rock Physics, Southampton, UK.

Mikhaltsevitch, V., M. Lebedev, and B. Gurevich, 2012, An experimental study of low-frequency wave dispersion and attenuation in water saturated sandstone, 74th EAGE Conference and Exhibition, Expanded Abstracts, P315.

Mikhaltsevitch, V., M. Lebedev, and B. Gurevich, 2013, An experimental study of modulus dispersion and attenuation in sandstones at seismic frequencies, ASEG-PESA 23rd International Geophysical Conference, ASEG Extended Abstracts, 1-4.

Mikhaltsevitch, V., M. Lebedev, and B. Gurevich, 2013, An experimental study of attenuation in sandstones at seismic frequencies, EAGE Workshop on Seismic Attenuation, Singapore, Extended Abstract, O16.

Chapter 3:

Journal paper:

Mikhaltsevitch, V., M. Lebedev, and B. Gurevich, 2016, Practical application of the Kramers-Kronig relationship for validation of the laboratory measurements at seismic frequencies: Geophysical Research Letters, **43**, 4986-4991.

Chapter 4:

Journal papers:

Mikhaltsevitch, V., M. Lebedev, and B. Gurevich, 2014, Measurements of the elastic and anelastic properties of sandstone flooded with supercritical CO_2: Geophysical Prospecting, **62**, 1266-1277.

Mikhaltsevitch, V., M. Lebedev, and B. Gurevich, 2014, A laboratory study of the elastic and anelastic properties of the sandstone flooded with supercritical CO_2 at seismic frequencies: Energy Procedia, **63**, 4289-4296.

Conference proceedings:

Mikhaltsevitch, V., M. Lebedev, and B. Gurevich, 2012, Laboratory measurements of elastic and anelastic parameters of sandstone flooded with supercritical CO_2 at seismic frequencies, CO2CRC Research Symposium, Adelaide, Australia, 1-2.

Mikhaltsevitch, V., M. Lebedev, and B. Gurevich, 2013, Low frequency laboratory measurements of the elastic and anelastic properties of the sandstone flooded with supercritical CO_2, ASEG-PESA 23rd International Geophysical Conference and Exhibition, ASEG Extended Abstracts, 1-4.

Mikhaltsevitch, V., M. Lebedev, and B. Gurevich, 2013, Low frequency measurements of the elastic and anelastic properties of the sandstone flooded with supercritical CO_2, 75th EAGE Conference and Exhibition, Extended Abstracts, Th P09 07.

Mikhaltsevitch, V., M. Lebedev, and B. Gurevich, 2014, Laboratory study of the elastic and anelastic properties of the sandstone flooded with supercritical CO_2 at seismic frequencies, GHGT-12 The Greenhouse Gas Control Technologies Conference, Austin, USA, #271.

Chapter 5:

Journal paper:

Mikhaltsevitch, V., M. Lebedev, and B. Gurevich, 2016, Laboratory measurements of the effect of fluid saturation on elastic properties of carbonates at seismic frequencies: Geophysical Prospecting, **64**, 799-809.

Conference proceedings:

Mikhaltsevitch, V., M. Lebedev, and B. Gurevich, 2013, Laboratory measurements of the elastic and anelastic parameters of limestone at seismic frequencies, SEG International Exposition and 83rd Annual Meeting, SEG Technical Program Expanded Abstracts, 2974-2978.

Mikhaltsevitch, V., M. Lebedev, and B. Gurevich, 2014, Low-frequency laboratory measurements of the acoustic parameters of Savonnieres limestone, SEG International Exposition and 84th Annual Meeting, SEG Technical Program Expanded Abstracts, 2978-2982.

Mikhaltsevitch, V., M. Lebedev, and B. Gurevich, 2014, A laboratory study of elastic and anelastic properties of Savonnieres limestone, 76th EAGE Conference and Exhibition, Extended Abstracts, We P12 01.

Chapter 6:

Conference proceedings:

Mikhaltsevitch, V., M. Lebedev, B. Gurevich, M. Pervukhina, and S. Zandi, 2016, Elastic anisotropy of the Wellington shale at seismic frequencies: Laboratory measurements, SEG International Exposition and 86th Annual Meeting, SEG Technical Program Expanded Abstracts, 392-397.

Mikhaltsevitch, V., M. Lebedev, and B. Gurevich, 2016, A laboratory study of the elastic anisotropy in the Mancos shale at seismic frequencies, SEG International Exposition and 86th Annual Meeting, SEG Technical Program Expanded Abstracts, 3174-3178.

Mikhaltsevitch, V., M. Lebedev, and B. Gurevich, 2017, Effects of water saturation on P-wave anisotropy in the Mancos Shale at seismic frequencies, 79th EAGE Conference and Exhibition, France, Extended Abstracts, Tu P3 11.

Chapter 1

A laboratory apparatus for measurements of elastic and anelastic properties of rocks at low frequencies

1.1 Introduction

Laboratory studies of pore fluid effects on the seismic properties of sedimentary rocks play a crucial role in geophysical exploration and in the interpretation of the field data. Laboratory measurements of the elastic and anelastic properties of reservoir rocks provide the physical background required for seismic data analysis as well as for monitoring reservoir fluid production and enhanced oil recovery processes.

Depending on the frequency band, there are three main categories of laboratory tests used to measure the seismic properties of rocks.

The high-frequency tests comprising various ultrasonic techniques are extensively used for determination of the elastic parameters of rock since the 1950s (Hughes and Jones, 1950, 1951; Wyllie et al., 1956) and currently are the most popular experimental instruments due to their nondestructive nature, simplicity of implementation and low cost. The ultrasonic devices operate at frequencies from several hundred kHz to the MHz region (Ellis and Singer, 2007). However, conventional sonic tools used for well-logging operate in a frequency range under 25kHz (Ellis and Singer, 2007), and the dominant frequencies of the seismic waves with sufficient energy for recording in exploration seismology lie in a range from 2Hz to 120Hz (Sheriff and Geldart, 1995). The large difference in frequency renders

difficult direct use of the ultrasonic results for interpretation of sonic or seismic field data.

The laboratory tests based on resonant-bar techniques have been reported since 1930s (Ide, 1935, 1936; Birch and Bancroft, 1938). The resonant-bar techniques utilize the relationship between the elastic properties and the resonance frequencies of the examination object. The resonance frequencies are determined by the boundary conditions and therefore are dependent on the dimensional sizes and shape of the object. The frequency band for measuring the elastic properties is determined by the fundamental resonant frequency and its first few overtones corresponding to the kilohertz frequency range which is in a good match with standard sonic frequencies (Jackson, 1986; Weidner, 1987).

The low-frequency (LF) laboratory tests that have been considerably developed in recent decades, utilize a stress-strain relationship and differ by the type of the forced oscillations applied to a specimen under investigation: torsional (Jackson et al., 1984; Paffenholz and Burkhardt, 1989), longitudinal (Spencer, 1981; Paffenholz and Burkhardt, 1989; Batzle et al., 1999; Takei et al., 2011) and volumetric (Adelinet et al., 2010).

However, only a few out of the given above devices (Jackson et al., 1984; Spencer, 1994; Batzle et al., 1999; Adelinet et al., 2010) are able to measure elastic properties of rocks at an elevated confining pressure of over 10 MPa.

Jackson et al. (1987) constructed a device to study of rock anelasticity by observing the forced torsional oscillations of a series combination of a rock and a steel standard subjected to a harmonic torque under confining pressure. The device uses argon as a pressure medium and operates at frequencies of 3 mHz to 1 Hz and a confining pressure of 0-300 MPa. The performance of the machine is limited to measurements of shear modulus and shear attenuation.

In the apparatuses proposed by Spencer (1994) and Batzle et al. (1999) the confining pressure is applied by placing the entire device into a gas pressure vessel. Using the gas pressure vessel puts some considerable constrains on the sizes of rock samples and the mechanical assembly of the apparatus. The latter should be massive enough to avoid spurious acoustic resonances (Batzle et al., 2006) in the mechanical parts of the device.

The medium used for confining pressure in the apparatus described by Adelinet et al. (2010) is hydraulic oil. Saw-like oscillations of the confining pressure are

managed by a hydraulic ram along with two pressure intensifiers. The bulk modulus of rock is measured as a ratio of oscillating pressure to the resulting volumetric strain in the rock. The frequency band of the confining pressure oscillations used in the apparatus is limited by a low segment of the teleseismic domain and lies in the range between 0.01 Hz and 0.1 Hz. The apparatus is unable to measure shear modulus and operate in the uniaxial mode.

This chapter describes a LF laboratory apparatus based on the strain-stress technique with the longitudinal type of the forced oscillations designed and constructed in the Rock Physics Laboratory at the Department of Exploration Geophysics of Curtin University (Mikhaltsevitch et al., 2011a, 2011b, 2012; Lebedev et al., 2012). The apparatus operates in the frequency range from 0.01 Hz to 100 Hz and measures the complex Young's moduli and Poisson ratio of rock samples at confining or uniaxial pressures from 0 to 70 MPa and at pore pressures from 0 to 20 MPa. Using the results of the Young's modulus and Poisson ratio measurements, the shear and bulk moduli also can be determined. The performance of the apparatus is tested with dry Berea sandstone, Eagle Ford shale and polymethyl methacrylate (PMMA).

1.2 Experimental Setup

The mechanical assembly of the LF apparatus is presented in Figure 1.1. The assembly comprises the frame formed by two massive steel platforms (the total mass of the platforms is ~ 400 kg), four steel poles joining the platforms, and a set of units placed in the center of the frame (Figure 1.2). The set includes a hydraulic actuator, a Hoek's triaxial cell (model 45-D0554, Controls Group), a piezoelectric stack actuator PSt 1000/35/60 (APC International Ltd) with the limit of maximum load of 70,000 N and with the frequency of its mechanical resonance >20 kHz, an aluminum calibration standard, and two steel plugs with passages for a fluid injection. A rock sample to be tested is placed inside a sleeve made of elastomer, which is mounted within the triaxial cell. The fluid passages in the steel plugs attached to the sample enable the flow of fluids through the sample and provide the means for pore pressure control. The triaxial cell and the hydraulic actuator (model RCS201, Enerpac) are connected via fluid lines with two manual hydraulic pumps (model P392, Enerpac)

providing lateral and longitudinal static forces applied to the rock. The dynamic stress applied to the sample and the strains in the rock are controlled by three identical semiconductor strain gauges (type KSP-6-350-E4, Kyowa Ltd). One gauge is glued in the axial direction to the aluminum standard and the other two are glued to the sample with an epoxy adhesive (Selleys Araldite Super Strength). The same adhesive is also used to jacket the sample with a thin epoxy layer to prevent pore-fluid flow through the boundary (Batzle et al., 2006). The strain gauges attached to the sample are orientated to measure axial and radial strains. All strain gauges are connected with a set of electric bridges (BCM-1 Wheatstone Bridge, Omega Engineering Ltd). The connection of the gauges fixed to the rock is implemented with a feedthrough assembly (Spectite WFS), which is shown in Figure 1.3. To minimize friction between the rock and sleeve, the rock sample is covered by a few layers of teflon tape.

The schematic diagram of the electrical part of the apparatus is shown in Figure 1.4. The multilayer piezoelectric actuator transforms the periodic voltage, applied by an oscillator, into mechanical stress, which causes displacements in the aluminum standard and tested sample mounted in series. The displacements modulate the conductivity of the strain gauges. A set of electric bridges transforms the modulated conductivity into electric signals, which, after digitizing by an analogue-to-digital converter (model 100, InstruNet, Omega Engineering Ltd), are received by an acquisition computer, where the signals are averaged and processed. The value of extensional attenuation is derived from the phase delay between the stress applied to the sample and the strain in the rock.

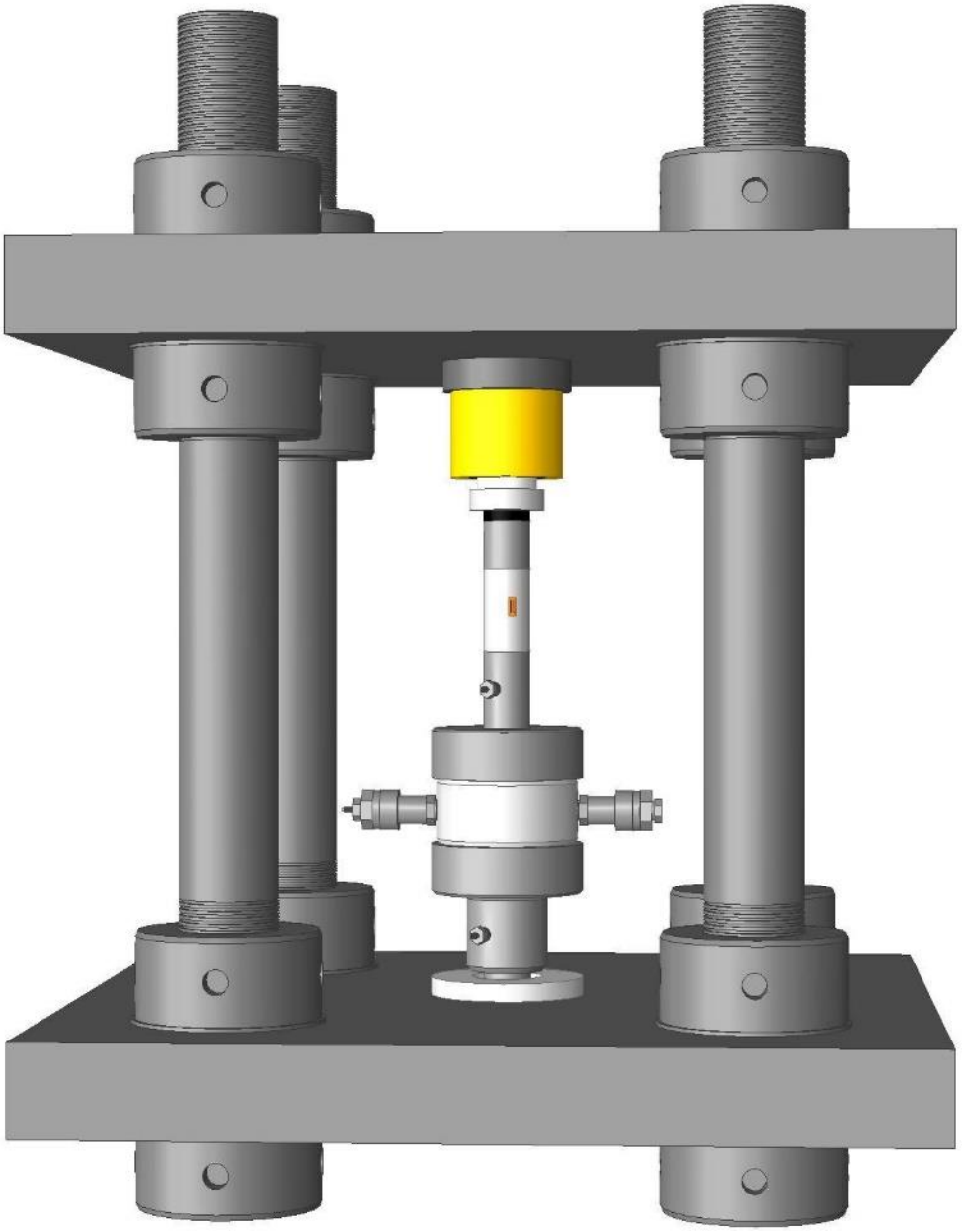

Figure 1.1 The mechanical assembly of the low-frequency laboratory rig.

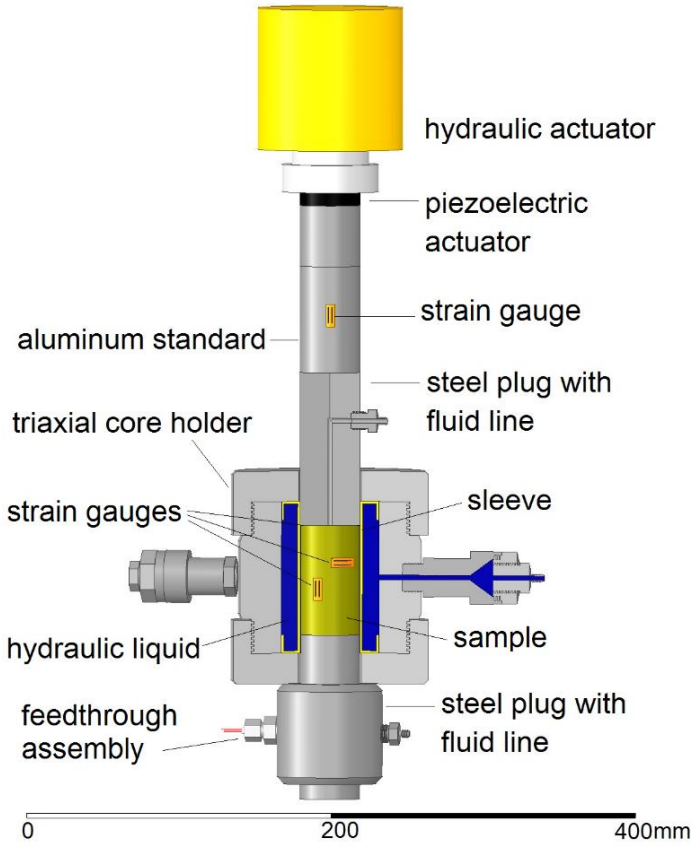

Figure 1.2 The central part of the low-frequency laboratory rig.

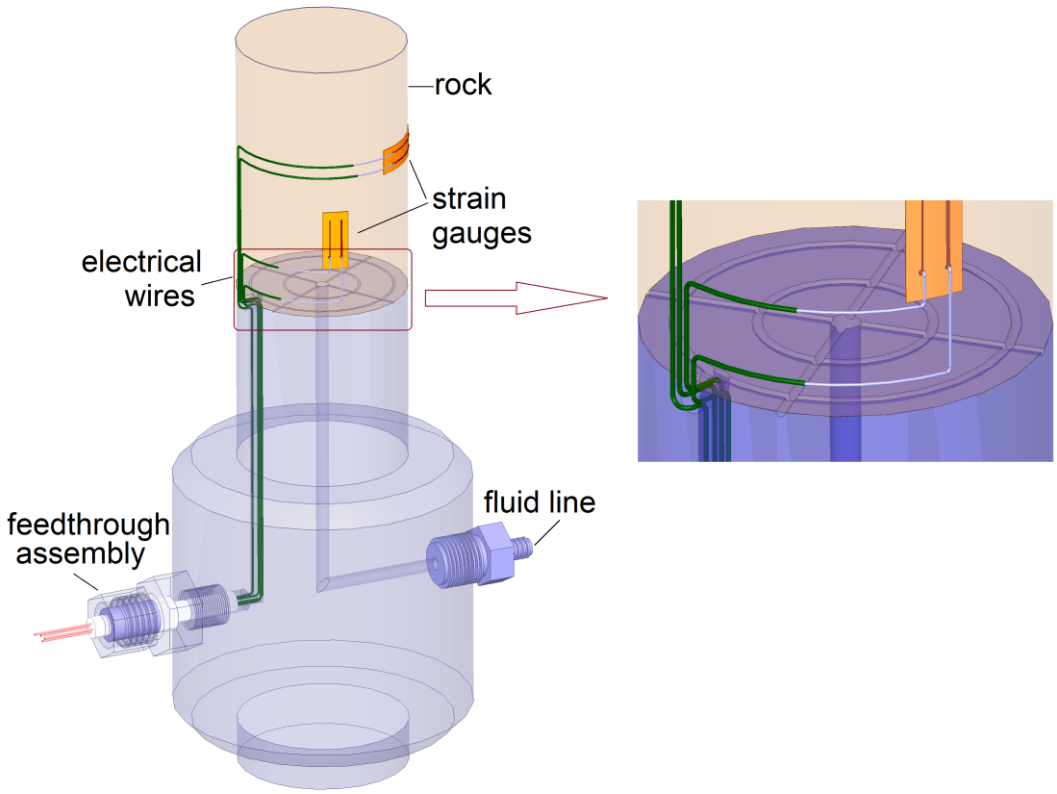

Figure 1.3 Connection of the electrical wires with the strain gauges glued to a sample.

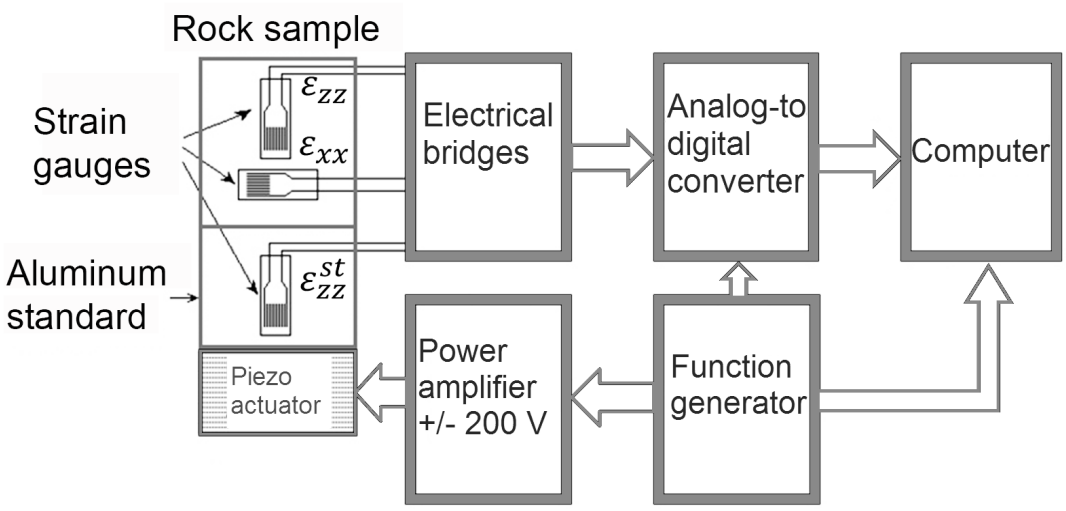

Figure 1.4 The electrical schematics of the low-frequency laboratory apparatus.

1.3 Method and operation

Measurements are performed using a modified version of the stress-strain technique employed by Spencer (1981), Paffenholz and Burkhardt (1989), and Batzle et al., (1999). Our approach is outlined below in more detail.

Consider a uniform harmonic stress applied to a homogeneous and isotropic rock sample. The wavelength λ of the stress oscillations meets the condition $\lambda >> L$, where L is the length of the sample.

If stress is applied along z-axis, then using Hooke's law (e.g. Mavko et al., 2009)

$$\varepsilon_{ij} = \frac{1}{E}[(1+\nu)\sigma_{ij} - \nu\delta_{ij}\sigma_{\alpha\alpha}], \tag{1.1}$$

where ν is the Poisson ratio, ε_{ij} are the elements of the rock strain tensor, σ_{ij} are the elements of the stress tensor, $\sigma_{\alpha\alpha} = \sum_{i=1}^{3}\sigma_{ii}$.

Equation 1.1 can be re-written in a matrix form:

$$\begin{pmatrix}\sigma_{xx}\\ \sigma_{yy}\\ \sigma_{zz}\\ \sigma_{xy}\\ \sigma_{yz}\\ \sigma_{zx}\end{pmatrix} = \frac{E}{(1+\nu)(1-2\nu)}\begin{pmatrix}1-\nu & \nu & \nu & 0 & 0 & 0\\ \nu & 1-\nu & \nu & 0 & 0 & 0\\ \nu & \nu & 1-\nu & 0 & 0 & 0\\ 0 & 0 & 0 & 1-2\nu & 0 & 0\\ 0 & 0 & 0 & 0 & 1-2\nu & 0\\ 0 & 0 & 0 & 0 & 0 & 1-2\nu\end{pmatrix}\begin{pmatrix}\varepsilon_{xx}\\ \varepsilon_{yy}\\ \varepsilon_{zz}\\ \varepsilon_{xy}\\ \varepsilon_{yz}\\ \varepsilon_{zx}\end{pmatrix}, \tag{1.2}$$

Using equation 1.2 and also taking into account rotational symmetry $\sigma_{xx} = \sigma_{yy}$ and $\varepsilon_{xx} = \varepsilon_{yy}$, we can express axial σ_{zz} and lateral σ_{xx} dynamic stresses as

$$\sigma_{zz} = [\nu\varepsilon_{xx} + \nu\varepsilon_{yy} + (1-\nu)\varepsilon_{zz}]\frac{E}{(1+\nu)(1-2\nu)} = [(1-\nu)\varepsilon_{zz} + 2\nu\varepsilon_{xx}]\frac{E}{(1+\nu)(1-2\nu)}, \quad (1.3)$$

$$\sigma_{xx} = \sigma_{yy} = [(1-\nu)\varepsilon_{xx} + \nu\varepsilon_{yy} + \nu\varepsilon_{zz}]\frac{E}{(1+\nu)(1-2\nu)} = [\varepsilon_{xx} + \nu\varepsilon_{zz}]\frac{E}{(1+\nu)(1-2\nu)}. \quad (1.4)$$

After dividing equation 1.4 by 1.3 we get the following relation for the Poisson ratio

$$\nu = \frac{c - \frac{\varepsilon_{xx}}{\varepsilon_{zz}}}{1 + c - 2c \cdot \frac{\varepsilon_{xx}}{\varepsilon_{zz}}} = \frac{c+u}{1+c+2c\cdot u}, \quad (1.5)$$

where $c = \frac{\sigma_{xx}}{\sigma_{zz}}$ and $u = -\frac{\varepsilon_{xx}}{\varepsilon_{zz}}$. Given that coefficient c can vary from 0 to 1, we get a range of possible values for ν between u and 0.5.

The Young's modulus of the rock can be found from equation 1.3

$$E = \sigma_{zz}\frac{(1+\nu)(1-2\nu)}{(1-\nu)\varepsilon_{zz} + 2\nu\varepsilon_{xx}}, \quad (1.6)$$

The stress can σ_{zz} be expressed in terms of the aluminum standard parameters as

$$\sigma_{zz} = E_{st}\varepsilon_{zz}^{st}, \quad (1.7)$$

where E_{st} is the Young's modulus of aluminum (which is assumed known) and ε_{zz}^{st} is a measured amplitude of longitudinal strain in the aluminum standard. The Young's modulus of the rock sample can be obtained by substituting equation 1.7 into 1.3. This yields

$$E = E_{st}\varepsilon_{zz}^{st}\frac{(1+\nu)(1-2\nu)}{2\nu\varepsilon_{xx} + (1-\nu)\varepsilon_{zz}} = E_{st}\frac{\varepsilon_{zz}^{st}}{\varepsilon_{zz}}\cdot\frac{1-\nu-2\nu^2}{1-\nu-2\nu u} \approx E_{st}\frac{\varepsilon_{zz}^{st}}{\varepsilon_{zz}}. \quad (1.8)$$

The parameter c, which is required for determination of the Poisson ratio ν in equation 1.5, can be found as follows. The lateral stress σ_{xx} can be presented as

$$\sigma_{xx} = -K_{com}\frac{\Delta V}{V} \approx -2K_{com}\varepsilon_{xx}\frac{V_{rock}}{V}, \quad (1.9)$$

where K_{com} is the bulk modulus of the composition comprising the hydraulic oil and sleeve covering the sample; V is the part of the Hoek's cell volume occupied by hydraulic oil and sleeve; ΔV is the volume change resulting from applied stress oscillations; $\Delta V / V_{rock} \approx 2\varepsilon_{xx}$. Taking into account that

$$\sigma_{zz} = E_{st}\varepsilon_{zz}^{st}, \tag{1.10}$$

we obtain

$$c = \frac{\sigma_{xx}}{\sigma_{zz}} = -\frac{K_{com}}{E_{st}\varepsilon_{zz}^{st}} \cdot \frac{\Delta V}{V} \approx -2\frac{K_{com}}{E_{st}} \cdot \frac{\varepsilon_{xx}}{\varepsilon_{zz}^{st}} \cdot \frac{V_{rock}}{V}. \tag{1.11}$$

If we introduce a factor

$$k_c = \frac{K_{com}}{E_{st}}, \tag{1.12}$$

then equation 1.11 can be re-written in the form

$$c = -k_c \frac{2\varepsilon_{xx}}{\varepsilon_{zz}^{st}} \cdot \frac{V_{rock}}{V}, \tag{1.13}$$

or

$$c = -k_c \frac{2\varepsilon_{xx}}{\varepsilon_{zz}^{st}} \cdot \frac{r^2 L_s}{(R^2 - r^2)L}, \tag{1.14}$$

where L_s and r are the length and radius of the specimen, L and R are the internal length and radius of the core holder, correspondingly.

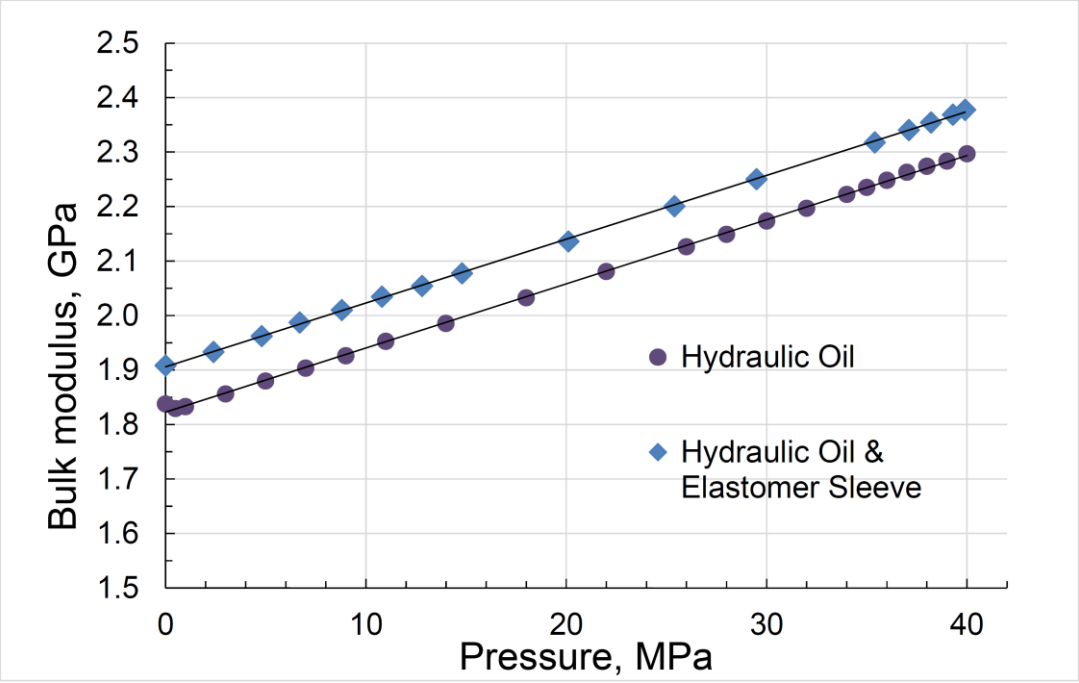

Figure 1.5 The pressure dependence of the bulk modulus of the oil-sleeve composition and hydraulic oil. The volume of oil and sleeve corresponds to Hoek's triaxial cell model 45-D0554 (Controls Group).

Note that inasmuch as the dynamic strains ε_{xx} and ε_{zz}^{st} have opposite phases, the coefficient c has to be positive.

The parameter $k_c = K_{com} / E_{st}$ can be estimated using the dependence of the bulk modulus K_{com} on pressure given in Figure 1.5.

The dependence was obtained using an ultrasonic system at a frequency of 1 MHz. The Young's modulus of the aluminum standard was found using an ultrasonic system and is equal to 69.0 GPa. Utilizing the graph presented in Figure 1.5, it is easy to show that, for example, at a confining pressure of 12 MPa, $k_c \approx 0.03$. Importantly, k_c does not depend on the type of a tested rock and can be applied to any sample.

The bulk K and shear μ moduli can be found via the Young's modulus determined by equation 1.8:

$$K = \frac{E}{3(1-2\nu)},\ \mu = \frac{E}{2(1+\nu)}. \tag{1.15}$$

In our experiments the extensional attenuation Q_E^{-1} in the sample is measured as a phase shift $\Delta\varphi$ between harmonic stress applied to the sample and resulting strain detected in that sample:

$$Q_E^{-1} = \Delta\varphi. \tag{1.16}$$

middle and bottom signals are obtained correspondingly from the axial and circumferential gauges attached to the rock sample. The number of averages is 100.

To derive relation 1.16, let us present the stress σ and strain ε in the complex form

$$\sigma = \sigma_0 \exp(i\omega t), \tag{1.17}$$

$$\varepsilon = \varepsilon_0 \exp(i\omega t - \Delta\varphi), \tag{1.18}$$

where σ_0 and ε_0 are the magnitudes of stress and strain, correspondingly. The complex Young's modulus of the rock is equal to

$$E = \frac{\sigma}{\varepsilon} = E_0 \exp(\Delta\varphi) = E_0(\cos\Delta\varphi + i\sin\Delta\varphi). \tag{1.19}$$

Here E_0 is the absolute value of the Young's modulus E.

The extensional attenuation Q_E^{-1} can be expressed as the ratio of the imaginary and real parts of E:

$$Q_E^{-1} = \frac{\mathrm{Im}(E)}{\mathrm{Re}(E)} = \tan\Delta\varphi \approx \Delta\varphi\,. \tag{1.20}$$

In our study, we used the following procedure to estimate $\Delta\varphi$. The signals obtained from two axial strain gauges attached to the sample and standard, were first digitized, averaged and subjected to Fourier transform, then the complex Fourier transform amplitudes of those signals were computed at the frequency of the harmonic stress, and, finally, the target value $\Delta\varphi$ was calculated as the difference between the phases of the found complex amplitudes.

The example of the signals obtained from dry Berea sandstone and an aluminum standard at a frequency of periodical stress oscillations equal to 1 Hz and at a confining pressure of 10 MPa, is given in Figure 1.6.

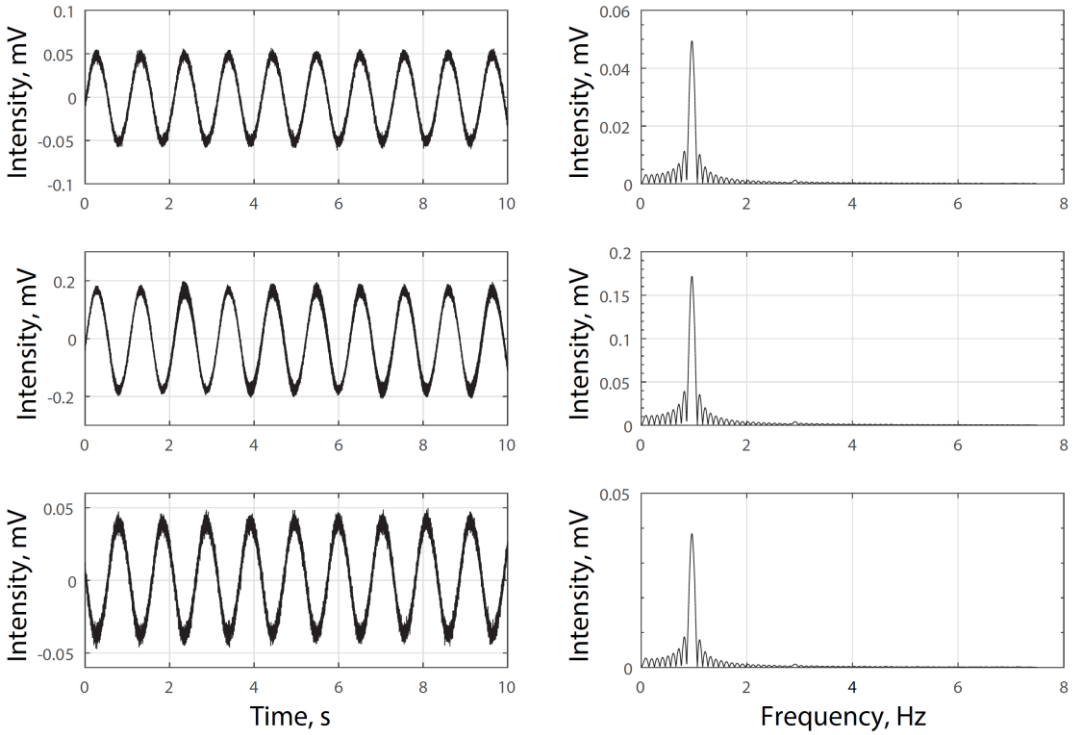

Figure 1.6 Signals and their Fourier transforms obtained from dry Berea sandstone at the frequency of the periodical stress oscillations equal to 1 Hz and at a confining pressure of 10 MPa. The top signal was obtained from the gauge attached to the aluminum standard, the middle and bottom signals were obtained correspondingly from the axial and circumferential gauges attached to the rock sample. The number of averages is 100.

1.4 Calibration

The experimental setup was calibrated using dry Berea sandstone, dry/water-saturated Eagle Ford shale and PMMA (acrylic material ASTM-D-5436, Spartech Townsend). First, the measuring accuracy of the apparatus was assessed by a comparison between data obtained for Berea sandstone and Eagle Ford shale with the LF apparatus and an ultrasonic system. Then, the role of a strain gauge position on the sample surface was determined using an acrylic specimen. To improve the signal-to-noise ratio 10 times, the number of signal averages in all tests was 100.

1.4.1 Berea sandstone

The results of the LF and ultrasonic calibrations with Berea sandstone are shown in Figures 1.7-1.9. The error bars for all measured parameters were estimated using the uncertainty analysis technique proposed in Adam (2009) and Adam et al. (2009).

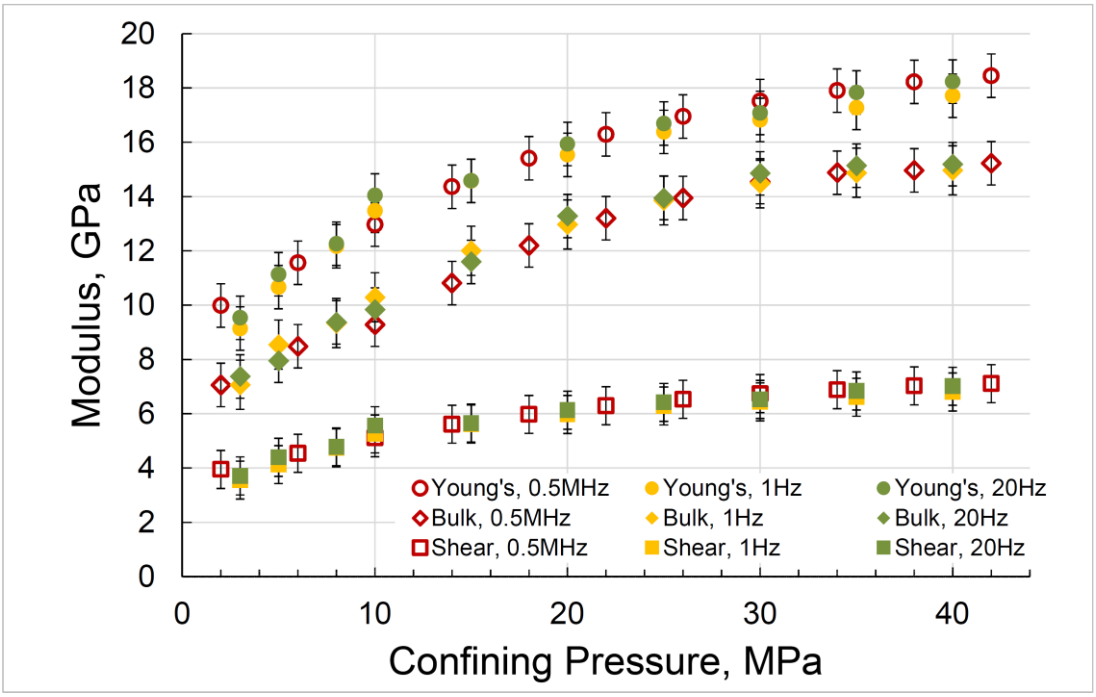

Figure 1.7 The pressure dependences of the Young's, bulk and shear moduli measured on the dry Berea sandstone sample. The LF measurements are conducted at two frequencies of 1 Hz and 20 Hz, the ultrasonic results are obtained at a frequency of 0.5 MHz.

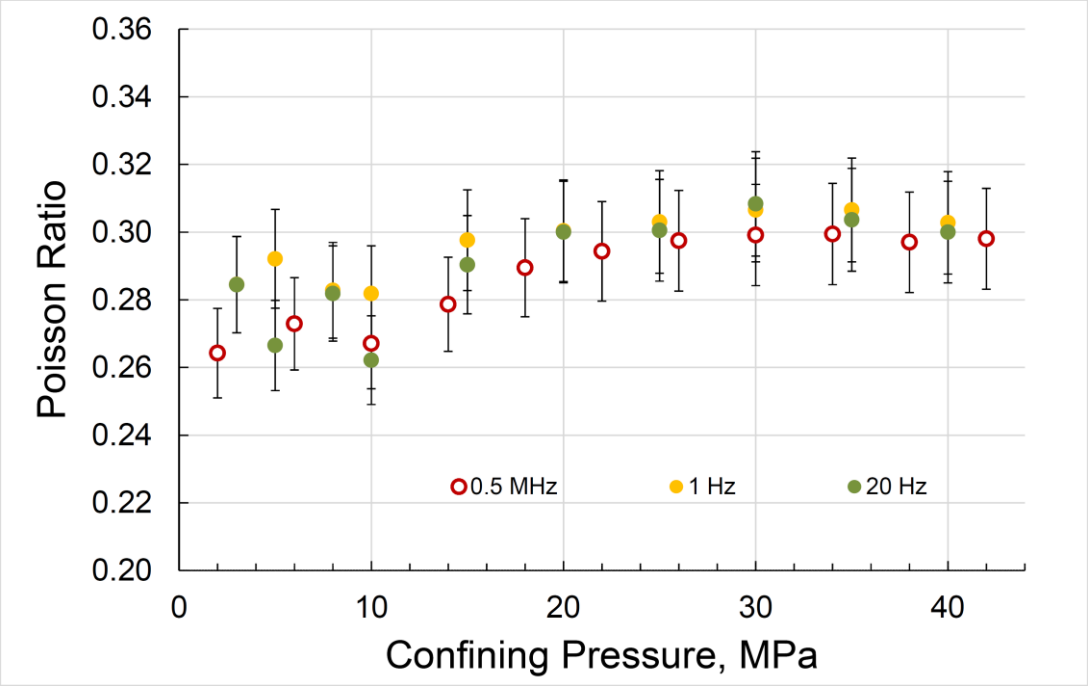

Figure 1.8 The pressure dependences of the Poisson ratio measured on the dry Berea sandstone sample at three frequencies of 1 Hz, 20 Hz and 0.5 MHz. All experimental parameters are the same as in Figure 1.7.

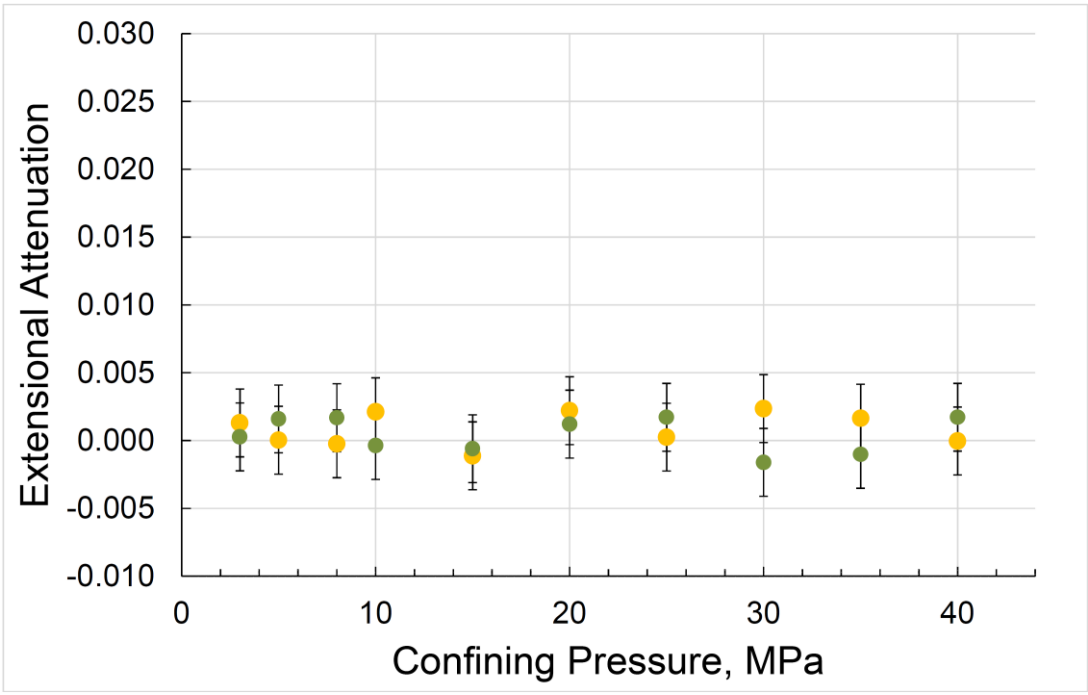

Figure 1.9 The pressure dependences of the extensional attenuation measured on the dry Berea sandstone sample at frequencies of 1 Hz and 20 Hz. The measurement parameters are the same as in Figure 1.7.

The experiments were performed at confining pressures from 2 MPa to 42 MPa and at an ambient pore pressure (0.1 MPa). In the ultrasonic tests, the compressional V_p and shear V_s velocities were measured using the time-of-flight technique. The bulk K and shear μ moduli were computed as

$$K = \rho\left(V_p^2 - \frac{4}{3}V_s^2\right), \quad \mu = \rho V_s^2, \tag{1.21}$$

where ρ is the density of a sample. The ultrasonic pulses with a carrier frequency of 0.5 MHz were generated and recorded using a pulser/receiver unit (5077PR, Olympus, Ltd.) and a digital oscilloscope (TDS3034C, Tektronix, Ltd.).

The Berea sandstone sample is made as a cylinder of 38 mm diameter and 70 mm length. The density of dry sandstone is 2305 kg/m^3. The elastic moduli and Poisson ratio of dry Berea sandstone are measured at two low (1 Hz and 20 Hz) and one ultrasonic (0.5 MHz) frequencies under confining pressures of 2 MPa to 42 MPa. As can be seen in Figures 1.7 and 1.8, the LF and ultrasonic results are in close agreement. The extensional attenuation Q_E^{-1} in dry Berea sandstone, expressed via the phase shift between stress and strain $\Delta\varphi$, is shown in Figure 1.9. The phase shift measurements are repeatable with an accuracy of ±0.0025 rad, which also characterizes the accuracy of the corresponding attenuation Q_E^{-1}. All measurements were conducted under a room temperature (~20° C).

1.4.2 Eagle Ford Shale

The elastic moduli and extensional attenuation of Eagle Ford shale were measured under dry and wet conditions at a confining pressure of 10 MPa and an ambient pore pressure. The LF and ultrasonic measurements were carried out at frequencies of 0.1 to 100 Hz and 0.5 MHz, correspondingly.

The Eagle Ford shale sample cut out in the direction normal to the formation bedding was selected after its homogeneity was thoroughly tested with an X-ray micro CT-scanner (Model VersaXRM-500, Xradia). The cross-section scans of the sample are presented in Figure 1.10. The sizes of the sample are: length – 69.4 mm, diameter – 38.0 mm. The mass and density of the dry/wet sample are 183.3/190.1 g and 2301/2402 kg/m^3, accordingly. The difference in density of the sample in dry and wet states corresponds to porosity of 9 %.

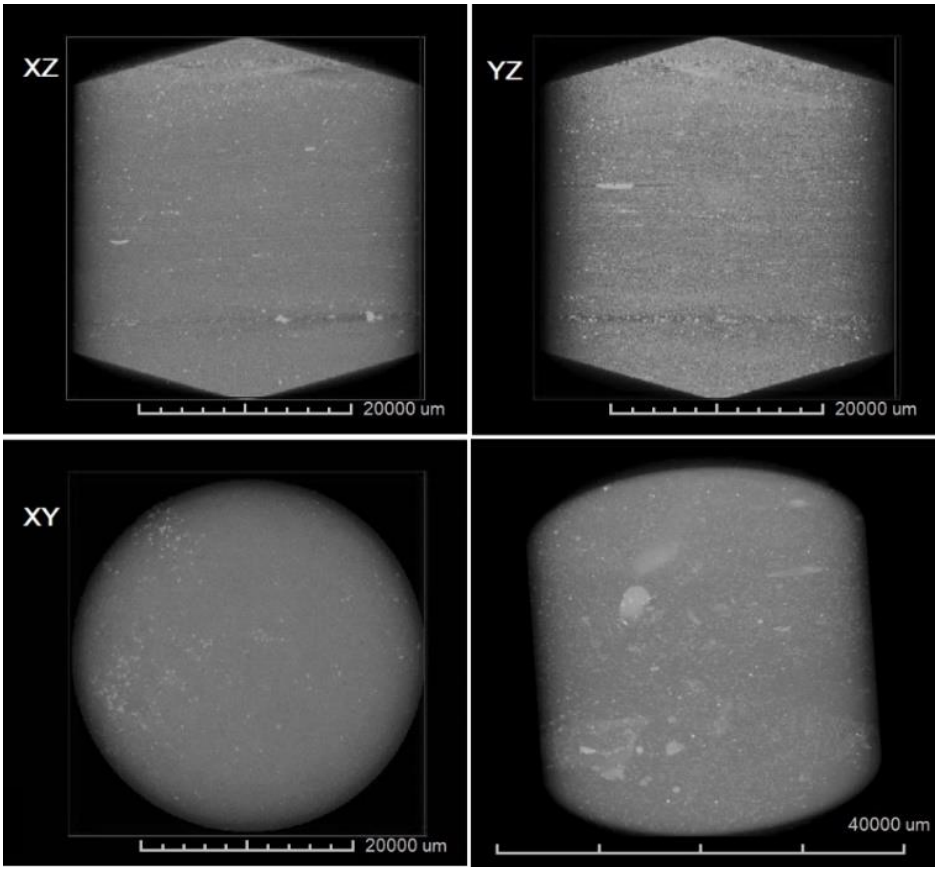

Figure 1.10 X - ray scans of the Eagle Ford shale sample.

The flowchart of the measurements performed on the sample was as follows:

- The elastic parameters and extensional attenuation of the vacuum-dry sample were measured at seismic frequencies at a confining pressure of 10 MPa.
- The ultrasonic elastic parameters of the sample were measured at confining pressures of 0 to 56 MPa.
- The sample was vacuum-dried for three weeks and after that placed in a container with distilled water inside a vacuum chamber for two months.
- The LF tests with the partially saturated sample were repeated in the same seismic frequency range as for the dry cycle.
- The ultrasonic measurements were conducted on the wet sample at confining pressures of 0 to 60 MPa.

The Young modulus E of the specimen and Poisson ratio ν presented in Figure 1.11 were measured at seismic frequencies by comparing the strains detected in the shale sample and in the aluminum standard.

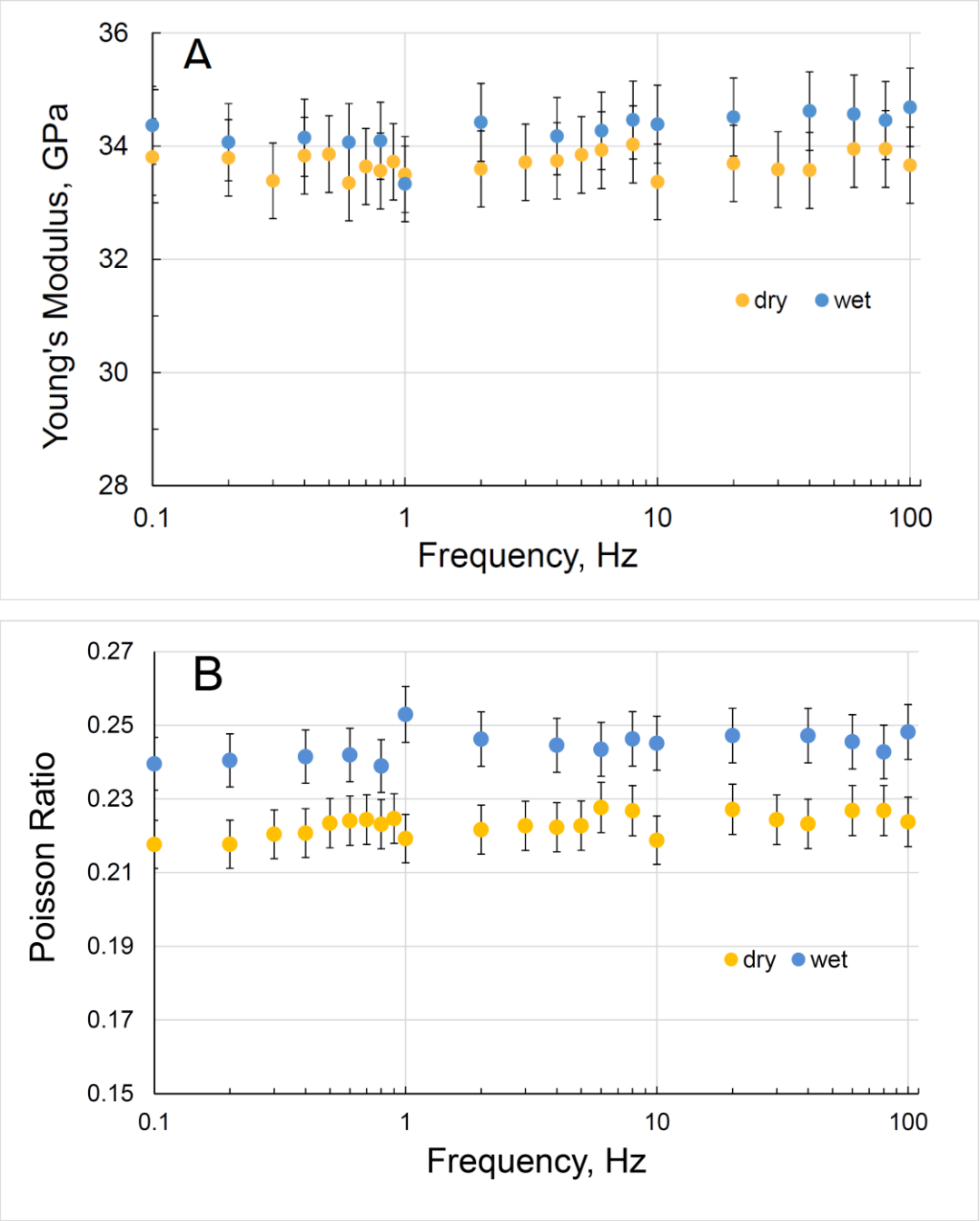

Figure 1.11 Young's modulus (A) and Poisson ratio (B) measured on the dry and wet Eagle Ford sample at a confining pressure of 10 MPa.

The bulk K and shear μ moduli of the sample shown in Figure 1.12 were computed using equations (1.15). The value of extensional attenuation was derived from the phase shift between the stress applied to a sample and the strain in the sample caused by that stress (O'Connell and Budiansky, 1978). The uncertainty in the measurements of the extensional attenuation is about ± 0.002.

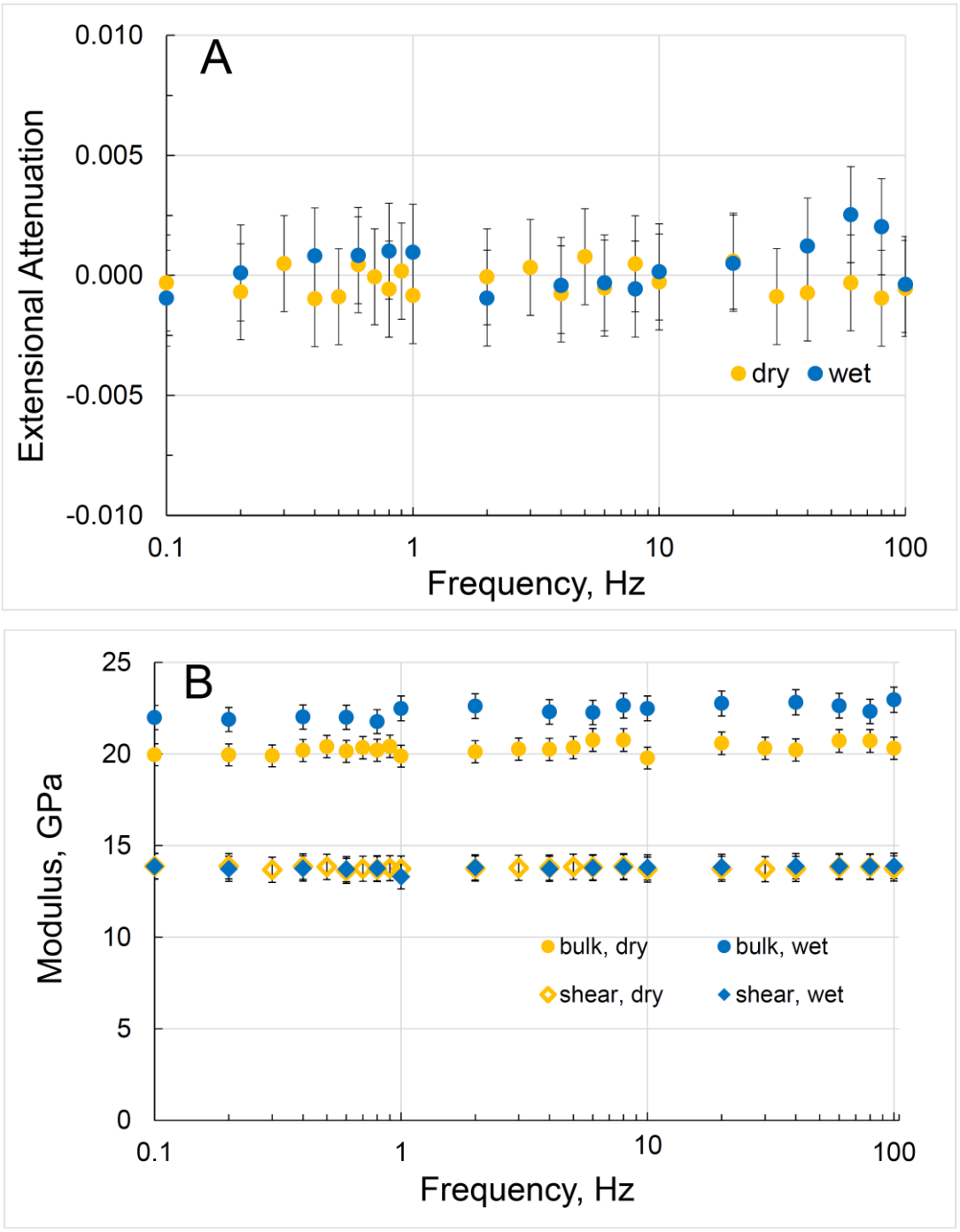

Figure 1.12 The extensional attenuation (A) and the bulk and shear moduli (B) obtained for the dry and wet shale sample at a confining pressure of 10 MPa.

The ultrasonic compressional V_P and shear V_S velocities were measured using the 'time of flight' method with a carrier frequency of ultrasonic pulses equal to 0.5 MHz. The results of the velocity measurements at ultrasonic frequency are presented in Figure 1.13A. The bulk and shear moduli were found using expressions 1.21 and presented in Figure 1.13B. In Figure 1.13B, for comparison, we also plotted the averaged moduli obtained in the tests at seismic frequencies.

The results obtained at seismic frequencies using the strain-stress technique are in good agreement with the data obtained in the ultrasonic tests (Figure 1.13B). This agreement can result from the high homogeneity of the shale sample on the scale of its characteristic size.

The absence of moduli dispersion in the partly saturated Eagle Ford shale in the frequency range from 0.1 Hz to 500 kHz is rather an important result of our measurements which should be considered in more detail.

The characteristic frequency f_c of dispersion/attenuation peaks in partially water saturated rock can be found as (Dutta and Seriff, 1979)

$$f_c = \frac{1}{\pi}\frac{kK_f}{\phi\eta h^2}, \tag{1.22}$$

where η = $8.9\cdot10^{-4}$ Pa·s is the water viscosity, ϕ=0.09 is the porosity of the rock, K_f = 2.2 GPa is the bulk modulus of water, k is the shale permeability, h = 0.07 m is the (characteristic) size of the sample. If we take into account that typical permeability of the Eagle Ford shale does not exceed 1 μD (Walls and Sinclair, 2011), we obtain $f_c \approx 0.002$ Hz. The lower limit of the seismic frequencies used in our experiments is two orders higher than this characteristic frequency f_c. Thus, all our measurements are not in the dispersive region and the measurements at seismic frequencies are equivalent to the measurements at ultrasonic frequencies. This result confirms the statement by Batzle et al. (2006) that for sedimentary rocks with very low intrinsic permeability even seismic frequencies can conform to the high-frequency regime where pore pressure is in non-equilibrium state.

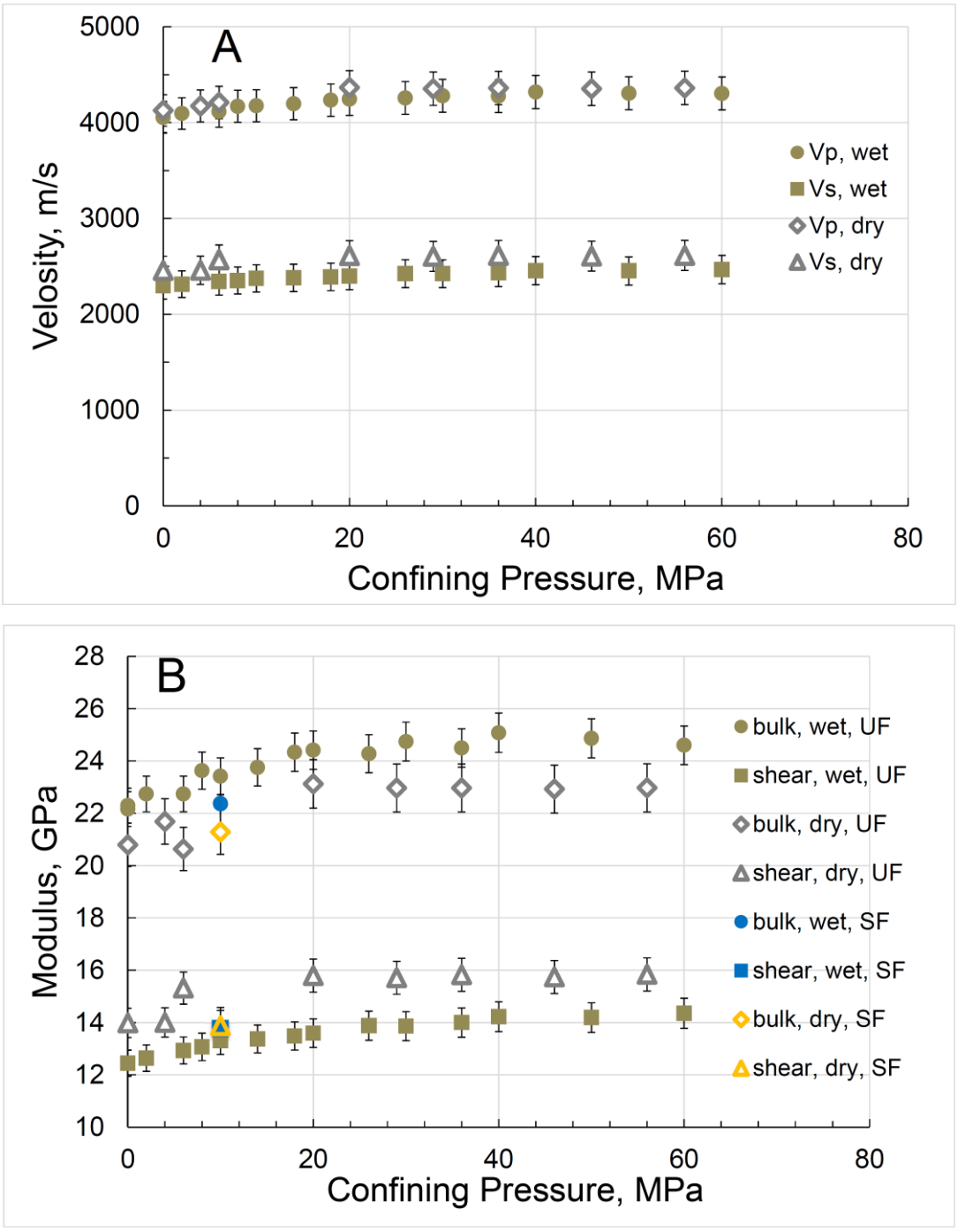

Figure 1.13 The ultrasonic P- and S-velocities (A) and the bulk and shear moduli (B) measured on the dry and wet Eagle Ford shale sample. For comparison, the averaged bulk and shear moduli obtained at seismic frequencies are also plotted on graph B.

1.4.3 Acrylic

In all LF laboratory experiments tested samples (mainly of cylindrical shape) are located between metal plugs at high pressure applied to their ends. Because of the frictions at the interface between the sample and the plug ends, a tested sample would not deform uniformly, resulting in "barrel" shaped geometry during compression (Figure 1.14). This effect might not be important for stiff samples with the elastic properties similar to the surrounding metal plugs, one of each is an aluminium standard, but it can be significant if the sample is much more compliant than aluminium. In this study we investigated the "barrel shape" effect in a cylindrical viscoelastic PMMA sample 150 mm long with a diameter of 38.0 mm and a density of 1185 kg/m^3 (acrylic material ASTM-D-5436, Spartech Townsend) using the LF laboratory apparatus. We used two pairs of strain gauges attached in the middle of the sample and at two centimetres from one of the ends. Each pair measures both axial and radial strains. To increase the effect, only axial pressure was applied to the sample; the measurements were conducted under two axial pressures of 7 MPa and 15 MPa.

The uniaxial version of the LF apparatus presented in Figure 1.15. A specimen to be tested is placed between the aluminium standard and the steel plug. To avoid the frictions between the tested sample and surrounding plugs, the ends of the sample are glued to the plugs with epoxy adhesive (Selleys Araldite Super Strength). A static axial force is applied to the specimen by a hydraulic actuator (model RCS201, Enerpac).

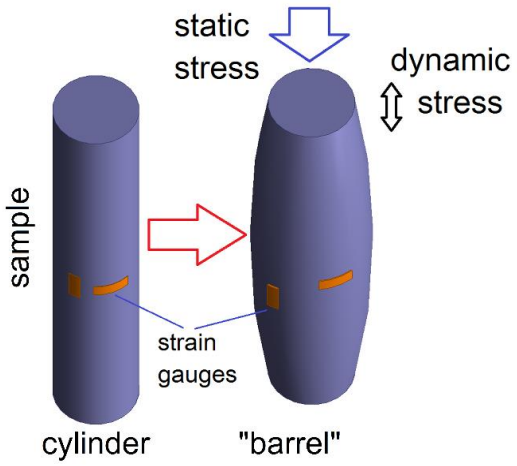

Figure 1.14 The "barrel shape" effect taking place in sold cylindrical samples under uniaxial pressure.

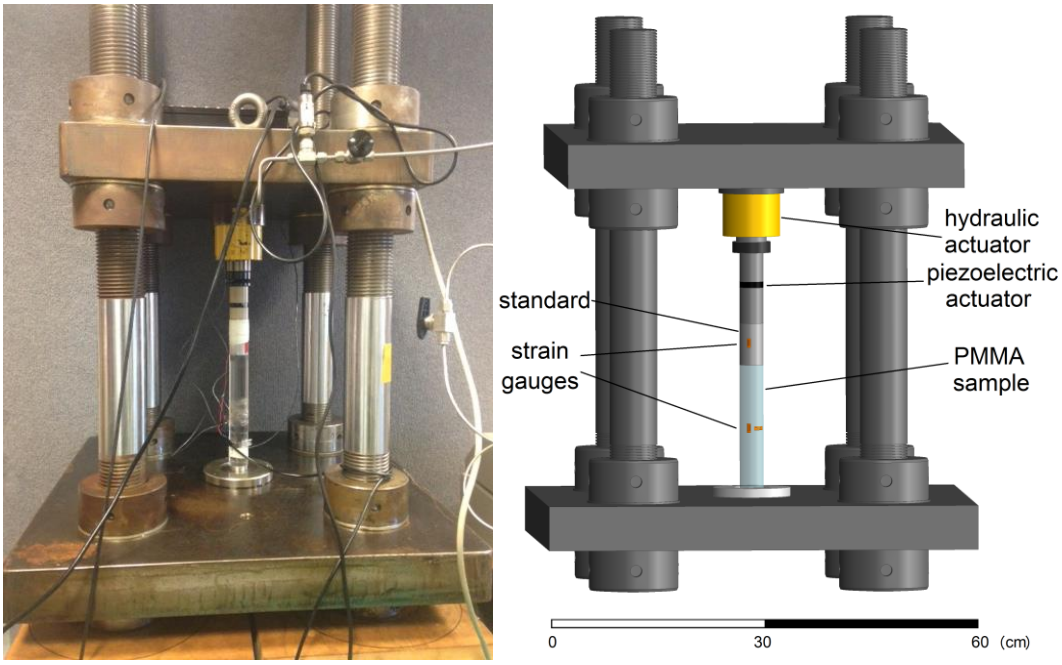

Figure 1.15 The LF apparatus for measurements of elastic and anelastic properties of solids.

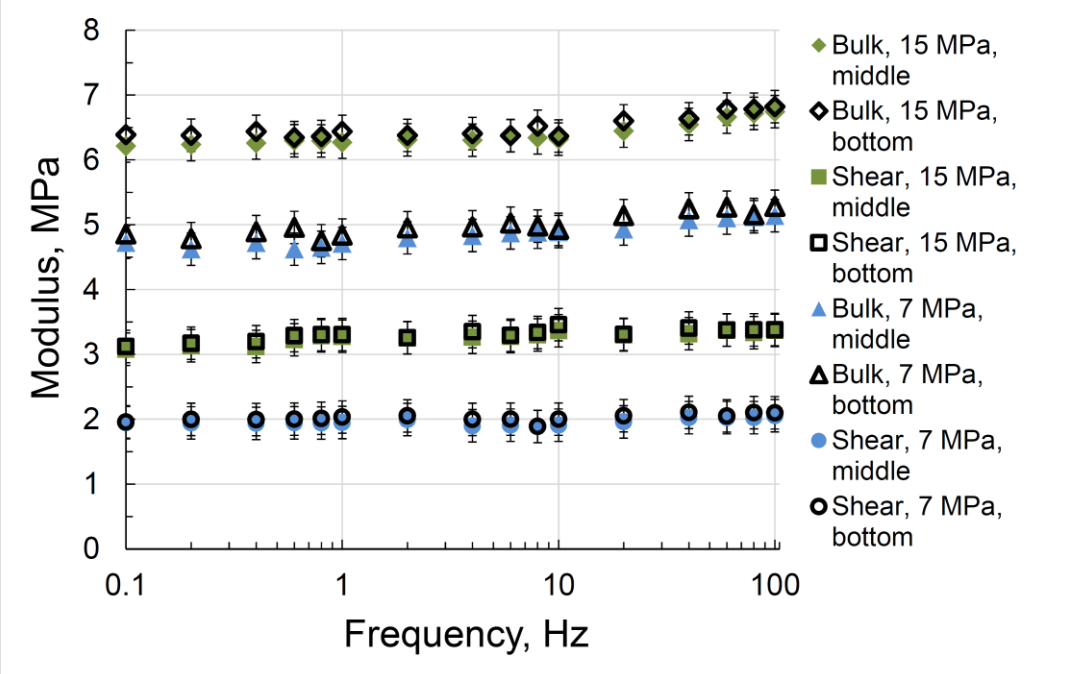

Figure 1.16 Frequency dependencies of the bulk and shear moduli of the cylindrical acrylic sample measured in the middle and at 2 cm from the bottom end of the sample at axial pressures of 7 MPa and 15 MPa.

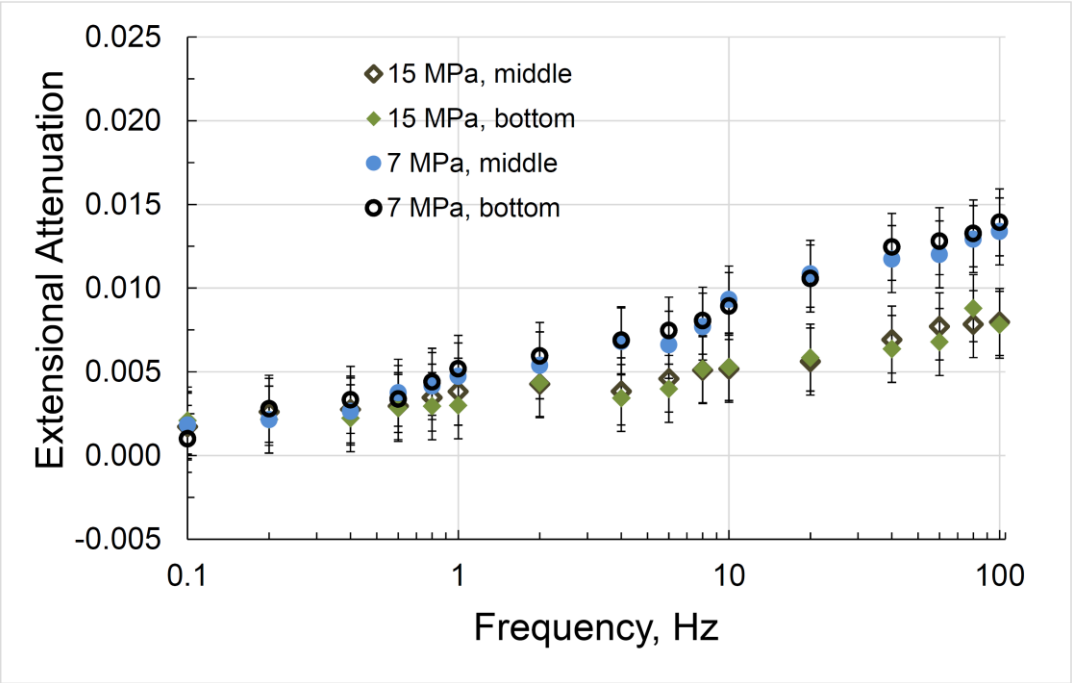

Figure 1.17 Frequency dependencies of the extensional attenuation in the cylindrical acrylic sample measured in the middle and at 2 cm from the bottom end of the sample at axial pressures of 7 MPa and 15 MPa.

The bulk and shear moduli of the samples were computed using equation 1.15, where the Poisson ratio ν and Young's modulus E were found as

$$\nu = -\frac{\varepsilon_{xx}}{\varepsilon_{zz}} \text{ and } E = E_{st}\,\varepsilon_{zz}^{st}/\varepsilon_{zz}\,. \tag{1.23}$$

The value of extensional attenuation is derived from the phase shift between the applied stress and the strain in the sample caused by that stress (O'Connell and Budiansky, 1978). The uncertainty in the measurements of extensional attenuation is about ± 0.002.

The results of the experiments are presented in Figures 1.16 and 1.17. Figure 1.16 demonstrate the increase of the bulk modulus with the frequency increase. According to the principle of causality, presented for linear viscoelastic systems by the Kramers-Kronig relations (O'Donnel et al. 1981), the increase of moduli should correspond to attenuation increase which is consistent with our experimental data presented in Figure 1.17. As can be seen, the barrel shape of a sample does not affect the results of the measurements.

Let us analyse this result. An output voltage of the electric bridge connected to a radial strain gauge is proportional to $\Delta V \sim \delta R / R$, where R is the resistance of the gauge, δR is the variation of the resistance at periodical stress. On the other

hand, ΔV is proportional to a radial strain $\Delta V \sim \delta r / r$, where r is the radius of the sample, δr is the radius variation when a periodical stress is applied. So, we get $\Delta V \sim \delta R / R \sim \delta r / r$. If we assume that the barrel shape of the sample does not affect significantly the axial strain measured along the length of the sample, we come to the conclusion that the results of our LF measurements should not depend on the radius of the sample (which varies if the sample has a barrel shape), but should depend only on relative change of the radius. This is true until the dynamic deformations are linear.

1.5 Conclusions

Chapter 1 presents the design, operation and calibration of the LF apparatus developed to measure extensional attenuation and elastic moduli of cylindrical rock samples in the seismic frequency range. The apparatus utilizes a stress-strain technique and measures the complex Young's modulus and Poisson's ratio of the rock sample at the range of strain amplitudes between 10^{-8} and 10^{-6} under confining or uniaxial pressures of 0 to 70 MPa.

The main peculiarities of the proposed design are as follows:

- A combination of the multilayer piezoelectric adaptor, having a high limit of maximum load, and the Hoek triaxial core holder provides the means to separate uniaxial and lateral pressures applied to the sample, which makes feasible the experiments with either uniaxial or confining pressures.
- Two massive platforms as a part of the mechanical assembly completely prevent spurious mechanical resonances in the apparatus. The top limit of the frequencies of operation is limited exclusively by the frequency of the mechanical resonance in the piezoelectric actuator.
- The sizes of the rock samples, which can be measured in this apparatus, are determined by the sizes of the triaxial core holder only.

The LF system was calibrated using dry Berea sandstone, dry/water-saturated Eagle Ford shale and PMMA (acrylic material ASTM-D-5436, Spartech Townsend). Calibration tests showed the accuracies of the extensional attenuation measurements were ±0.0025 rad.

The measurements on dry Berea sandstone conducted at two seismic frequencies of 1 Hz and 20 Hz, and one ultrasonic frequency of 0.5 MHz showed that LF and ultrasonic results are in very close agreement.

The Eagle Ford shale sample, recovered from a core drilled in the direction normal to the formation bedding, was tested under dry and water saturated conditions at seismic (0.1 Hz – 100 Hz) and ultrasonic (0.5 MHz) frequencies. According to the experimental procedure, the sample was first vacuum-dried for three weeks and then placed in a container with distilled water inside a vacuum chamber for two months. The elastic parameters measured at low frequencies for the dry and saturated sample are close to those measured at an ultrasonic frequencies. Our analysis demonstrates that LF and ultrasonic measurements on water saturated shale are conducted in non-dispersive high-frequency range where the measurements at seismic and ultrasonic frequencies are equivalent. This conclusion is confirmed by good agreement between the LF and ultrasonic results.

The uniaxial LF experiments carried out on acrylic demonstrate that measured elastic and anelastic parameters of a cylindrical solid sample are independent from the location of the strain gauges on the sample. The conducted tests confirm that the barrel shape of the sample caused by axial force does not affect reliability of LF laboratory measurements.

Chapter 2

Dispersion and attenuation in water/brine saturated sandstones at seismic frequencies

2.1 Introduction

Understanding the effects of the pore fluid on the elastic and anelastic properties of sedimentary rocks is important for interpreting seismic data obtained for reservoirs containing various fluids as well as for monitoring the fluid movement during hydrocarbon extraction in producing fields. It is generally accepted that the presence of fluid in the pore space leads to attenuation of acoustic waves and dispersion of the acoustic velocities and elastic moduli of rocks, see Pride et al. (2003) and Müller et al. (2010) for recent reviews.

Although a number of theoretical models have been developed to describe seismic attenuation and dispersion in fluid-saturated rocks, their practical use is very limited due to lack of systematic experimental validation and calibration. This lack of experimental data is the result of the fact that elastic wave velocities (and occasionally attenuation) in rocks are usually measured at ultrasonic frequencies, where dispersion and attenuation may be dominated by very different mechanisms than at seismic frequencies. Thus measurements of attenuation and dispersion at seismic frequencies is an issue of critical importance.

It has been demonstrated (Gordon and Davis, 1968; Mavko, 1979; Winkler et al., 1979) that linear loss mechanisms of attenuation in the rocks, which are relevant to seismic waves, become dominant at strain amplitudes $<10^{-6}$. This threshold level of strain amplitudes should be considered as a major constraint implied on the laboratory experiments.

The first seismic frequency (SF) laboratory measurements of elastic and anelastic properties of rocks at a strain amplitude $<10^{-6}$ were reported by Spencer (1981). Spencer used an apparatus based on the stress-strain relationship where sinusoidal stress was applied to a sample in a longitudinal direction; no lateral stress on the sample was set. Spencer observed significant Young's moduli dispersion and attenuation at frequencies of a few hundreds of Hertz in water saturated Navajo sandstone and at frequency ~10 Hz in water saturated Spergen limestone. The measurements were conducted under ambient conditions.

The SF laboratory experiments undertaken by Paffenholz and Burkhardt (1989) included measurements of the Young's moduli and extensional attenuation in fully water saturated rocks at frequencies between 0.03 and 300 Hz. Paffenholz and Burkhardt found substantial attenuation in Mittelrhaet and Obemkirchner sandstones with the peaks of attenuation at a few tens of Hertz, and also in limestone and dolomite, where the peaks of attenuation were observed at ~0.1 and ~20 Hz respectively. The measurements were carried out under uniaxial pressure of 1.5 MPa using the approach similar to the one used by Spencer.

When analysing Spencer's experiments, White (1986) and Dunn (1986) demonstrated that the attenuation observed by Spencer (1981) was due to radial fluid flow caused by the open-pore boundary condition on the sample surface and, to some extent, due to anelasticity of the rock matrix. The same remarks can be attributed to the measurements of the extensional attenuation performed by Paffenholz and Burkhardt (1989).

Batzle et al. (2006) conducted SF measurements (5 – 2500 Hz) on brine saturated low-permeability sandstone with high smectite content at various differential pressures. Applying the Cole-Cole relations to measured elastic parameters, Batzle at al. found that a peak of attenuation for distilled water saturated sandstone with low permeability (a few millidarcies or less) can be at a frequency below the seismic band. This result indicates that for sedimentary rocks with low intrinsic permeability and low fluid mobility, the pore pressure may be out of

equilibrium even at seismic frequencies (the undrained regime). Therefore, measurements conducted only at seismic frequencies are not always sufficient to validate commonly used theoretic models of fluid substitution and theories of elastic moduli dispersion and attenuation.

However, so far no laboratory experiments using confining pressure to prevent the open-pore boundary effect, have been conducted on the water/brine saturated sedimentary rocks in seismic and teleseismic frequency domains together.

This study is an attempt to fill the gap in the experimental study of the elastic and anelastic properties of low-permeability rocks at seismic frequencies. The work is based on a comparison of elastic moduli dispersion and extensional attenuation measured in sandstone samples with very low and very high permeability. Two sandstone samples with permeability of 0.7 mD and 425 mD were quarried in Donnybrook, Western Australia, and one sandstone sample with permeability of 1.1 mD was obtained from the region of Western Australia Harvey. The measurements were carried out with dry and fully water/brine saturated samples at various effective pressures and room temperature (22º C) using a new SF apparatus, based on stress-strain relationship. The apparatus can operate at strain amplitudes 10^{-8}–10^{-6} and provides the means for measurements that require independent control of pore, uniaxial or confining pressures.

2.2 Sample description and experimental procedure

The physical characteristics of the sandstones and their mineral composition retrieved from X-ray fluorescence and diffraction analysis, are summarised in Table 2.1. The mineral bulk moduli of the samples were computed using Voigt-Reuss-Hill average on the basis of the bulk moduli of the constituents given in Table 2.2.

Sample	**A Donnybrook**	**B Donnybrook**	**C Harvey**
Porosity, %	20.6	14.8	18.0
Helium permeability, $\times 10^{-15}$ m^2 (mD)	582 (590)	7.7 (7.8)	9.5 (9.6)
Water permeability, $\times 10^{-15}$ m^2 (mD)	~ 420 (425)	0.7 (0.7)	1.1 (1.1)
Density, kg/m^2	2261	2099	2110
Length, mm	70	70	72
Diameter, mm	38	38	38
Quartz, %	88.5	62	73
K-feldspar, %			11
Siderite, %	2.6		
Microcline, %	4.9	15	
Calcite, %			3
Albite, %		6	
Kaolinite, %	4	17	13
Mineral bulk modulus, GPa	36.3	30.9	32.3

Table 2.1 Petrophysical data for the sandstone samples.

Mineral	**Bulk Modulus, GPa**
Quartz	36.6 (Mavko et al., 2009)
K-feldspar	57 (Angel et al., 1988)
Siderite	117 (Zhang et al., 1998)
Microcline	55.4 (Mavko et al., 2009)
Calcite	67 (Zhang and Reeder, 1999)
Albite	56.4 (Tenner et al., 2007)
Kaolinite	11 (Vanorio et al., 2003)

Table 2.2. Bulk moduli of the sandstones minerals.

In case of inhomogeneous rock, the stress in the cross-sections of the rock will not be uniform, thus violating the assumptions of the stress-strain measurements. Thus, we would like to ensure that the samples are as homogeneous as practically

possible. To verify the homogeneity of our rock samples, they were scanned using an X-ray microscope VersaXRM-500 (Xradia Ltd). The cross-section scans obtained in three directions for each sample are presented in Figure 2.1. Based on these X-ray images, we assume that all three sandstone samples tested in this study are homogeneous on a macroscopic (wavelength and sample-size) scale. Note that applicability of our experimental techniques does not require the homogeneity on a microscopic (pore- or grain-size) scale.

The experimental procedure was organized in the following way. For avoiding the influence of moisture on acoustic properties, which can be significant in sandstones (Murphy, 1984), prior to the measurements, each sample was vacuum dried in oven at a temperature of 60^0 C. Then a set of ultrasonic measurements of dry sandstones, which serves the purpose of strain gauge calibration, was carried out at the same confining (differential) pressures that are used later for SF measurements. The ultrasonic compressional and shear velocities were measured using the "time of flight" method with a carrier frequency of ultrasonic pulses equal to 0.5 MHz. After the completion of the ultrasonic measurements, each sample was subjected to seismic frequency tests in the range of frequencies from 0.1 Hz to 100 Hz at a given confining pressure. After the SF measurements of the sample in dry state, the sample was saturated with distilled water and tested again under the differential pressure corresponding to the confining pressure of the dry cycle. Each sample was saturated at a confining pressure of 10 MPa. To ensure the full saturation at least 10 pore volumes of water were pumped through the samples. For sample A we used a back pressure regulator. The flow rate of water during saturation did not exceed 0.02 cm^3/s (1.2 cm^3/min). In sample C, after the completion of the SF tests with distilled water as a pore fluid, water was replaced with brine (45,000 ppm NaCl) and measurements were repeated at the same confining and pore pressures.

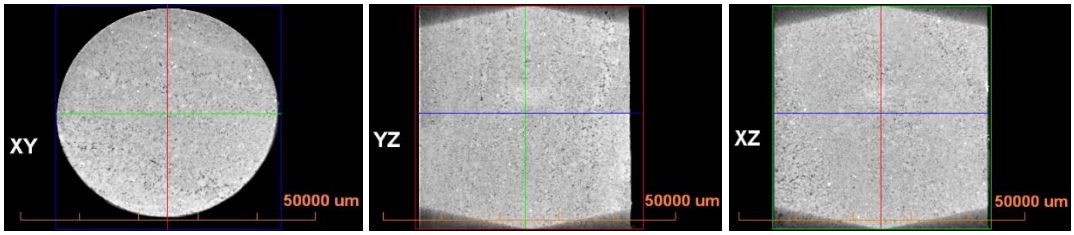

A

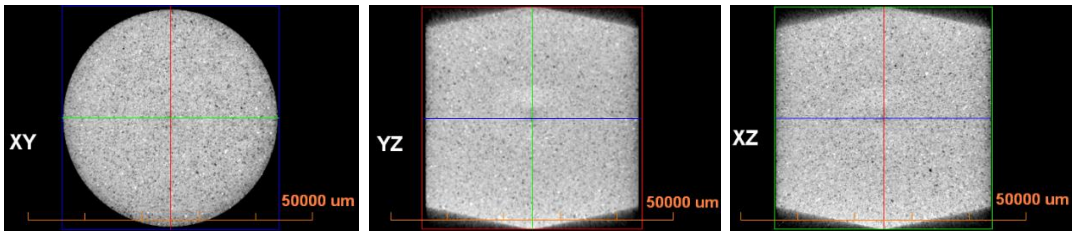

B

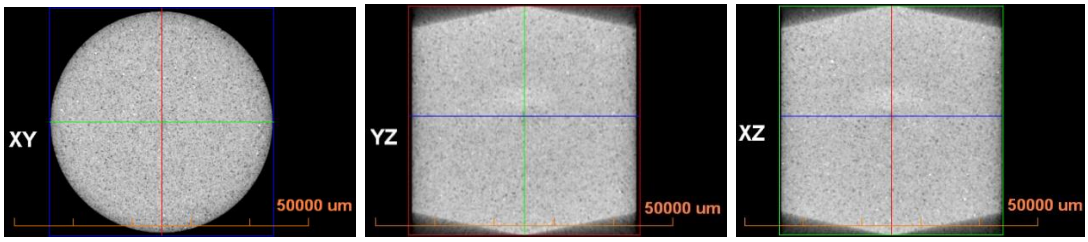

C

Figure 2.1 2D mutually perpendicular X - ray cross-sections of: (A) sample A, (B) sample B, (C) sample C.

2.3 Results

The SF experiments with dry and water saturated sandstone A were conducted at three confining pressures of 2.5 MPa, 7 MPa and 15 MPa and at a pore pressure of ~0.1 MPa. The confining and pore pressures in the measurements of dry sample B were 18 MPa and 0.1 MPa, respectively. In the measurements of sample B in water saturated condition both confining and pore pressures were 2 MPa higher, so the differential pressure was unchanged.

In dry state sample C was tested at confining pressures of 9 MPa and 23 MPa and a pore pressure of ~0.1 MPa. The measurements for water/brine saturated sample C were performed at confining pressures of 15 MPa and 29 MPa and a pore pressure of 6 MPa.

The experimental results obtained for all sandstone samples are presented in Figures 2.2 – 2.12. The error bars for the moduli estimates were computed in accordance with the uncertainty analysis procedure elaborated for LF stress-strain measurements in Adam (2009) and Adam et al. (2009). The number of signal averages in our experiments was 100.

The dependences of the bulk, shear and Young's moduli on frequency of the sinusoidal stress applied to sample A are presented in Figures 2.2 and 2.3. In Figure 2.2 one can see that a change of the sample condition from dry to water saturated increases the bulk modulus of the sandstone in reasonable agreement with the predictions of Gassmann's fluid substitution theory (Gassmann, 1951). A slight increase of the shear modulus of the sandstone after saturation is within the limits of the experimental error. The magnitudes of the extensional attenuation measured in dry and water saturated sample A are virtually identical (Figure 2.4).

The frequency range of the periodic stress used in the tests with samples B and C was 0.1 ÷100 Hz and 0.1÷120 Hz, respectively. The dependences of the bulk, Young's and shear moduli on frequency obtained for both samples are presented in Figures 2.5-2.7 and 2.9-2.11. Significant dispersion of the bulk and Young's moduli was found in both sandstones (Figures 2.5-2.6 and 2.9-2.10). The bulk moduli of the water-saturated samples are consistent with Gassmann prediction computed from the dry moduli at the lower end of the frequency range, but the saturated moduli are getting much larger at higher frequencies (Figures 2.5 and 2.9). The dispersion of shear moduli, as can be seen in Figures 2.7 and 2.11, is within the accuracy of the

measurements. The frequency dependence of the extensional attenuation measured for sample B (Figure 2.8) displays a distinct peak at a frequency of ~0.8 Hz. The frequency shift of the attenuation peak with the increase of the differential pressure from 2.5 MPa to 15 MPa is insignificant. A peak of the extensional attenuation was also detected in sample C at a frequency of ~7 Hz (differential pressure is 23 MPa) and ~20 Hz (differential pressure is 9 MPa) as demonstrated in Figure 2.12. In contrast with the behavior of the extensional attenuation in sample B, the frequency of the attenuation peak observed in sample C shifts significantly with the change of the differential pressure applied to the sample.

The bulk, Young's and shear moduli measured for sample C saturated with brine (45,000 ppm NaCl) are practically identical to the same moduli measured in distilled water saturated state (Figures 2.9-2.11). The change in the extensional attenuation in response to the replacement of the saturant is also within the experimental error (Figure 2.12).

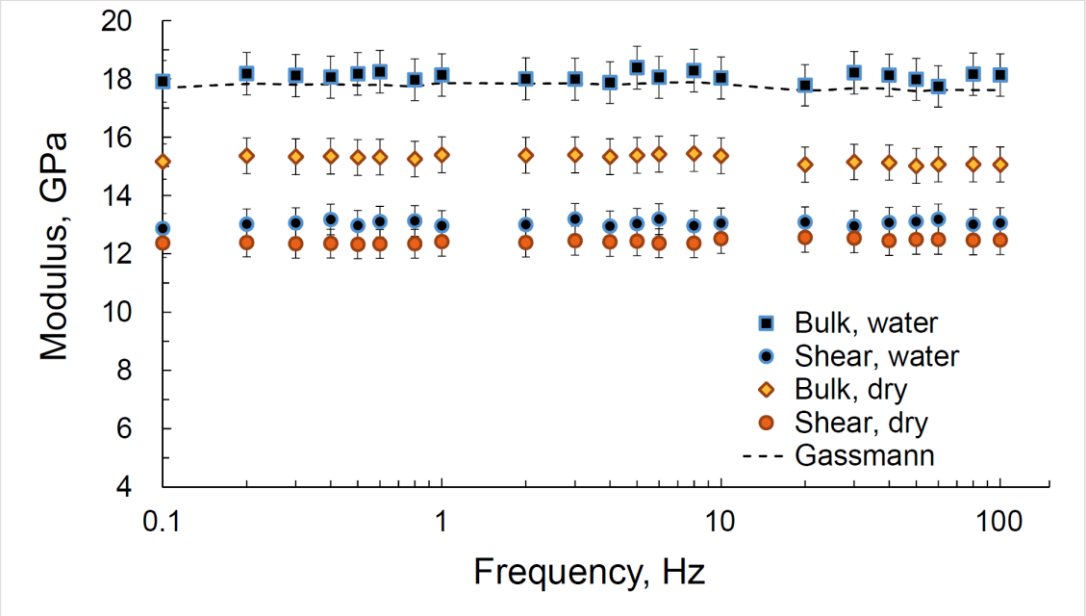

Figure 2.2 The frequency dependence of the bulk and shear moduli measured for dry and distilled water saturated sandstone sample A. The measurements with the dry and water saturated sample are conducted in frequency range from 0.1 Hz to 100 Hz at a differential pressure of 18 MPa; the pore pressure is ~ 0.1 MPa and 2 MPa for dry and distilled water saturated sandstone, correspondingly.

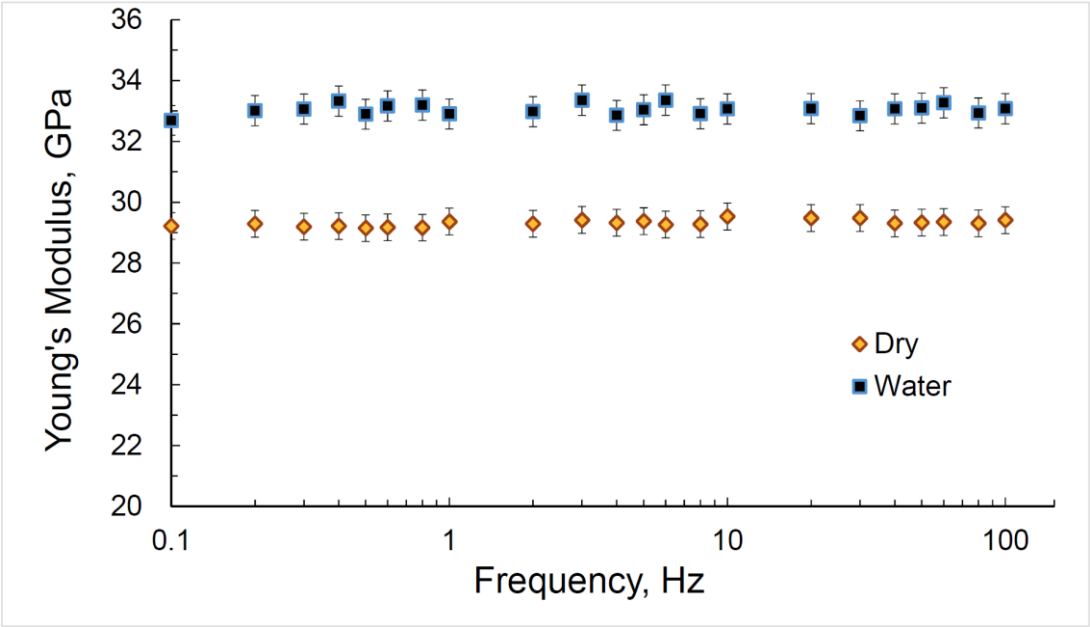

Figure 2.3 The frequency dependence of the Young's modulus measured for dry and distilled water saturated sandstone sample A. The measurement parameters are the same as in Figure 2.2.

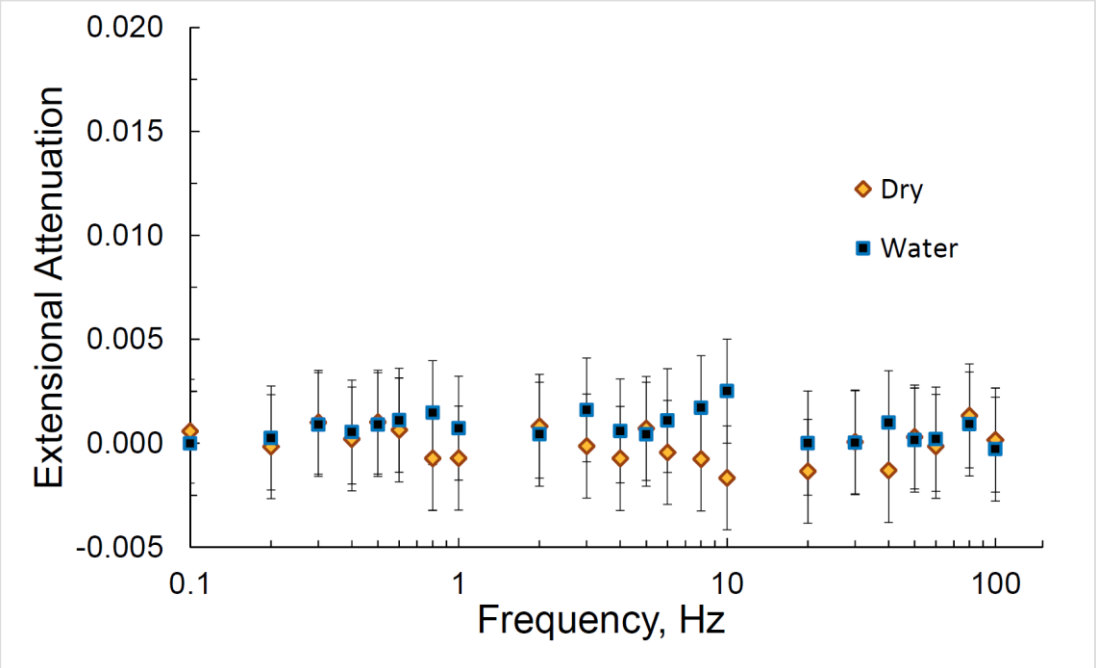

Figure 2.4 The frequency dependencies of the extensional attenuation Q_E^{-1} in sample A. Frequency range, pore and confining pressures are the same as in Figure 2.2.

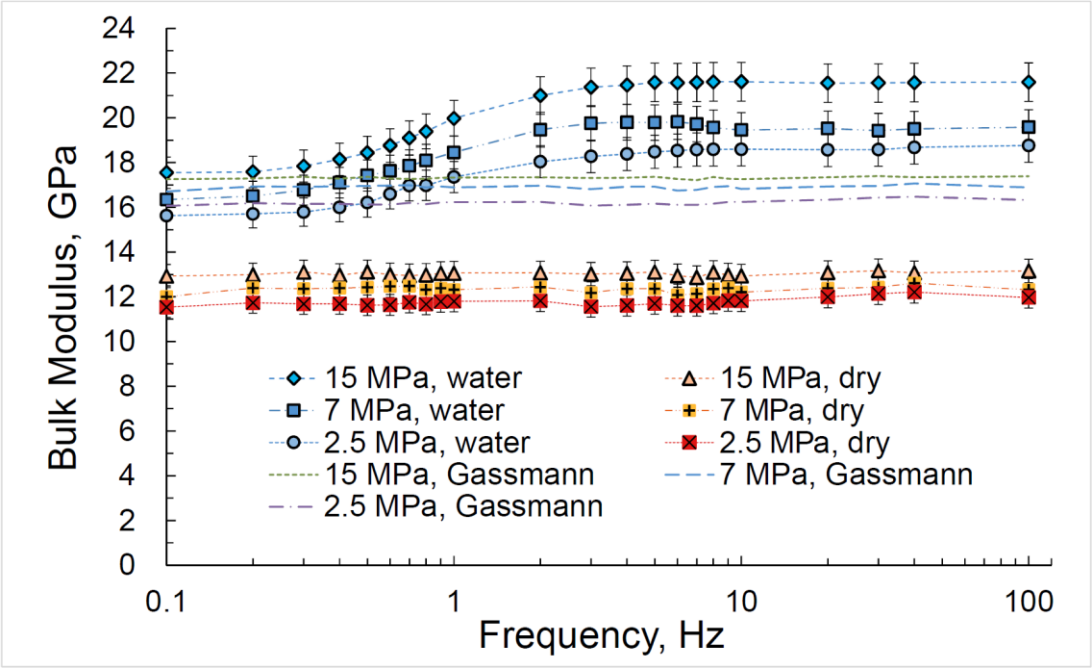

Figure 2.5 The frequency dependences of the bulk moduli measured for dry and distilled water saturated sandstone sample B. The measurements with the dry and distilled water saturated sample are conducted in frequency range from 0.1 Hz to 100 Hz at differential pressures of 2.5, 7 and 15 MPa; the pore pressure is ~ 0.1 MPa.

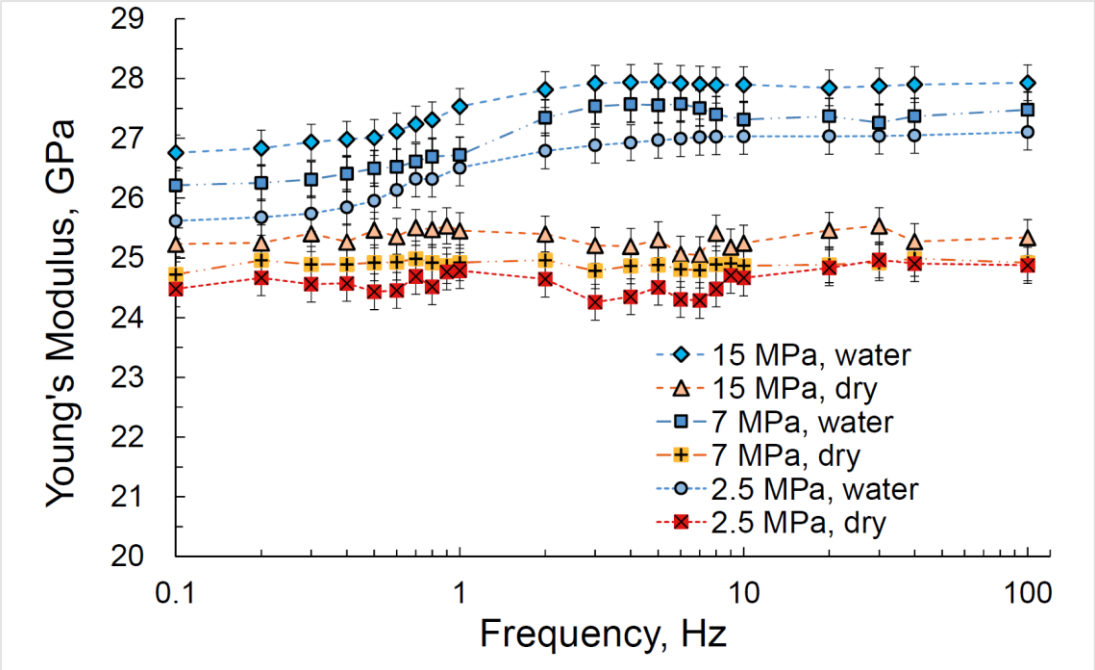

Figure 2.6 The frequency dependences of the Young's moduli measured for dry and distilled water saturated sandstone sample B. The experimental parameters are the same as in Figure 2.5.

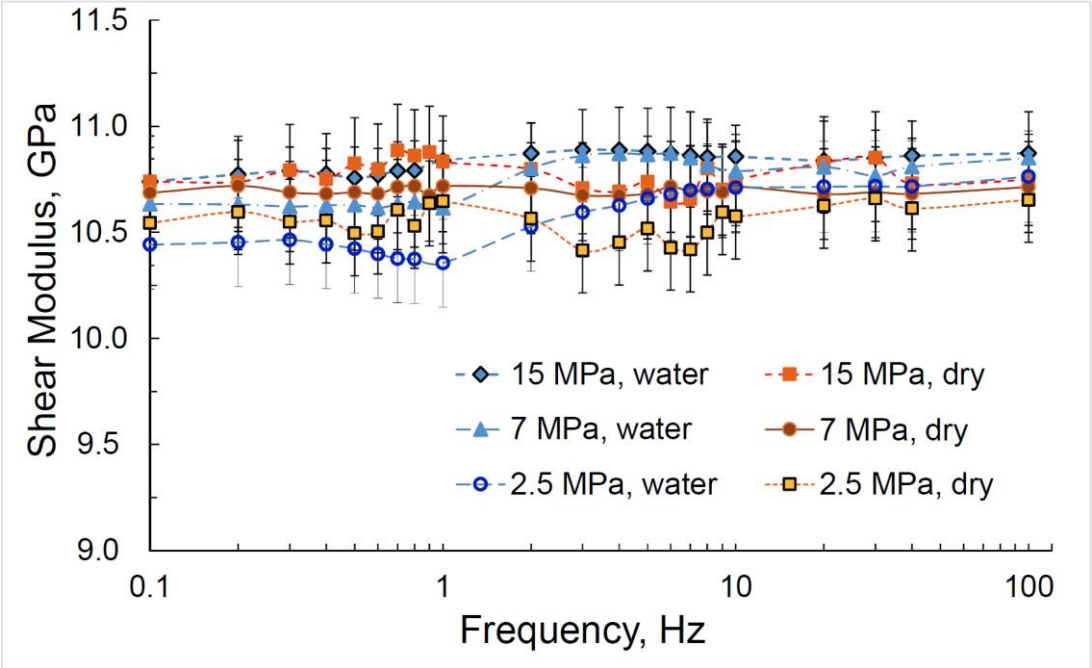

Figure 2.7 The dependences of shear moduli on frequency measured for dry and distilled water saturated sample B. The frequency range, pore and confining pressures are the same as in Figure 2.5.

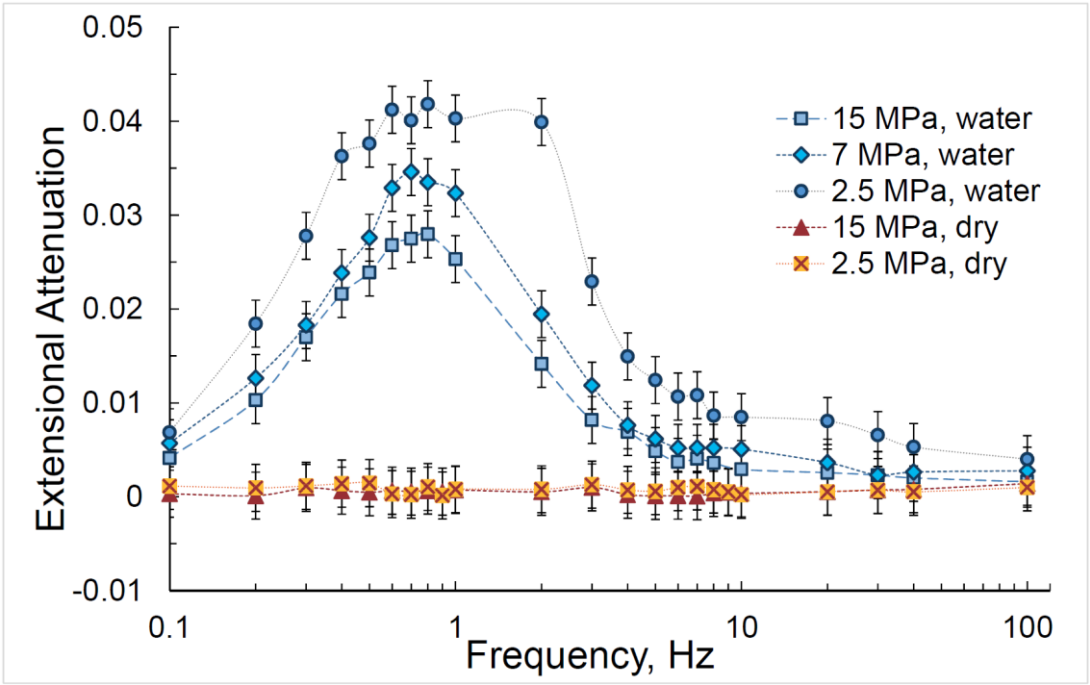

Figure 2.8 The frequency dependencies of the extensional attenuation Q_E^{-1} in sample B measured at two confining pressures of 2.5 and 15 MPa in dry state and at three confining pressures of 2.5,7 and 15 MPa in water saturated state. The measurement parameters are the same as in Figure 2.5.

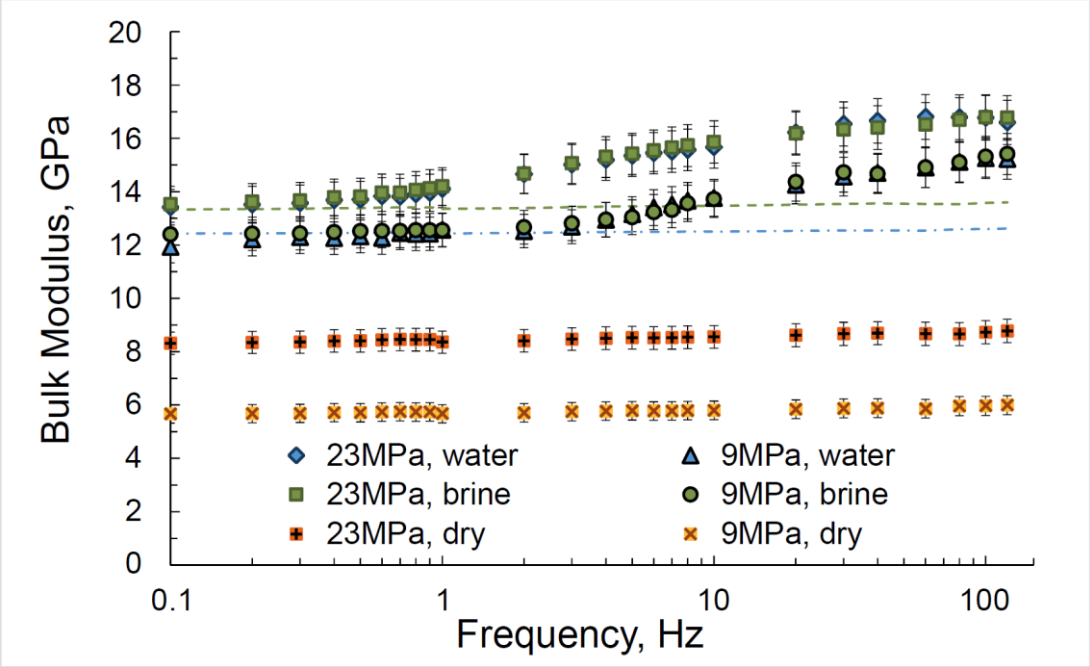

Figure 2.9 The frequency dependence of the bulk modulus measured for dry and distilled water saturated sandstone sample C. The measurements with the dry and distilled water saturated sample are conducted in frequency range from 0.1 Hz to 120 Hz at differential pressures of 9 MPa and 23 MPa; the pore pressure is ~ 0.1 MPa and 6 MPa for dry and distilled water saturated sandstone correspondingly.

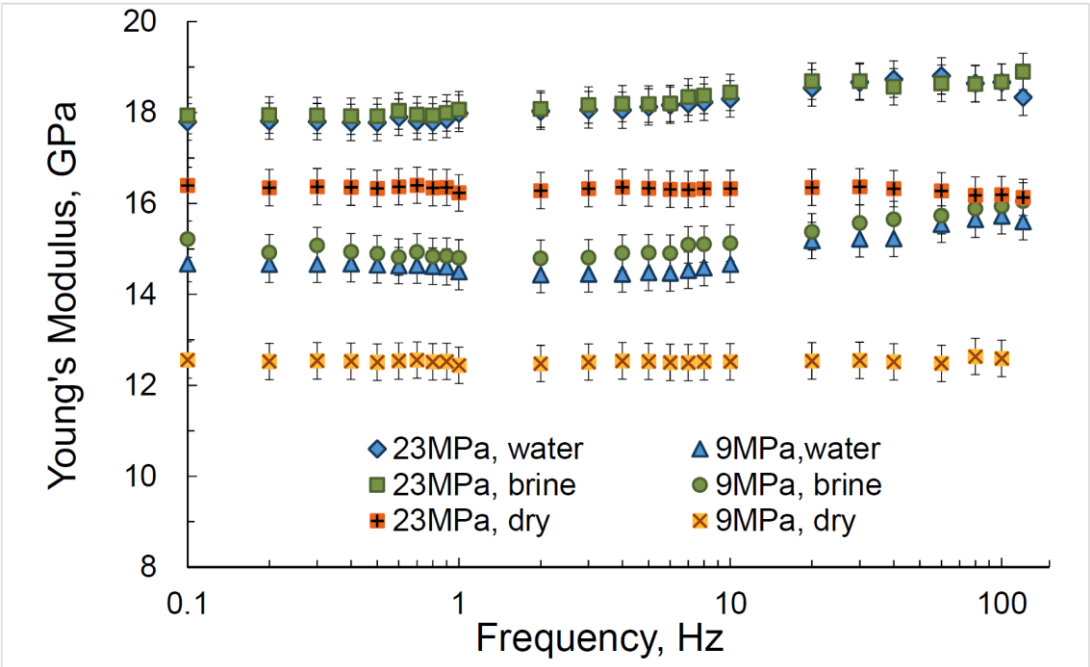

Figure 2.10 The Young's moduli measured for dry and distilled water saturated sample C. The experimental parameters are the same as in Figure 2.9.

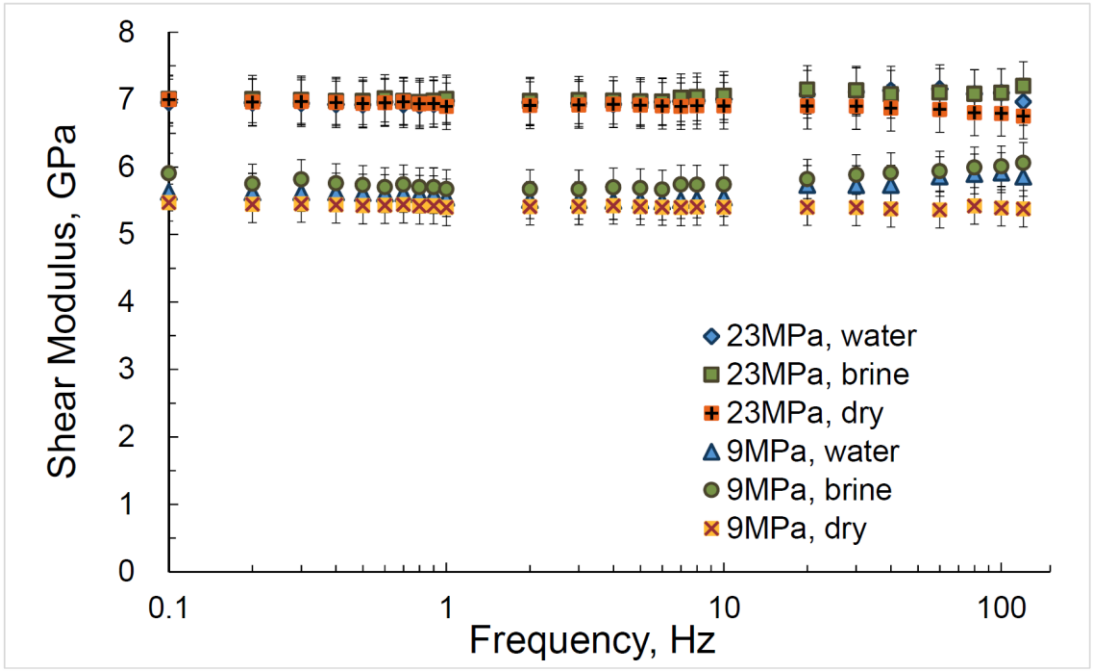

Figure 2.11. The shear moduli measured for dry and distilled water saturated sample C. The experimental parameters are the same as in Figure 2.9.

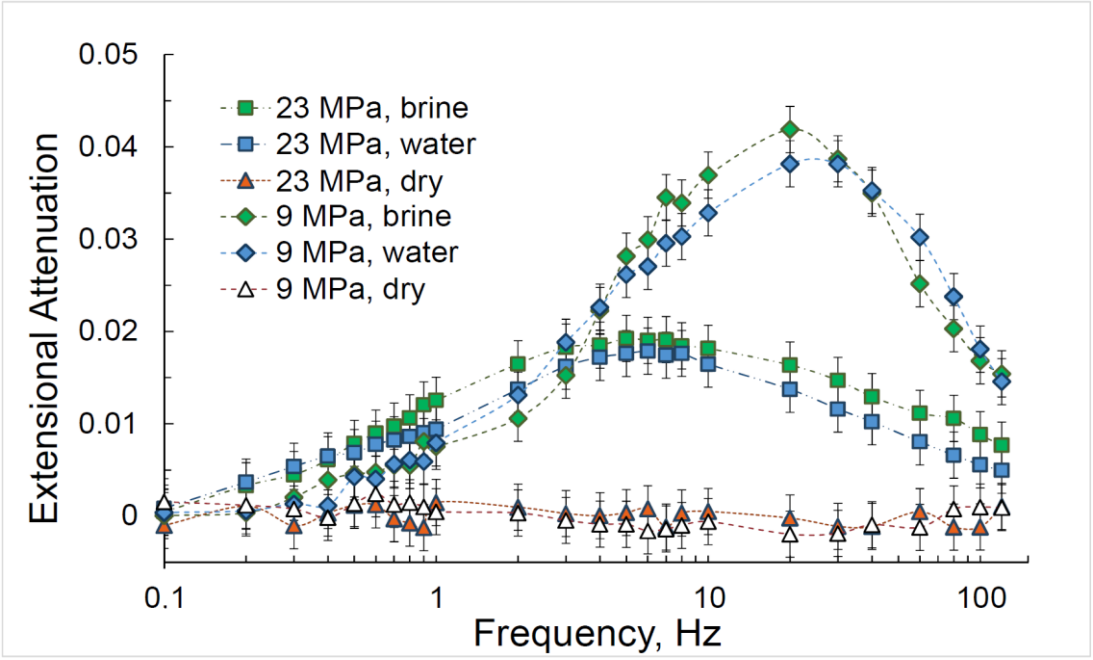

Figure 2.12 Frequency dependencies of the extensional attenuation Q_E^{-1} in sample C measured in dry and water/brine saturated conditions at two differential pressures of 9 MPa and 23 MPa.

2.4 Analysis of the results

Let us now consider some physical mechanisms which can be responsible for the dispersion and attenuation observed in our experiments in more detail.

Two possible artificial sources of apparent attenuation and modulus dispersion in SF experiments are the open-boundary effect (Dunn, 1986; White, 1986) and the effect of the fluid movement in the pore-fluid lines next to the sample (Batzle et al., 2006). In each of these effects the liquid saturating the sample is not completely sealed in the pore space and can move in and out of the pores when variable stress is applied to the sample. These effects, in principle, may produce dispersion/attenuation peaks that look similar to those observed in our experiments. The crossover frequency of such peaks can be estimated using the following expression (Dutta and Seriff, 1979)

$$f_c = \frac{1}{\pi}\frac{kK_f}{\phi\eta h^2}, \tag{2.1}$$

where η is the fluid viscosity, ϕ is the porosity of the rock, K_f is the bulk modulus of the saturant, and k is the fluid permeability, h is the (characteristic) size of the rock sample. For samples A, B and C saturated with distilled water (K_f = 2.2 GPa, η = $8.9\cdot10^{-4}$ Pa·s) the corresponding characteristic frequencies are

$$f_{cA}\approx 300 \text{ Hz}, \quad f_{cB}\approx 0.8 \text{ Hz}, \quad f_{cC}\approx 0.6 \text{ Hz}.$$

If the measurement frequencies are much lower than the crossover frequency f_c, there is enough time for the fluid pressure to equilibrate between the pore space and the external reservoir, and we get a drained regime, where the measured moduli are close to those of the dry sample. This drained bulk modulus has to be significantly lower than the bulk modulus predicted by the Gassmann theory. A good agreement between the bulk moduli calculated according to the Gassmann equation and the saturated bulk moduli measured at the lower portion of our frequency range (Figures 2.5 and 2.9) indicates that neither of these effects is observed in the tests.

Thus we conclude that the attenuation and dispersion are likely caused by physical body wave attenuation in the medium. Furthermore, since dispersion in the dry samples is negligible, the most likely cause of the measured dispersion and attenuation in samples B and C is wave induced fluid flow (Pride et al., 2003; Müller

et al., 2010). This wave induced flow is caused by equilibration of wave induced pressure gradients, which may occur on several scales. Biot's global is related to pressure relaxation between peaks and troughs of the wave. Mesoscopic flow is caused by pressure gradients between rock segments with different compliance. Local or squirt flow results from relaxation of local (pore-scale) pressure gradients between adjacent pores and cracks of different shapes and orientations.

One possible source of attenuation and dispersion is the global flow caused by pressure gradients in a rock (Biot, 1956a, 1956b; White, 1983; Bourbié et al., 1987; Pride, 2005). The global flow mechanism is the largest in the vicinity of the Biot characteristic frequency (Biot, 1956a, b)

$$f_B = \frac{\eta\phi}{2\pi\rho_f k}, \tag{2.2}$$

where ρ_f is fluid density; k, η and ϕ are water permeability, water viscosity and sample porosity, correspondingly.

For both samples B and C the Biot characteristic frequency is about 30 MHz. Hence, the Biot's global flow attenuation cannot be observed in our experiments.

The attenuation and dispersion in our experiments can also stem from spatial variations of mesoscopic heterogeneities in the rock (White, 1975; White et al., 1975; Murphy, 1982; Norris, 1993; Gurevich and Lopatnikov, 1995; Gelinsky et al., 1998; Cadoret et al., 1998). Let us analyse a hypothetical numerical example to estimate the possible attenuation in sample B caused by mesoscopic heterogeneities. In our analysis we assign all macroscopic parameters of sample B to a hypothetical heterogeneous rock composed of randomly distributed macroscopic regions of two elastic porous materials. The maximum attenuation and dispersion in this rock correspond to the highest contrast of the elastic moduli of those materials. Because the moduli of clay are lower than the moduli of other minerals presented in sample B, to achieve the desired contrast we choose clay (kaolinite) as one of two materials forming the hypothetical rock. The second material is the sandstone which has the same mineralogy as sample B with the exception of clay. To ensure that overall sample has the measured moduli, the absence of clay in the sandstone portions of the sample has to be compensated by a proportional increase of all other mineral constituents. We also presume that both materials are saturated with distilled water and their porosities are the same as the porosity of sample B ϕ = 0.15.

It was demonstrated by Müller and Gurevich (2005) that dispersion and attenuation curves in one- and three-dimensional randomly inhomogeneous media are quite similar, so, to simplify our analysis, we choose a one-dimensional approach developed by Gurevich and Lopatnikov (1995). In this approach the regions of clay and clay-free sandstone randomly distributed in the rock are randomly distributed layers of the two substances.

The parameters of the first material (kaolinite) are: fraction of kaolinite in the rock Φ_1=0.17, mineral bulk modulus K_1^m = 11 GPa, dry bulk modulus K_1^{dry} = 7.85 GPa, dry shear modulus μ_1^{dry} = 4.5 GPa. The dry moduli were found in accordance with the empirical equations proposed by Vanorio et al. (2003):

$$\mu_1^{dry} = 6 - 10\phi \text{ (GPa)}, \tag{2.3}$$

$$K_1^{dry} = 11 - 21\phi \text{ (GPa)}. \tag{2.4}$$

Considering the shear modulus as independent of saturation, we get $\mu_1^{sat} = \mu_1^{dry}$. Using the Gassmann equation one can obtain the bulk modulus of water saturated kaolinite

$$K_1^{sat} = 9.3 \text{ GPa}. \tag{2.5}$$

The mineral bulk modulus of the second material (clay-free sandstone) can be computed as the Voigt-Reuss-Hill average using the mineral bulk moduli presented in Table 2.2 and equals

$$K_2^m = 39 \text{ GPa}. \tag{2.6}$$

Using Backus' formulas

$$\frac{1}{K^{sat} + \frac{4}{3}\mu^{sat}} = \frac{\Phi_1}{K_1^{sat} + \frac{4}{3}\mu_1^{sat}} + \frac{1-\Phi_1}{K_2^{sat} + \frac{4}{3}\mu_2^{sat}} \tag{2.7}$$

and

$$\frac{1}{\mu^{sat}} = \frac{\Phi_1}{\mu_1^{sat}} + \frac{1-\Phi_1}{\mu_2^{sat}}, \tag{2.8}$$

where K^{sat} = 15.6 GPa and μ^{sat} = 10.4 GPa are bulk and shear moduli of saturated sample B at a differential pressure of 2.5 MPa, we find the moduli of the second material

$$K_2^{sat} = 18.6 \text{ GPa}, \ \mu_2^{sat} = 13.34 \text{ GPa}. \tag{2.9}$$

The maximum of P-wave attenuation in randomly layered saturated porous media can be found as follows (Gurevich and Lopatnikov, 1995)

$$Q_{P\max}^{-1} = \frac{1}{\sqrt{2}} \frac{\left(C_1 H_1^{-1} - C_2 H_2^{-1}\right)^2}{(H_1^{-1} - H_2^{-1})(N_1 + N_2)}, \tag{2.10}$$

where

$$H_i = K_i^{sat} + \frac{4}{3}\mu_i^{sat} + \sigma_i C_i, \tag{2.11}$$

$$C_i = \sigma_i M_i, \tag{2.12}$$

$$M_i = \left(\frac{1 - \sigma_i - \phi}{K_i^m} + \frac{\phi}{K_F} \right)^{-1}, \tag{2.13}$$

$$N_i = \frac{M_i}{H_i}(K_i^{sat} + \frac{4}{3}\mu_i^{sat}), \tag{2.14}$$

$$\sigma_i = 1 - K_i^{sat} / K_i^m, \tag{2.15}$$

K_F =2.2 GPa is the bulk modulus of water, i =1, 2.

Substituting the moduli K_i^m, K_i^{sat} and μ_i^{sat} into equations 2.11 – 2.15, and then parameters C_i, H_i and N_i into equation 2.10, we get

$Q_{P\max}^{-1} \approx 2 \cdot 10^{-4}$.

The same calculations performed with the hypothetical rock modelled for sample C give the following maximum of P-wave attenuation:

$Q_{P\max}^{-1} \approx 1.6 \cdot 10^{-4}$.

Since attenuation parameters Q_P^{-1} and Q_E^{-1} have the same order of magnitude, one can conclude that a contribution of the mesoscopic heterogeneities to the attenuation and dispersion effects observed in our SF measurements, is negligible compared to the values obtained in our measurements.

One remaining possibility is that the observed dispersion and attenuation in samples B and C are caused by the local (squirt) flow between compliant grain contacts and stiff inter-granular pores (Mavko and Nur, 1975, 1979; O'Connell and Budiansky, 1977; Palmer and Traviolia, 1980; Dvorkin et al., 1995; Pride et al., 2004; Gurevich et al., 2010). Qualitatively, such a hypothesis looks plausible. In particular, attenuation is the largest at low confining pressure and decreases with increasing pressure. This is consistent with the fact that increase of confining

pressure tends to close compliant grain contacts. One unusual observation is that the attenuation/dispersion peaks are observed at very low frequencies. Usually, squirt flow is assumed to be most prominent at much higher frequencies. However De Paula et al. 2012 predicted that significant squirt flow attenuation can also occur at seismic frequencies. Another feature that requires explanation is the variation of peak frequency with pressure for sample C. Characteristic frequencies of squirt-flow attenuation are controlled by the aspect ratio of compliant pores (Jones, 1986; Murphy et al., 1986; Gurevich et al., 2010). Distribution of aspect ratios also controls the pressure variation of dry elastic moduli of the rock. Thus characteristic frequencies of the squirt dispersion and attenuation can be independently inferred from hydrostatic pressure tests on dry samples (De Paula et al., 2012). Such quantitative analysis is beyond the scope of this study but will be a subject of a further research.

2.5 Conclusions

In our experiments we have studied three sandstone samples, one of which has high water permeability (~425 mD) and low clay content (~4%), but two others have low water permeability (~ 0.7 mD and 1.1 mD) and relatively high clay content (17% and 13%). All samples are not very different in porosity (20.6% for the high-permeability rock, 14.8% and 18% for the low-permeability rocks).

We found that for the high-permeability sandstone (sample A) the relations between the elastic moduli of the fully water saturated rock and those of the dry rock are in good agreement with the Gassmann predictions. The measurements in the frequency range from 0.1 Hz to 100 Hz demonstrate that the dispersion and attenuation in the dry and water saturated sample A are negligible.

The SF measurements of water/brine saturated low-permeability sandstones (samples B and C) revealed dispersion of the bulk and Young's moduli and significant extensional attenuation. Prominent peaks of extensional attenuation were found at frequency of 0.8 Hz in sample B and at frequencies ~20 Hz and 7 Hz under a differential pressure of 9 MPa and 23 MPa, correspondingly, in sample C. The dispersion of the bulk and Young's moduli of both samples taking place at seismic frequencies was also detected. The magnitudes of dispersion of the dry moduli were within the accuracy of the measurements.

Our analysis shows that the attenuation and dispersion exhibited in two low-permeability sandstones B and C cannot result from the global flow mechanism. It was also found out that a contribution of the mesoscopic heterogeneities to the attenuation and dispersion is beyond the instrument's sensitivity.

We can conclude that the dispersion and attenuation detected in our experiments are most likely caused by the squirt flow, but an additional series of ultrasonic experiments with dry and wet sandstones are required to confirm the nature of the observed effect.

Chapter 3

Validation of the laboratory measurements at seismic frequencies using the Kramers-Kronig relationship

3.1 Introduction

The progress of the modern methods of geophysical exploration is tightly linked to the development of the new effective indicators distinguishing the types of reservoir rocks and fluids. The attenuation and moduli dispersion of a reservoir rock, being direct signs of anelasticity, are an important source of information about the key characteristics of the subsurface interior such as rock composition, permeability, pore fluid properties and saturation. The numerous theoretical and laboratory studies, which examined the opportunity of using the attenuation and dispersion attributes as indicators of reservoir properties, led to the development of the laboratory techniques and instruments enabling to measure simultaneously elastic moduli and attenuation in the seismic-frequency (SF) range (see, e.g., Jackson and Paterson (1987), Spencer (1981), Batzle et al. (2006), and Adelinet et al. (2010), Tisato and Madonna, (2012)).

One of the central problems that emerge when using the SF devices are the acoustic resonances occurring in the mechanical parts of the devices, which overlap and distort the signals obtained from the sample (Adam et al., 2009). The solution of this problem requires a diagnostic instrument to validate the quality of experimental data, which would be able to corroborate the physical nature of the detected signals, in other words, monitor the artefacts caused by uncontrolled experimental conditions. Considering that the measurements of attenuation and elastic moduli are independent

and take place in the same frequency range, it appears natural to use the consistency of the experimental data with the casualty principle as a quality control measure.

Mathematically, the causality principle is often expressed through Kramers-Kronig equations which link real and imaginary parts of a complex function that controls wave propagation in medium, such as a complex wavenumber or a complex elastic modulus. For acoustic waves, a convenient approximate form of Kramers-Kronig relations (KKR) was found by O'Donnel et al. (1978), who derived an expression linking a phase velocity with attenuation at a specific frequency which was successfully used for validating the results of the ultrasonic experiments conducted on haemoglobin solutions. Later, O'Donnel et al. (1981) presented a model of attenuation for the class of loss mechanisms associated with relaxational phenomena, which was applied to validate the ultrasonic data obtained for materials exhibiting relaxation such as polyethylene and $CoSO_4$-water solution. A relaxation model with a Cole-Cole distribution of relaxation times was used by Spencer (1981) for verification of the attenuation and Young's modulus dispersion measurements carried out on liquid-saturated sandstone, limestone and granite at seismic frequencies. Dvorkin and Mavko (2006) developed a model of the attenuation estimation based on the standard linear solid approximation that links the attenuation to the corresponding elastic modulus.

It should be noted, that the attenuation models elaborated in O'Donnel et al. (1981), Spencer (1981) and Dvorkin and Mavko (2006) are based on assumptions of the physical properties of materials which go beyond the casualty principle and have a restricted area of application.

The aim of this Chapter is to illustrate the applicability of KKR for validating the data obtained in SF experiments. It is shown that for the sub-resonance type of SF measurements, the relation between the measured Young's modulus and extensional attenuation can be verified using an approximation of KKR, whereby the reliability of SF tests might be significantly enhanced. It is important to emphasize that no assumption about the physical characteristics of materials is necessary for this validation.

3.2 Kramers-Kronig relation for the Young's modulus

Let us consider an isotropic viscoelastic material regarded as a dynamic system for which the stress-strain relationship is linear and whose mechanical property is characterised by the complex Young's modulus

$$E^*(\omega) = \frac{\sigma}{\varepsilon} = \left|E^*(\omega)\right| \exp(i\varphi(\omega)) = E_m(\cos\varphi + i\sin\varphi) = E'(\omega) + iE''(\omega), \quad (3.1)$$

where $E_m = \left|E^*(\omega)\right|$ is the absolute magnitude of the Young's modulus E^*, the real E' and imaginary E'' parts of E^* are the storage and loss moduli, correspondingly, $\varphi(\omega)$ is the phase angle between the force applied to the sample and its displacement (loss angle), $\omega = 2\pi f$, f is the frequency of the periodical stress σ. Christensen (1982) showed that if the imaginary part E'' is slowly changing with respect to ω, the nearly-local approximation of the integral Kramers-Kronig equations takes the form:

$$E''(\omega) = \frac{\pi}{2}\omega\frac{dE'(\omega)}{d\omega}. \quad (3.2)$$

Taking into account that the extensional attenuation defined as the inversed quality factor Q_E^{-1} and the phase angle $\varphi(\omega)$ are connected by the relation

$$Q_E^{-1} = \frac{E''}{E'} = \tan(\varphi), \quad (3.3)$$

and dividing both parts of equation 3.2 by $E'(\omega)$, we find the relationship connecting attenuation Q_E^{-1} and storage modulus $E'(\omega)$:

$$Q_E^{-1} = \frac{\pi}{2}\frac{\omega}{E'(\omega)}\frac{dE'(\omega)}{d\omega}, \quad (3.4)$$

which yields the expression for E' at a frequency f

$$E'(f) = E'_0 \exp\left[\frac{2}{\pi}\int_{f_0}^{f}\frac{Q_E^{-1}}{f'}df'\right]. \quad (3.5)$$

Taking into account that modulus dispersion and attenuation are usually considered on a logarithmic frequency scale, equation 3.5 can be transformed to

$$E'(f) = E'_0 \exp\left[\frac{2}{\pi \lg(e)} \int_{\lg(f_0)}^{\lg(f)} Q_E^{-1} d\lg(f')\right] \approx E'_0 \exp\left[1.466 \int_{\lg(f_0)}^{\lg(f)} Q_E^{-1} d\lg(f')\right], \quad (3.6)$$

where e is Euler's number, lg is the decimal logarithm, E'_0 is the storage modulus measured at some reference frequency f_0.

If the magnitude of attenuation is small $Q_E^{-1} \ll 1$, equations 3.3 and 3.6 can be simplified to

$$Q_E^{-1} \approx \varphi, \quad (3.7)$$

and

$$E'(f) = E'_0 + 1.466 E'_0 \int_{\lg(f_0)}^{\lg(f)} \varphi d\lg(f'). \quad (3.8)$$

Equations 3.5, 3.6 and 3.8 connect the attenuation and storage modulus and can be used for verification of the SF experimental data. Equations 3.7 and 3.8 are strikingly simple and allow visual check of causality by comparing the behaviour of the storage modulus and phase angle. However for calculations it is more accurate to use the full expressions 3.5 or, equivalently, 3.6.

It should be pointed out that the relationships identical with equation 3.2 were also derived for imaginary and real parts of two other commonly used characteristics of viscoelastic materials: complex compressibility (O'Donnel et al., 1978, 1981) and complex shear modulus (Booij and Thoone, 1982).

3.3 Experimental setup

In this study two versions of the SF apparatus, with and without confining pressure (Figures 1.1 and 1.15), were used. For the measurements on the polymethyl-methacrylate (PMMA) sample, we used the simplified uniaxial configuration presented in Figure 1.15, when for the tests carried out on the sandstone samples, we used the configuration comprising the Hoek triaxial cell as it is shown in Figure 1.1. The detailed description of the apparatus and its operation are presented in Chapter 1.

3.4 Samples and experimental procedure

We apply equation 3.8 to the experimental data obtained at seismic frequencies for four specimens: a cylindrical viscoelastic PMMA sample, two low-permeability sandstone samples retrieved from the regions of Donnybrook and Harvey, Western Australia, and one Berea sandstone sample. The parameters of the PMMA sample, which for convenience is designated here as sample A, are given in Section 1.4.3 of Chapter 1. The petrophysical parameters of the two low-permeability sandstone samples, which were considered in Section 2.2 of Chapter 2 and designated as samples B (Donnybrook) and C (Harvey), are presented in Table 2.1. The petrophysical properties of the Berea sandstone sample, which we denote as sample D (Berea), are shown in Table 3.1.

Table 3.1. Petrophysical data for the Berea sandstone sample.

Sample	D (Berea)
Porosity, %	19.0
Glycerol permeability, $\times 10^{-15}$ m^2 (mD)	71 (72)
Density, kg/m^2	2080
Length, mm	70
Diameter, mm	38
Quartz, %	80
Feldspar, %	12
Kaolinite, %	8
Mineral bulk modulus, GPa	32.0

The Young modulus E is determined as follows. The periodic stress σ_{zz} provided by the multilayer piezoelectric actuator can be expressed as

$$\sigma_{zz} = E_{st}\varepsilon_{zz}^{st} = E\varepsilon_{zz}, \tag{3.9}$$

where ε_{zz}^{st} and ε_{zz} are the amplitudes of the longitudinal strains measured in the standard and specimen, correspondingly, E_{st} is the Young's modulus of the standard. Therefore, the Young's modulus E is

$$E = E_{st}\varepsilon_{zz}^{st} / \varepsilon_{zz}. \tag{3.10}$$

In our measurements the attenuation Q_E^{-1} is found as a phase angle φ between the force applied to the sample and its displacement (O'Connell and Budiansky, 1977).

The experimental procedure applied to samples A is described in detail in Section 1.4.3 of Chapter 1, and the procedure used for samples B and C is given in Section 2.2 of Chapter 2. Below for sample A, we use the data obtained from the strain gauges located at the center of the sample, and for sample C only the data corresponding to water saturation.

The experiments carried out on sample D were organized as follows. Dry sample D was first tested at a confining pressure of 10 MPa and an ambient pore pressure under a temperature of 23 °C. Then, the measurements on glycerol-saturated sample D were carried out at a confining pressure of 13 MPa and a pore pressure of 3 MPa under temperatures of 23, 31 and 37.5 ºC.

The frequency range of the periodic stress used in the tests was 0.1-100 Hz for samples A and B, 0.1-120 Hz for sample C, and 0.01-100 Hz for sample D. The number of signal averages was 100.

3.5 Experimental results

The experimental results obtained for all samples are presented in Figures 3.1 –3.4. The error bars for the moduli estimates were computed in accordance with the uncertainty analysis procedure developed for SF measurements in Adam et al. (2009). The dependences of the extensional attenuation and Young's modulus on frequency of the sinusoidal stress applied to sample A obtained for two static axial pressures are presented in Figure 3.1. In Figures 3.2 and 3.3 one can see the results of the attenuation and Young's modulus measurements carried out on sandstones B and C under dry and water-saturated conditions, respectively. The results of the measurements on dry and glycerol-saturated sample D are shown in Figure 3.4.

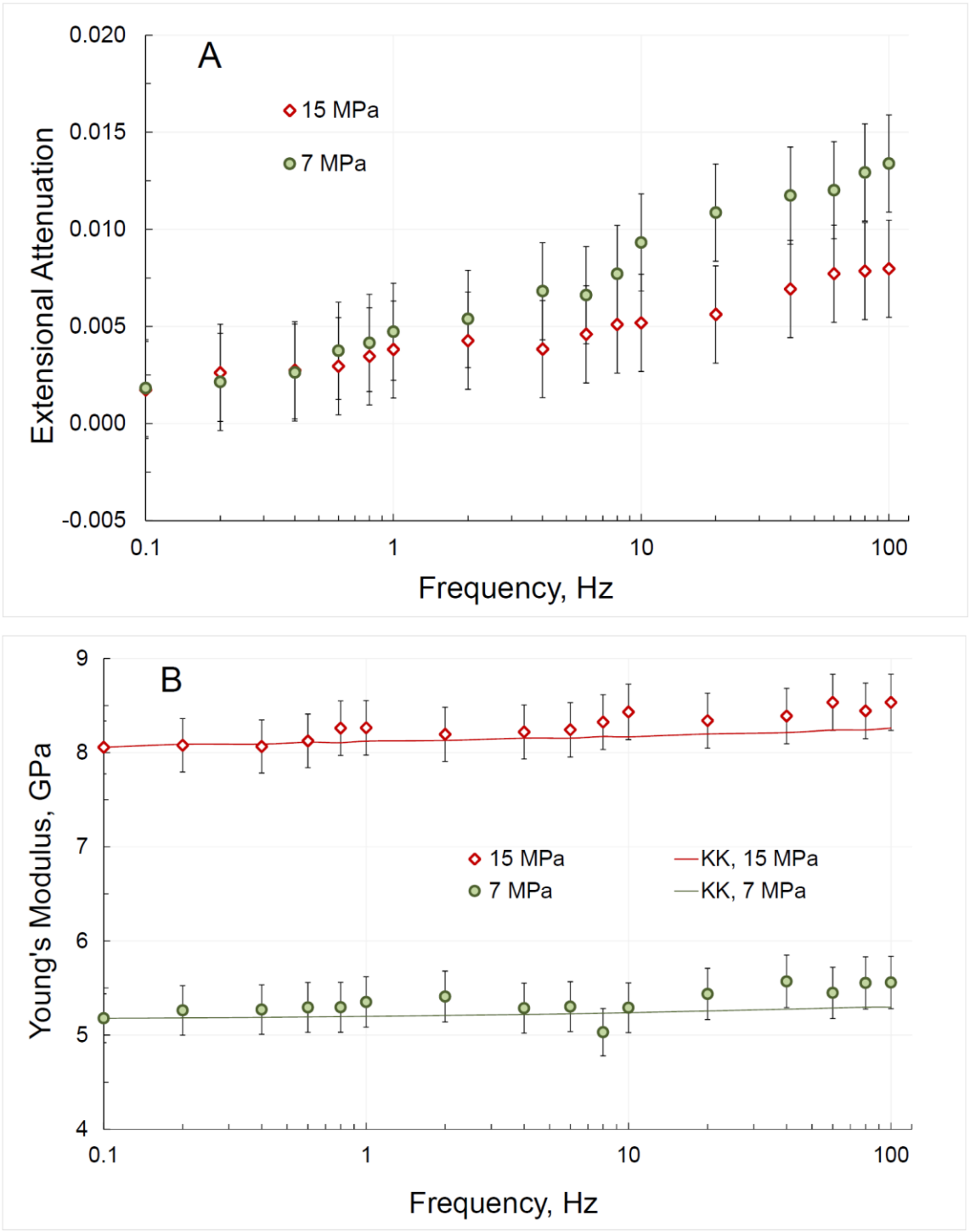

Figure 3.1 The attenuation Q_E^{-1} (A) and Young's modulus (B) measured and computed using KKR for sample A at two axial pressures of 15 and 7 MPa.

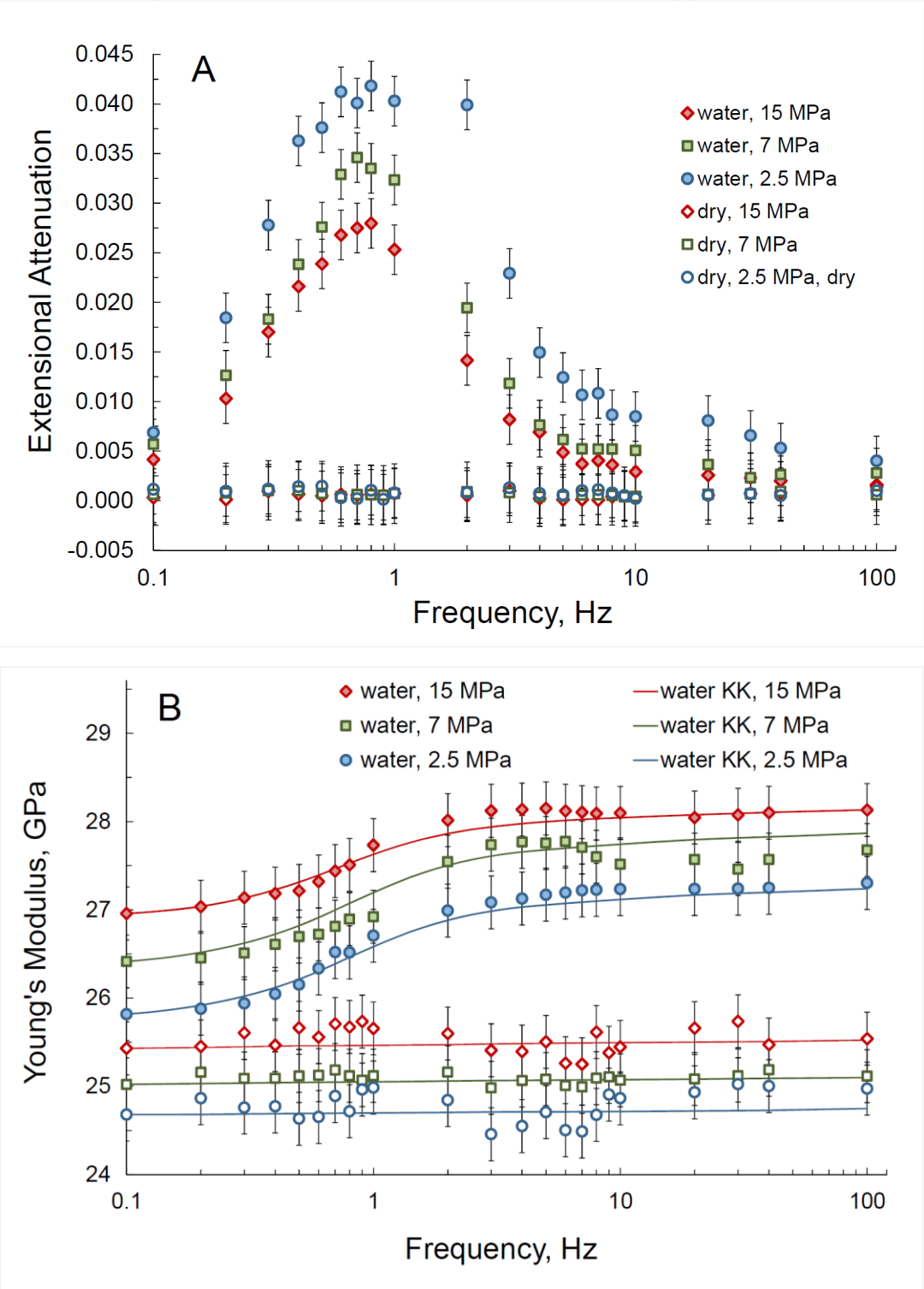

Figure 3.2 The attenuation Q_E^{-1} (A) and Young's moduli (B) measured and computed using KKR for sample B. The confining pressures are 2.5 and 15 MPa in dry state and 2.5, 7 and 15 MPa in water-saturated state. The pore pressure is ambient for both dry and saturated states.

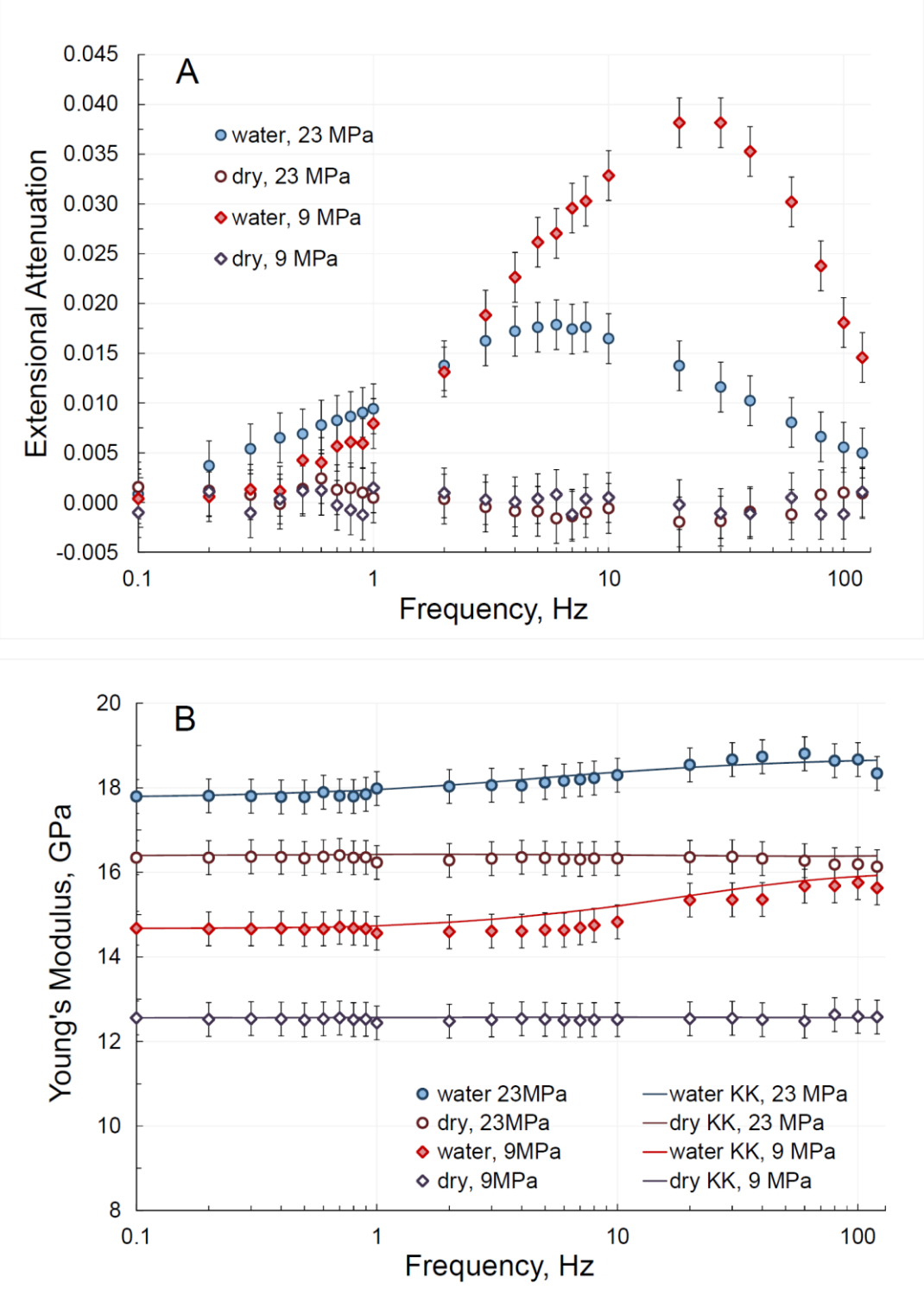

Figure 3.3 The frequency dependencies of (A) the attenuation Q_E^{-1} and (B) Young's moduli measured and computed using KKR for the sample C in dry and water-saturated conditions at two confining pressures of 9 MPa and 29 MPa; the pore pressure is ambient in dry state and 6 MPa under saturated conditions.

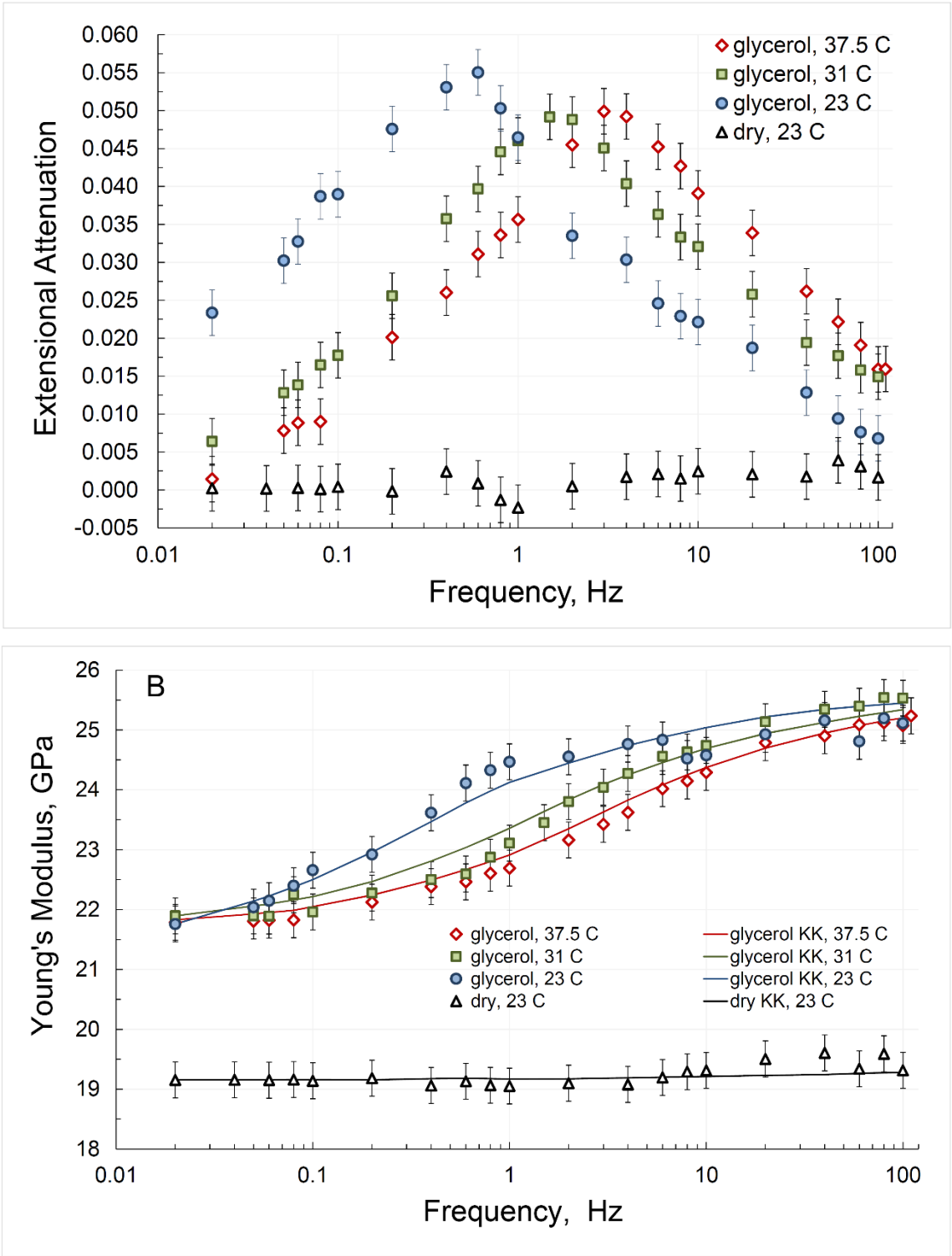

Figure 3.4 The dependencies on frequency for (A) the attenuation Q_E^{-1} and (B) Young's moduli of sample D measured in dry and glycerol-saturated states. The differential pressure is 10 MPa in both dry and saturated states. The Young's moduli computed using KKR are indicated by the dash lines. The measurements on the glycerol-saturated sample were conducted at 23, 31 and 37.5 ℃.

Let us note, that the attenuation and dispersion observed in sample A represent a typical behavior of acrylic plastic in the seismic frequency range (Spencer, 1981, Tisato and Madonna, 2012). The physical nature of the attenuation and modulus dispersion observed in samples B, C and D was discussed previously in Chapter 2.

3.6 Calculation of dispersion from attenuation

The simplest approximation of equation 3.6 suitable for computing the dependence of the storage modulus $E'(f)$ from attenuation data can be presented in the form

$$E'(f_L) = E'_0 \exp\left[0.733 \sum_{i=1}^{L-1} (\varphi_{i+1} + \varphi_i) \lg(f_{i+1} / f_i) \right]. \quad (3.11)$$

Here L is the number of the measurement frequencies f_i corresponding to the number of the measured stress-strain phase angles φ_i.

More accurate approximation can be achieved using cubic splines for data interpolation (see, e.g., Yang et al. (2005)) as

$$E'(f_M) = E'_0 \exp\left[0.733 \sum_{k=1}^{M-1} (\tilde{\varphi}(f_{k+1}) + \tilde{\varphi}(f_k)) \lg(f_{k+1} / f_k) \right], \quad (3.12)$$

where M is the number of the breakpoints chosen for the spline interpolation, $\tilde{\varphi}$ is the cubic spline function used for the interpolation of a given set of the measured phase values φ_i $(i = 1...L)$ at a frequency of f_k $(k = 1...M)$.

Using equation 3.12, we have computed the dependences of the Young's modulus from attenuation data. The results of numerical integration, presented in Figures 3.1B – 3.4B, demonstrate a good match between the dependences of the measured Young's moduli and Young's moduli computed using KKR. Thus, we conclude that the attenuation and dispersion measurements are consistent with the causality principle. This indicates that the dispersion and attenuation have a common physical source.

3.7 Conclusions

In this Chapter, we present a method relating to the application of the Kramers-Kronig relation for verification of the laboratory measurements of the extensional attenuation and Young's modulus carried out on the solid specimens at seismic frequencies. The method was applied to the results of the SF tests conducted on a set of samples comprising a viscoelastic PMMA sample, two sandstone samples excavated in Donnybrook and Harvey, Western Australia, and one Berea sandstone sample. The measurements on the sandstones were performed under dry, water-(Donnybrook and Harvey) and glycerol-saturated (Berea) conditions. It was demonstrated that the quantitative relationship between the extensional attenuation and frequency dependence of the Young's modulus measured for the PMMA sample and all sandstones is consistent with the causality principle expressed by the Kramers-Kronig relationship.

Chapter 4

Measurements of the elastic and anelastic properties of sandstone flooded with supercritical CO_2

4.1 Introduction

Laboratory studies of the CO_2 effects on the elastic and anelastic properties of sedimentary rocks are important for interpreting seismic data obtained during monitoring the processes caused by supercritical CO_2 ($scCO_2$) injected into depleted natural gas reservoirs. The injection of $scCO_2$ into brine/water saturated storage sandstone affects petrophysical, mechanical and acoustic properties of the rock, which require quantitative analysis to ensure CO_2 storage capacity and long-term reservoir behavior. Numerous studies have been conducted to investigate different aspects of the changes in sandstone properties during and after CO_2/$scCO_2$ injection. $ScCO_2$-rock chemical interactions can lead to dissolution and precipitation of minerals with increase of pore space (Le Guen et al. 2007; Zemke et al. 2010; Nover et al. 2013) and also to drying and disintegration of clay minerals (Rochelle et al. 2004; Forster et al. 2006). These processes may result in changes of the petrophysical and fluid transport properties of rocks (Rochelle et al. 2004; Nover et al. 2013). A change of the mechanical properties of sandstones induced by a chemical damage due to rock-fluid interactions was studied by Ross et al. (1982), Le Guen et al. (2007), Oikawa et al. (2008), Hangx et al. (2013). Oikawa et al. (2008) demonstrated that the differences in strength, the Young's modulus and Poisson ratio of CO_2-injected Berea sandstone were only slightly smaller than those for the water-saturated sandstone. This is also in line with the results obtained for quartz-cemented Captain

sandstone by Hangx et al. (2013), who showed that a continuous flushing of the rock with CO_2-saturated brine and a concomitant removal of calcite do not affect rock strength or elastic properties. Some other studies demonstrated that injection of CO_2-saturated brine into the sandstones composed of quartz grains that are cemented by dolomite and calcite, such as Triassic arkosic (Le Guen et al. 2007) or North Sea calcareous (Ross et al. 1982) sandstones, leads to dissolution of the cement, which can result in total collapse of the rock (Ross et al. 1982).

The influence of CO_2 saturation on the acoustic properties of reservoir rocks became a subject of intensive study in recent years. Wang and Nur (1989) measured ultrasonic velocities in seven sandstones saturated with n-hexadecane before and after CO_2 flooding; they found that the effect of CO_2 injection on compressional-wave velocities in hydrocarbon-saturated sandstones is close to that calculated with the Gassmann equation. Xue and Ohsumi (2004) measured ultrasonic P-wave velocities during CO_2 injection into Tako sandstone; they reported that the velocity changes caused by gaseous, liquid, and $scCO_2$ injection can be successfully modelled by the Gassmann equation. Ultrasonic experiments undertaken in Siggins (2006) and Siggins et al. (2010) on synthetic and field sandstones showed that the Gassmann predictions of both P-wave and S-wave velocities under CO_2 flooding are generally supported by experimental results. Xue and Lei (2006), Shi et al. (2007), and Lei and Xue (2009) conducted ultrasonic measurements using seismic difference tomography during the injection of CO_2 into water-saturated Tako sandstone. Xui and Lei (2006) found that the patchy saturation model can be used to estimate P-wave velocities if the wavelength of the applied seismic wave is less than the characteristic size of the inhomogeneous patches of CO_2 fractions. Shi et al. (2007) reported that the Gassmann equation can be used to predict the P-wave velocity changes caused by $scCO_2$ injection into sandstones if the fluids are mixed at a scale below the critical diffusion length. Lei and Xue (2009) showed that their experimental results are in good agreement with the White and Dutta–Odé theory for partial saturation; they also showed that P-wave attenuation increases with CO_2 saturation, achieves a peak at 30-40 % saturation, and then gradually decreases until full CO_2 saturation. The effects of sub-core scale heterogeneity on fluid distribution pattern and acoustic properties of sandstones during imbibition/drainage tests with CO_2/$scCO_2$ were studied by Alemu et al. (2013), who found that acoustic properties at ultrasonic frequencies can be influenced greater by a fluid distribution pattern than by a

variation in CO_2 saturation, and, therefore, the Gassmann theory is not suitable to predict the P- velocity variations. Nakagawa et al. (2013) used the split Hopkinson resonant bar method for sonic-frequency (1-2 kHz) measurements of brine-saturated sandstone during $scCO_2$ flooding and demonstrated that changes in acoustic velocities are generally agreed with the Gassmann model. Lebedev et al. (2013) investigated acoustic properties of brine-saturated shaly sandstones (the Otway Basin, South Australia) flooded with $scCO_2$ and showed that Gassmann's predictions are in a reasonable agreement with the ultrasonic measurements.

In this Chapter, we present the results of the low-frequency (0.1 – 100 Hz) and ultrasonic (~0.5 MHz) experiments conducted on a water saturated sandstone sample flooded with $scCO_2$. To our knowledge, these are the first experiments conducted at seismic frequencies on CO_2 injected sandstone. The aim of the experiments was to investigate the effects of $scCO_2$ injection on the elastic and anelastic properties of sandstone at seismic frequencies and compare the obtained data with the results of ultrasonic measurements. The applicability of Gassmann's fluid substitution theory for the interpretation of obtained data was also a subject of our study.

4.2 Experimental setup

The experiments at seismic frequencies were performed using the low-frequency laboratory apparatus described in Chapter 1 (Figures 1.1-1.4).

The same apparatus with a modified set of units placed between the steel platforms was also used in this study for ultrasonic measurements. The "ultrasonic set" configuration is displayed in Figure 4.1. The ultrasonic transducers were inserted in steel endcaps where they were fixed on the end butts facing a sample by steel springs. There were a Pulser and Receiver system (5077PR, Olympus, Ltd.) and a digital oscilloscope (TDS3034C, Tektronix, Ltd.) used for generation and recording of the ultrasonic pulses.

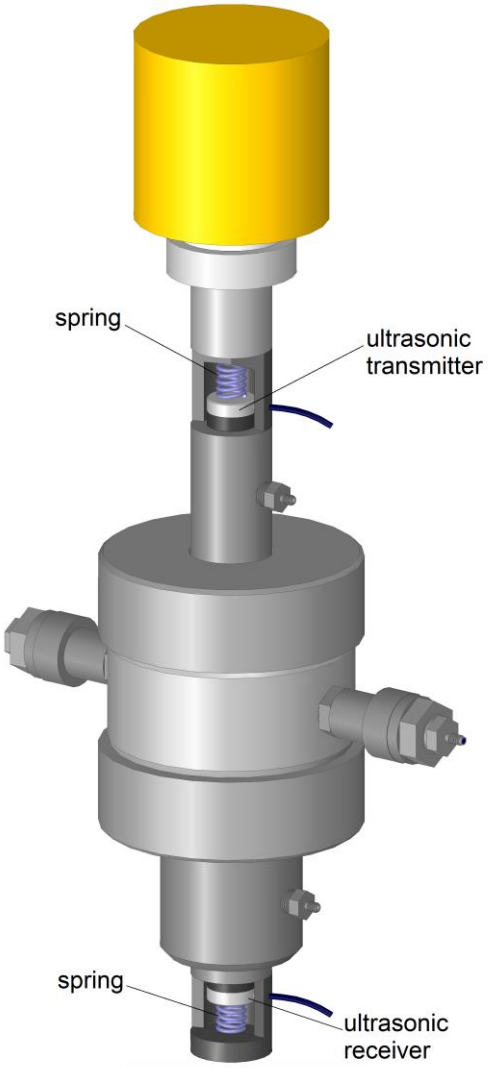

Figure 4.1 The arrangement for ultrasonic measurements.

A diagram of the experimental setup used in this study is presented in Figure 4.2. The setup comprises a CO_2 bottle, a CO_2 syringe pump (model 260D, Teledyne Isco Inc), an ultrasonic/low-frequency system, a distilled water container and a pump for water injection (model LC-20AT, Shimadzu Ltd). The water and scCO_2 were injected from the bottom end of the sample by the water or CO_2 syringe pump. The pumps were used to control the pore pressure and fluid flow during the experiment. To avoid changes of the elastic parameters of the rock caused by pore pressure variations, the pore pressure was kept constant and the same at both ends of the sample.

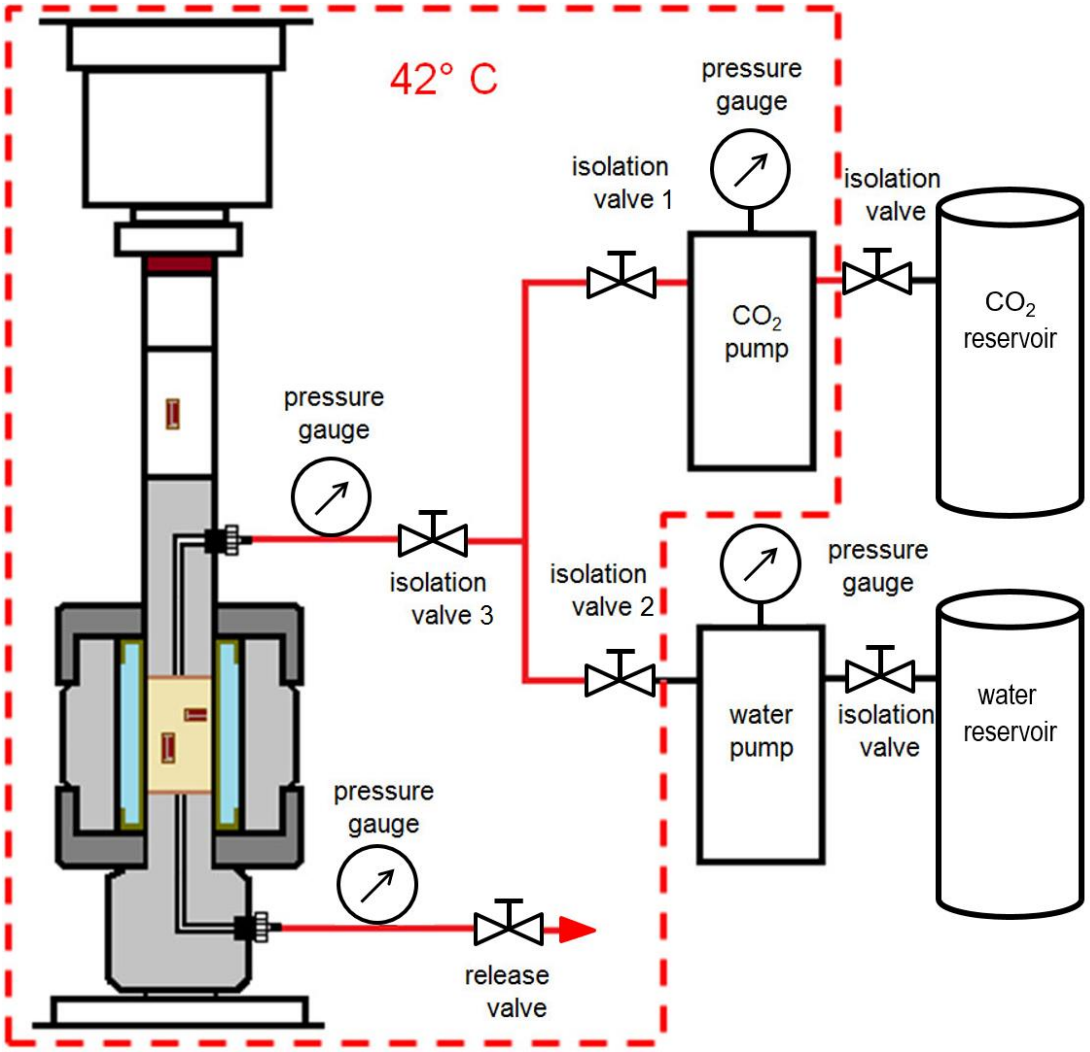

Figure 4.2 The diagram of the experimental setup.

4.3 Experimental procedure

The experimental procedure was organized in the following way. First, the sample was vacuum dried at a temperature of ~60^0 C for two days. Then a set of ultrasonic measurements was conducted where compressional and shear velocities were measured along the symmetry axis of the sample at a frequency of ~0.5 MHz. The ultrasonic measurements of the dry sandstone were carried out at differential (confining) pressures from 10 MPa to 60 MPa. In the tests with the dry sample the pore pressure did not exceed 0.1 MPa. After the experiments with the dry rock, the sample was saturated with distilled water by injecting water from the bottom inlet, and the ultrasonic tests were conducted again at the differential pressures corresponding to the differential pressures of the dry cycle and at a pore pressure of 10 MPa. At the final stage of the ultrasonic tests, the syringe pump, fluid lines, and triaxial cell with the sample inside were heated to a temperature of 42±0.3°C and the $scCO_2$ was injected into the sample. The injection lasted for 48 hours at a constant inlet-outlet pressure of 15 MPa to ensure the water in the sandstone is replaced with the maximum amount of the $scCO_2$, during this process the isolation valves 1 and 3 and the release valve (Figure 4.2) were open. When the process of saturation was finished, a pore pressure was set up at ~10 MPa and all valves were closed. The amount of the residual water in the sample after flooding with $scCO_2$ was estimated at ~ 40% of the pore space by measuring the volume of water removed from the sample. After the measurements at the ultrasonic frequency were finished, the sample was again dried and subjected to a set of low-frequency tests in the range of frequencies from 0.1 Hz to 100 Hz at a single confining pressure of 21 MPa. The procedures of water saturation and $scCO_2$ injection were the same as in the set of the ultrasonic tests.

4.4 Sample description

In this study we investigated the effects of $scCO_2$ on the acoustic properties of sandstone quarried in Donnybrook, Western Australia. A sandstone sample was cut in the direction perpendicular to a formation bedding plane. The physical parameters of the sample are as follows: water permeability – 0.28 mD, porosity – 11.54%. The density of the dry sample is 2249 kg/m^3, the density of the water saturated sample is 2364 kg/ m^3.

The mineral composition of the sandstone retrieved from X-ray fluorescence and diffraction analysis, and the bulk moduli of the found constituents are summarized in Table 4.1. The mineral bulk modulus of the sample was computed using Voigt-Reuss-Hill average and is equal to 31.7 GPa.

In case of inhomogeneous rock, the uniformity of the stress in the cross-sections of the rock cannot be ensured and consequently the elastic moduli and extensional attenuation cannot be measured with the stress-strain method. To verify the homogeneity of the sandstone sample, it was scanned using an X-ray microscope VersaXRM-500 (Xradia Ltd). The cross-section scans obtained in three directions are presented in Figure 4.3. Based on these X-ray images, we assume that the sandstone tested in this study is homogeneous on a macroscopic (wavelength and sample-size) scale. It is important to note that applicability of our experimental techniques does not require the homogeneity on a microscopic (pore- or grain-size) scale.

Table 4.1 The petrographic data for the Donnybrook sandstone sample.

Mineral	Percentage, %	Bulk Modulus, GPa
Quartz	60.7	36.6 (Mavko et al. 2009)
Siderite	1.7	117 (Zhang et al. 1998)
Microcline	5.4	55.4 (Mavko et al. 2009)
Plagioclase	9.4	75.6 (Mavko et al. 2009)
Kaolinite	22.8	11 (Vanorio et al. 2003)

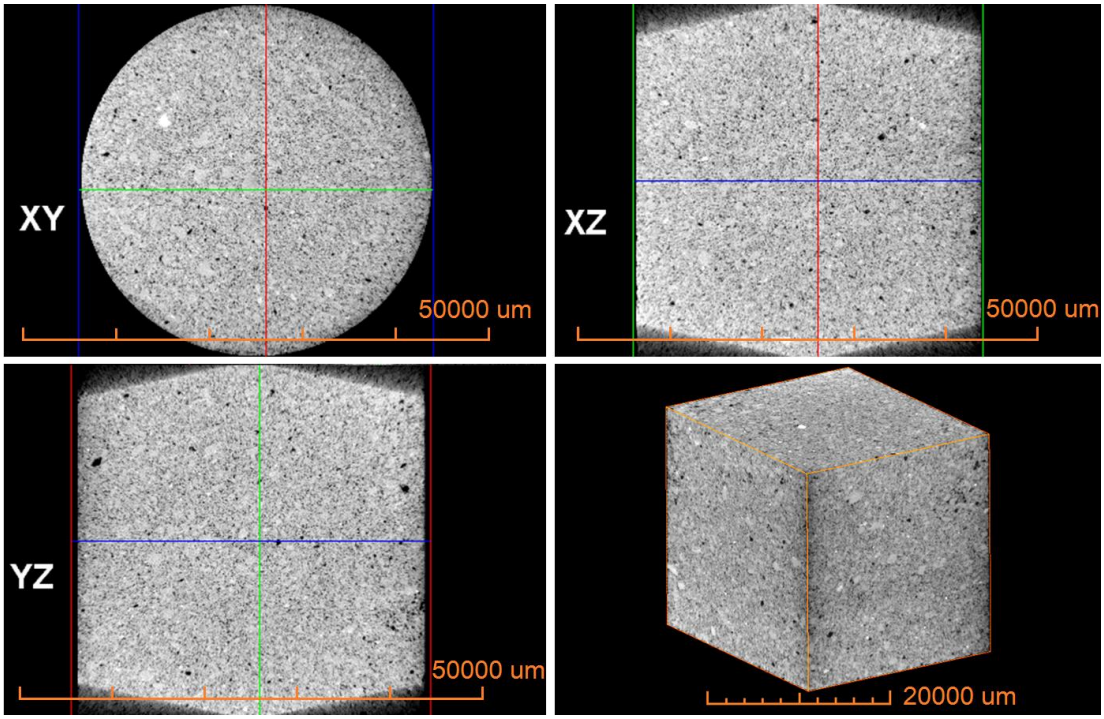

Figure 4.3 X-ray scans of the Donnybrook sandstone sample.

4.5 Results and discussion

The results of the ultrasonic tests are presented in Figures 4.4-4.6. Figure 4.4 shows the ultrasonic P- and S-wave velocities measured on the dry, water-saturated and $scCO_2$-injected sandstone. The confining pressures in these experiments were varied from 10 MPa to 60 MPa for the dry rock and from 21 MPa to 61 MPa for the water or $scCO_2$-water saturated rock; the pore pressure for the dry and fluid-saturated sample was ~0.1 MPa and 10 MPa, respectively. The results are presented against the differential pressure $P_{diff} = P_{conf} - P_{pore}$, where P_{conf} and P_{pore} are the confining and pore pressures. The bulk K and shear μ moduli presented in Figures 4.5-4.6 were computed from compressional V_P and shear V_S velocities:

$$K = \rho V_P^2 - \frac{4}{3}\rho V_S^2, \qquad \mu = \rho V_S^2. \tag{4.1}$$

where ρ is the density of the sandstone.

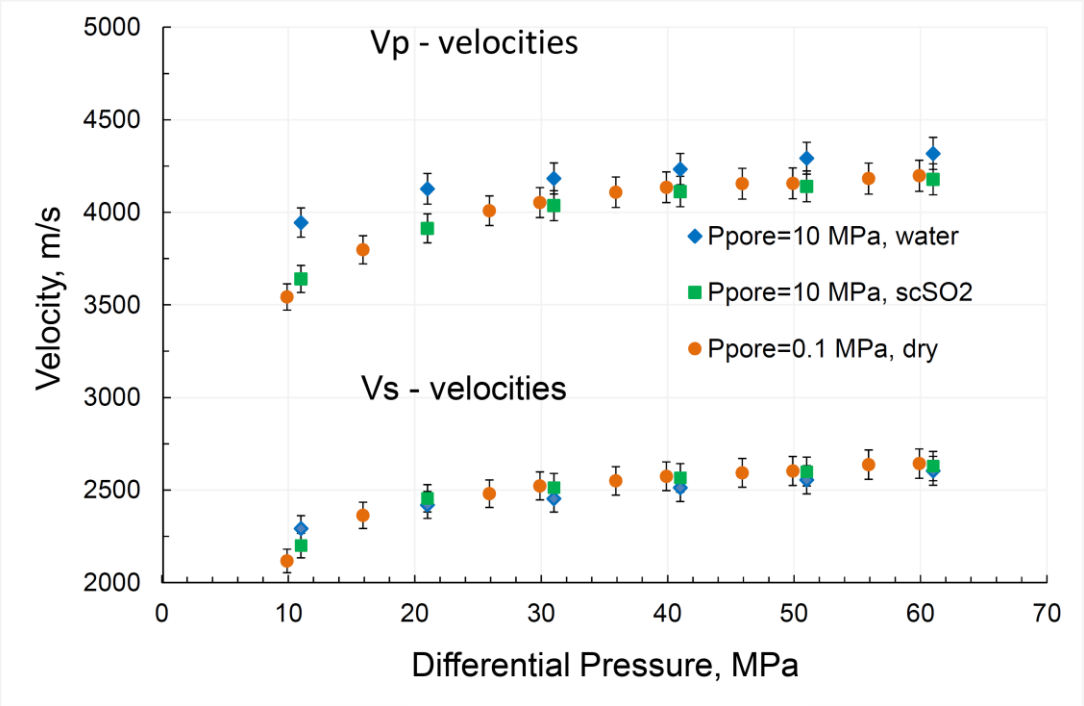

Figure 4.4 Ultrasonic P- and S-wave velocities measured in Donnybrook sandstone when dry, distilled water saturated, and flooded with $scCO_2$. The residual water saturation of the sample after flooding with $scCO_2$ was 40%. The measurements with the dry sandstone are conducted at confining pressures from 10 to 60 MPa and at a pore pressure of 0.1 MPa; the range of confining pressures for the sandstone with fluids is 21 MPa – 61 MPa and the pore pressure is 10 MPa.

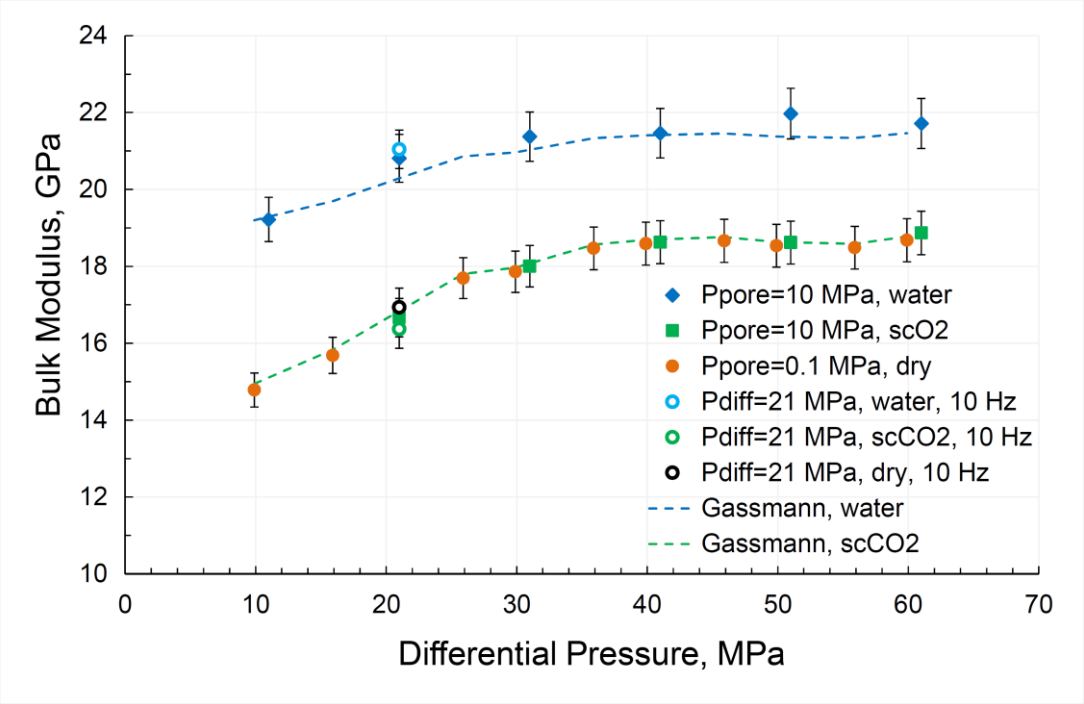

Figure 4.5 Bulk moduli measured for the dry, distilled water saturated, and flooded with $scCO_2$ sandstone at ultrasonic frequency. The residual water saturation after flooding with $scCO_2$ and pressure parameters are the same as in Figure 4.4. The bulk moduli calculated in accordance with the Gassmann fluid substitution equation presented with dash blue (water saturated sandstone) and dash green ($scCO_2$ injected sandstone) lines. For comparison, the bulk moduli obtained at 10 Hz are also presented.

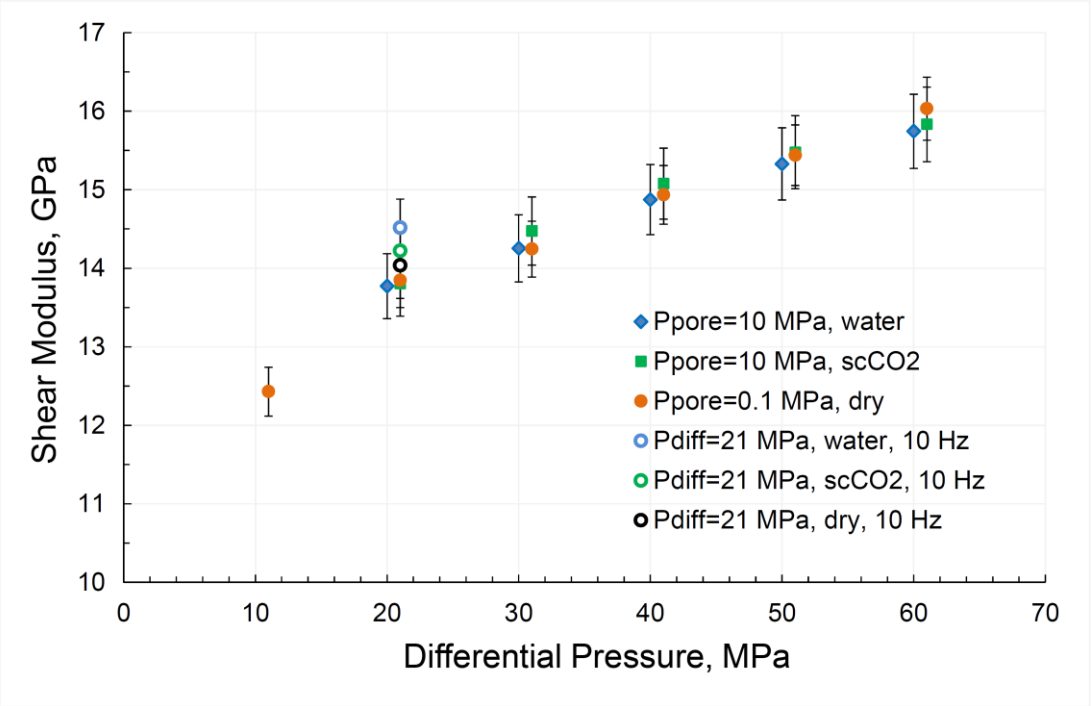

Figure 4.6 Shear moduli measured for dry, distilled water saturated, and flooded with $scCO_2$ sandstone at ultrasonic frequency. The residual water saturation after flooding with $scCO_2$ and pressure parameters are the same as in Figure 4.4.

In Figures 4.5 and 4.6 we also compare the ultrasonic bulk and shear moduli with the predictions of the Gassmann fluid substitution theory (Gassmann, 1951). For our calculations we used the following parameters for $scCO_2$ at a temperature of 42 °C: bulk modulus – 36 MPa, density – 582 kg/m^3, viscosity - 43μPa·s. These values were estimated with the Thermophysical Properties of Fluid Systems program developed by the National Institute of Standards and Technology (NIST) (Lemmon et al. 2011). For computing the bulk modulus of the mixture of $scCO_2$ and water, Wood's average (Wood, 1955) was used:

$$K_{\text{mix}} = \left(\frac{S}{K_{\text{water}}} + \frac{1-S}{K_{\text{scCO2}}} \right)^{-1}, \tag{4.2}$$

where K_{water} and K_{scCO2} are the bulk moduli of water and $scCO_2$, correspondingly, S is the fraction of water in the pores of the rock after $scCO_2$ injection; in our study $S \approx 0.4$. The bulk moduli of the rock predicted by the Gassmann model were found in accordance with the relation (Gassmann 1951):

$$K_{\text{sat}} = K_{\text{dry}} + \frac{\left(1 - \frac{K_{\text{dry}}}{K_{\text{min}}}\right)^2}{\frac{\phi}{K_{\text{mix}}} + \frac{1-\phi}{K_{\text{min}}} - \frac{K_{\text{dry}}}{K_{\text{min}}^2}}, \tag{4.3}$$

where K_{dry} and K_{sat} are the dry and fluid saturated bulk moduli, respectively, K_{min} is the bulk modulus of the minerals forming the rock, ϕ is the rock porosity. Note that in equation 4.3 we use the dry bulk modulus K_{dry} measured at room temperature to calculate the modulus K_{sat} of the saturated rock held at a temperature of 42 °C. As was shown in Lebedev et al. (2013), the changes of the elastic properties of dry sandstones in the temperature range from 23 to 45 °C are insignificant.

The results obtained for moduli, extensional attenuation, P-wave and S-wave velocities in the dry, water saturated and flooded with $scCO_2$ sandstone in the frequency range 0.1 – 100 Hz, and also Gassmann's predictions are presented in Figures 4.7 – 4.10. In Figures 4.5 – 4.6, for comparison, we plotted the low-frequency data obtained at a frequency of 10 Hz. As one can see, the low-frequency data are in fairly good agreement with the results of the ultrasonic experiments. The fact that the bulk and shear moduli of the sample flooded with $scCO_2$ are not frequency dependent suggests that the pressures in the pores filled with water or $scCO_2$-water mixture are in equilibrium for frequencies between 0.1 Hz and 500 kHz.

In our tests we also found that the elastic parameters measured for the $scCO_2$ injected rock are very close to the elastic parameters measured of the same rock in dry state. This result holds for both seismic and ultrasonic bands of frequencies. The differences in P-wave velocities are caused primarily by the contrast in the densities of the water and $scCO_2$-water mixture.

The absence of moduli dispersion in the partly saturated low-permeability sandstone is rather an unusual result of our measurements. Let us analyze this situation in more detail.

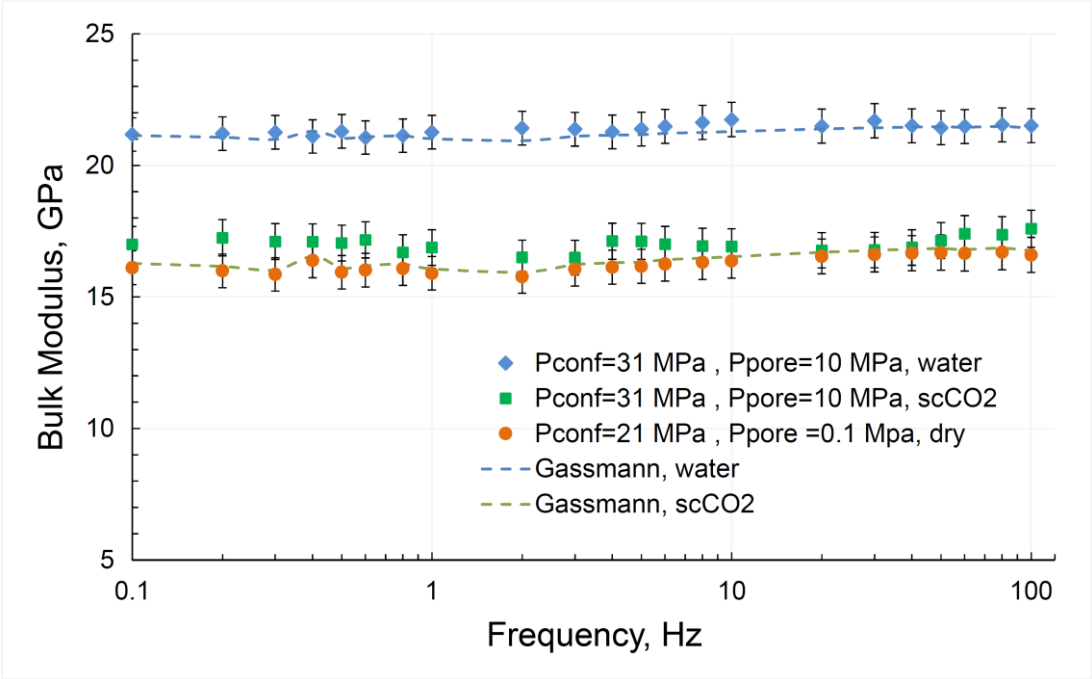

Figure 4.7 Bulk moduli measured for dry, distilled water saturated, and flooded with $scCO_2$ Donnybrook sandstone at the frequency range from 0.1 Hz to 100 Hz. The measurements on the dry sandstone are conducted at a confining pressure of 21 MPa and a pore pressure of 0.1 MPa; the confining and pore pressures for water saturated and flooded with $scCO_2$ sandstone are 31 MPa and 10 MPa, correspondingly; the residual water saturation after flooding with $scCO_2$ was 40%. The bulk moduli calculated in accordance with the Gassmann equation presented with dash blue (water saturated sandstone) and dash ($scCO_2$ injected sandstone) lines.

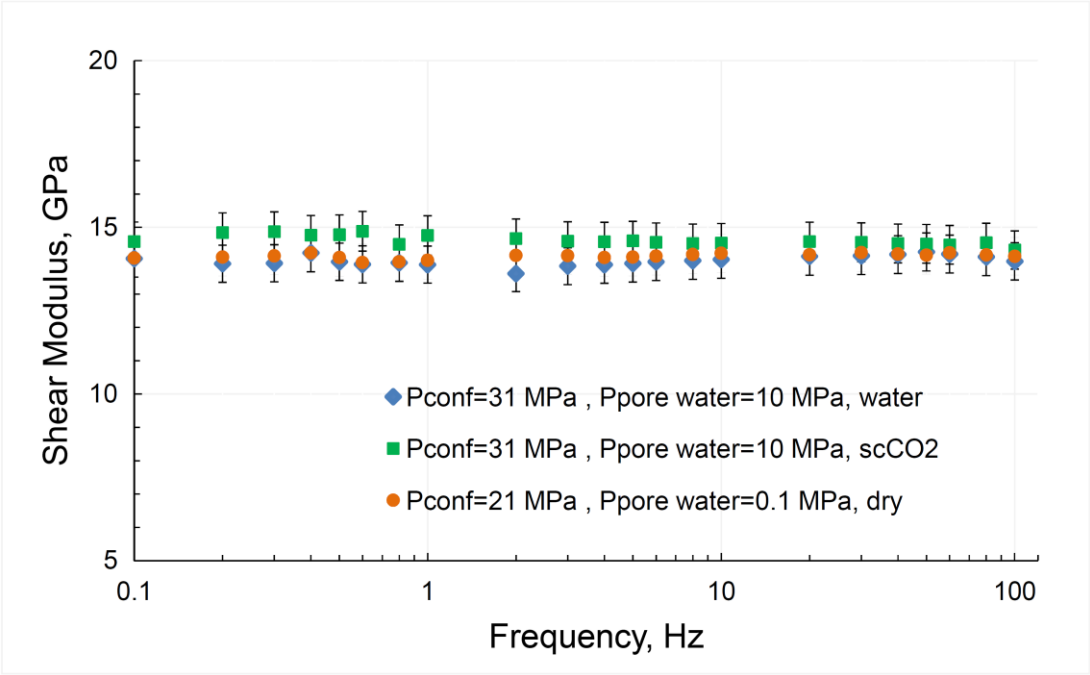

Figure 4.8 Shear moduli measured for dry, distilled water saturated and flooded with $scCO_2$ sandstone. The residual water saturation after flooding with $scCO_2$, pressure parameters and frequency range are the same as in Figure 4.7.

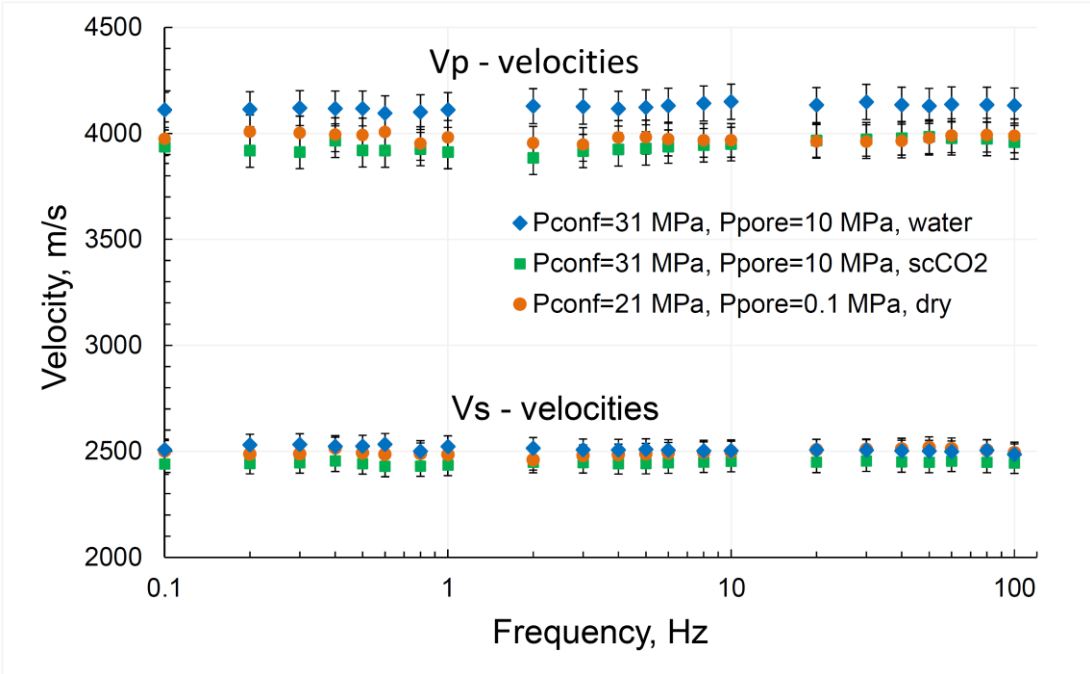

Figure 4.9 P- and S-wave velocities obtained for dry, distilled water saturated and flooded with $scCO_2$ sandstone. The residual water saturation after flooding with $scCO_2$, pressure parameters and frequency range are the same as in Figure 4.7.

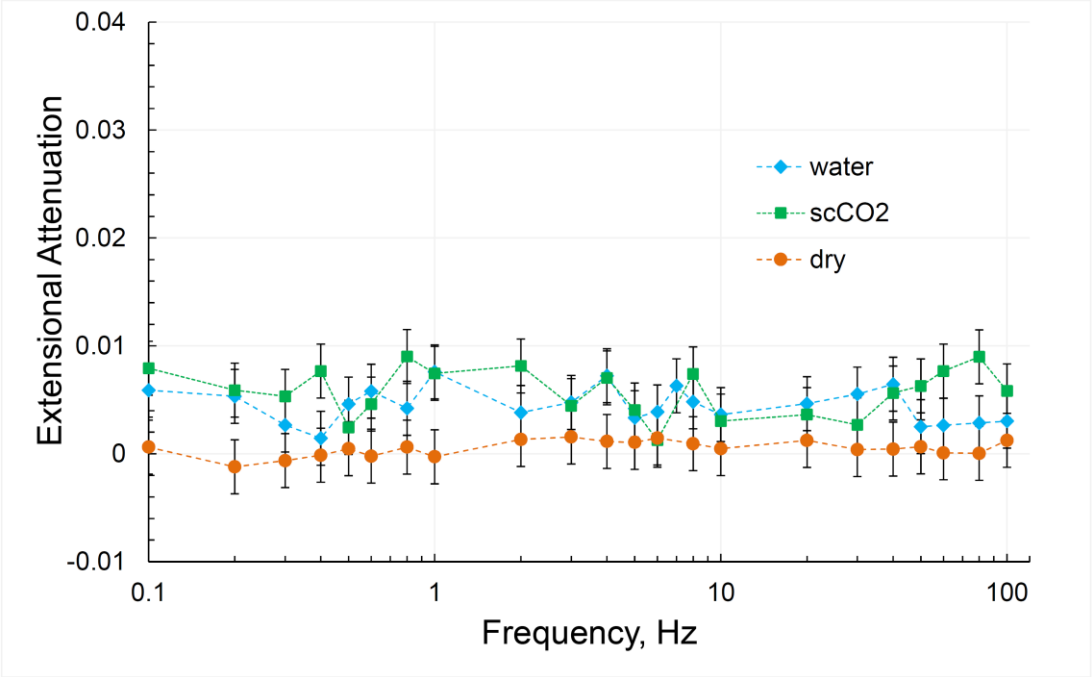

Figure 4.10 Extensional attenuation measured for dry, distilled water saturated and flooded with $scCO_2$ sandstone. The residual water saturation after flooding with $scCO_2$, frequencies of the measurements, confining and pore pressures are the same as in Figure 4.7.

During a period of stress oscillations, pore pressures equilibrate over spatial scales smaller than the characteristic diffusion length $L = \sqrt{\frac{D}{f}}$, where $D = \frac{kK_{\text{fl}}}{\phi\eta}$ is the diffusivity, f is the frequency of stress oscillations, k is the permeability, ϕ is the porosity, η and K_{fl} are the viscosity and bulk modulus of a fluid phase (Dvorkin et al. 2003; Pride 2005). Taking into account that the pores of the sample are filled with one of three fluids, such as water, $scCO_2$ or mixture of water and $scCO_2$, we have to consider three fluid phases inside the sample. The characteristic diffusion length L_w for the water phase is equal to 231 mm and 104 µm at frequencies of 0.1 Hz and 500 kHz, correspondingly. For the $scCO_2$ phase, the diffusion length L_{scCO_2} is 143 mm at 0.1 Hz and 65 µm at 500 kHz; the latter value is comparable with the mean pore size in medium-grained sandstones (Nelson 2009). It would appear reasonable that the diffusion length of uniformly mixed water and $scCO_2$ L_{mix} satisfies the condition $L_{\text{scCO}_2} \le L_{\text{mix}} \le L_{\text{w}}$. So, at a frequency of 0.1 Hz, all fluid phases of the sample are relaxed and the bulk modulus is given by equation 4.3. At

ultrasonic frequency, when all fluid-flow effects can be ignored, the bulk modulus of rock K_H can be found using Hill's equation (Mavko et al. 2009):

$$K_H = \left(\frac{S_{water}}{K_w + \frac{4}{3}\mu} + \frac{S_{sc}}{K_{sc} + \frac{4}{3}\mu} + \frac{S_{w\text{-}sc}}{K_{w\text{-}sc} + \frac{4}{3}\mu} \right)^{-1} - \frac{4}{3}\mu, \quad (4.4)$$

where S_{water}, S_{sc} and $S_{w\text{-}sc}$ are the saturations and K_w, K_{sc} and $K_{w\text{-}sc}$ are the Gassmann predictions of the bulk modulus of the rock saturated with water, $scCO_2$ and mixture of $scCO_2$ and water, correspondingly, μ is the shear modulus of the dry rock.

Let us assume that on average the fractions of water and $scCO_2$ in the pores with mixed fluids are the same as for the overall pore space and equal to 0.4 and 0.6, respectively. In this case the modulus $K_{w\text{-}sc}$ coincides with K_{sat} defined by equation 4.3. Equation 4.4 can be re-written in the following form:

$$K_H = \left(\frac{0.4(1-S_{w\text{-}sc})}{K_w + \frac{4}{3}\mu} + \frac{0.6(1-S_{w\text{-}sc})}{K_{sc} + \frac{4}{3}\mu} + \frac{S_{w\text{-}sc}}{K_{w\text{-}sc} + \frac{4}{3}\mu} \right)^{-1} - \frac{4}{3}\mu. \quad (4.5)$$

The bulk modulus dispersion can be estimated as the difference between K_H and K_{sat} which represent the bulk modulus of the saturated rock at the higher and lower frequency limits of our measurements, respectively. The modulus K_H, as a function of saturation $S_{w\text{-}sc}$, presented in Figure 4.11. To compute K_H and K_{sat} we used the average experimental values for the dry bulk and shear moduli: K_{dry} = 16.3 GPa, μ=14 GPa. As seen in Figure 4.11, the difference by 3% between K_H and K_{sat}, comparable with the experimental error, is reached at $S_{w\text{-}sc}$=0.6, and at $S_{w\text{-}sc}$>0.8 this difference is less than 1%. Thus, if more than 60% of the sample pores filled with the mixture of water and $scCO_2$, the dispersion of the bulk modulus becomes experimentally unobservable. Therefore, the absence of significant moduli dispersion in our experiments can be explained by the fact that a large proportion (>60%) of the sample pores comprises both fluids, water and $scCO_2$. In this case, according to the principle of causality, presented for linear viscoelastic systems by the Kramers-Kronig relations (O'Donnel et al. 1981; Dvorkin and Mavko 2006), the attenuation

also should be insignificant, which agrees with our experimental data showing that attenuation is barely above the experimental error (Figure 4.10).

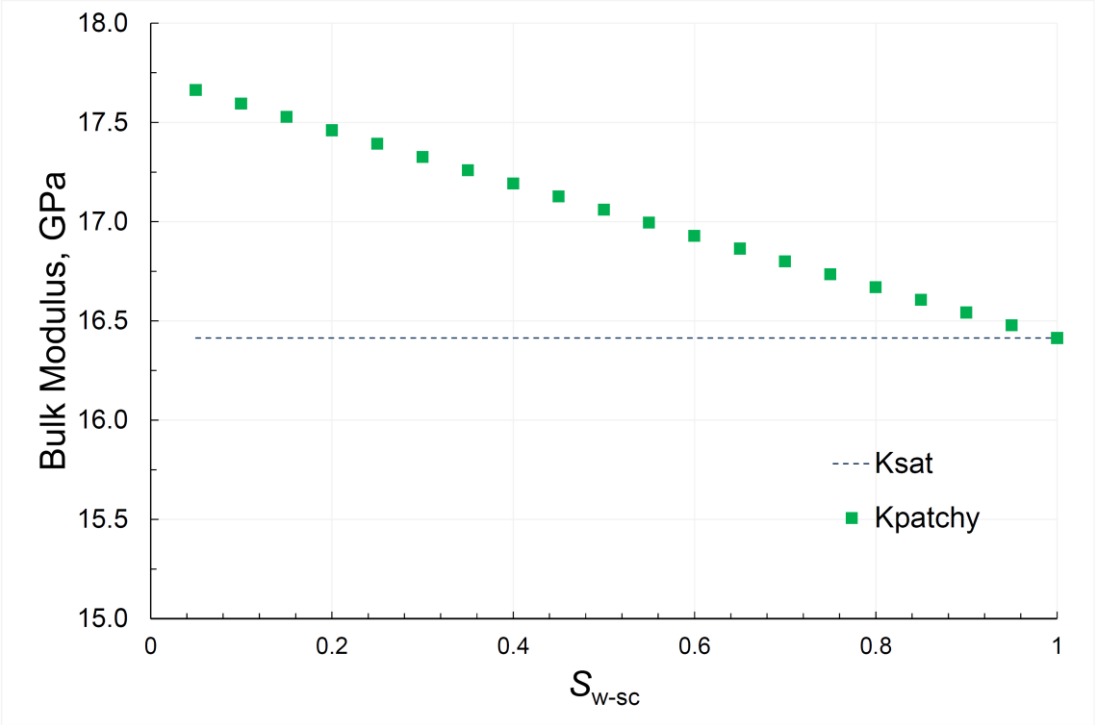

Figure 4.11 The bulk modulus K_H of the sandstone saturated with water (40%) and $scCO_2$ (60%) as a function of the proportion of the pores $S_{w\text{-}sc}$ filled with pore-size mixture of both fluids; the modulus K_H is computed on the basis of Hill's equation 4.5. For comparison, the bulk modulus K_{sat} computed using Gassmann's equation 4.3 is also presented.

4.6 Conclusions

The elastic properties and extensional attenuation of a low-permeability sandstone sample quarrried in Donnybrook, Western Australia, were investigated at ultrasonic (~0.5 MHz) and seismic (0.1 Hz – 100 Hz) frequencies during flooding tests with water and $scCO_2$. The measurements were first conducted on the dry and water saturated sandstone at room temperature (~22 º C). Then the Hoek triaxial pressure cell with the sample inside, the pump dispensing $scCO_2$ and fluid lines were heated to a temperature of 42º C, and the water saturated sample was flooded with $scCO_2$. The amount of the water in the sample after flooding with $scCO_2$ was estimated at ~40% of the pore space.

In both sets of our experiments, conducted at ultrasonic and seismic frequencies, we obtained a reduction (~5 % at a differential pressure of 21 MPa) in P-velocities after $scCO_2$ injection which agrees closely with the difference in P-velocity between the water saturated and dry sample. We found that the extensional attenuation measured in the water saturated sandstone before and after $scCO_2$ injection is practically unchanged.

It was also demonstrated that the dry elastic moduli and the moduli of the sample measured after flooding with $scCO_2$ are very close.

Our analysis shows that the Gassmann fluid substitution theory is applicable for the interpretation of the data measured on the Donnibrook sandstone in flooding tests with $scCO_2$.

Chapter 5

Laboratory measurements of the effect of fluid saturation on elastic properties of carbonates at seismic frequencies

5.1 Introduction

Carbonates are anionic complexes containing the carbonite group $(CO_3)^{2-}$ and metallic cations (Mg, Mn, Fe, Ba etc.) where the chemical bonds between the carbonite and metallic ions are weaker than the bonds inside the carbonite group, but the latter are weaker than the covalent bond in carbon dioxide CO_2 such that the carbonate group breaks up into CO_2 and water in the presence of hydrogen ions (Ahr 2008). The presence of two types of weak bonds in the carbonate minerals makes the petrophysical properties of carbonate reservoirs sensitive to any change in chemical, physical or thermodynamic conditions such as pressure, salinity, acidity/alkalinity, temperature, or a type of fluid. Physical and chemical fluid-rock interactions is one of the main factors changing the microstructure of the rock thereby affecting its porous network (Hoefner and Fogler 1988) and acoustic properties (Wang 1997; Marion and Jizba 1997; Adam et al. 2006; Vanorio 2008; Vialle and Vanorio 2011). Given the vast quantities of world's oil and gas reserves are contained in carbonate reservoirs, the laboratory studies of the elastic properties of fluid-saturated carbonates represent a research area of great importance.

Most common laboratory practices used for measuring elastic properties of carbonates are based on ultrasonic methods, such as the pulse transmission, pulse echo and spectral ratio methods, and the resonant bar method operating at sonic frequencies in the kilohertz range (Wang 1997). Literature on the laboratory

measurements of carbonates at seismic frequencies is very sparse (Adam et al. 2006; Adam and Batzle 2008; Adam et al. 2009). Recently the indentation method was proposed for measurements of the elastic properties of carbonate rocks (Lebedev et al. 2014).

One main implication of the laboratory studies conducted at ultrasonic and sonic frequencies is non-conformance of carbonate rocks to the assumptions of Gassman's fluid-substitution theory (Wang et al. 1991; Marion and Jizba 1997; Baechle et al. 2005; Sharma et al. 2006; Misaghi et al. 2010). In accordance with Gassmann's theory, fluid substitution increases the bulk modulus of a rock (Gassmann 1951), whereas the shear modulus remains constant (Berryman 1999). In most laboratory research carried out at ultrasonic frequencies, Gassmann's predictions mismatch the velocities observed in fluid-saturated carbonates (Wang et al. 1991; Wang 1997; Marion and Jizba 1997; Assefa et al. 2003; Baechle et al. 2005; Røgen et al. 2005; Sharma et al. 2006; Baechle et al. 2009; Misaghi et al. 2010; Lebedev et al. 2014; Wang et al. 2015). Considering that Gassmann's theory was established for low frequencies and that viscoelastic properties of fluid-saturated rocks displayed at ultrasonic (high) and seismic (low) frequencies might differ markedly, one possible cause of the difference between Gassmann-predicted and measured velocities may be the difference between high- and low-frequency regimes. This difference can be attributed to the dispersion of elastic moduli caused by the squirt effect due to microcracks and grain contacts or compliant clay-like intrapore minerals which can significantly affect measured velocities at ultrasonic frequencies (Best 1997, Assefa et al. 1999, Baechle et al. 2005). The existence of the squirt-flow effect in sedimentary rocks is reported in a number of studies. For example, Best et al. (1994) and Best and McCann (1995) demonstrated that in low-permeability sandstones with intrapore content presented by clays or carbonates the squirt flow mechanism is dominant at ultrasonic frequencies. Sams et al. (1997) observed velocity dispersion and frequency-dependent attenuation in the range of frequencies from 30 Hz to 900 kHz, using seismic, VSP, cross-hole, sonic and laboratory ultrasonic measurements at the Whitchester shallow borehole test site which comprises a finely layered sequence of limestones, sandstones, siltstones and mudstones. They showed that the intrinsic attenuation of compressional waves has a peak in the sonic frequency band and can be accounted for by squirt flow. Assefa et al. (1999) and Agersborg et al. (2008) found that at ultrasonic frequencies the squirt

flow is the source of attenuation in the limestones with moderate porosity and permeability. Thus, an examination of the applicability of Gassmann's theory to saturated carbonates has to be implemented at low frequencies. There are only a few studies which evaluate the effect of saturation on elastic properties of carbonate rocks in the low-frequency range. Adam et al. (2006) and Adam and Batzle (2008) examined various aspects of influence of fluid-rock interactions on attenuation and elastic properties of carbonates at seismic and ultrasonic frequencies. They observed the weakening of shear modulus in some carbonate samples at seismic frequencies when the rock condition changes from dry to saturated, while in the ultrasonic frequency domain the shear modulus strengthens. Another finding of these studies is that the shear modulus weakening and bulk modulus behavior are not correlated for brine-saturated carbonates (Adam et al. 2006).

Lebedev et al. (2014) conducted a laboratory study using the indentation (zero-frequency) method supplemented with ultrasonic measurements, specifically to assess the fabric weakening in the Savonnieres oolitic limestone under dry, water- and n-decane-saturated conditions. The grains in the sample measured in Lebedev et al. (2014), are presented mainly by two types of ooids: ooids surrounded by multiple laminae (ooid cortex) and superficial ooids with two or fewer laminae. Both types of ooids are infilled with peloids (peloid nuclei) and/or lithified peloidal sediments. The indentation tests showed water weakening for cement between ooids, peloid nuclei and ooid cortices, but peloidal sediments remained unchanged. Based on these results, a change in the bulk modulus of the water saturated sample might be expected, but this change has not been directly evaluated, however the weakening of the shear modulus was corroborated by ultrasonic measurements. No significant change in the indentation moduli were observed, when the rock changes from dry condition to n-decane-saturated condition.

This Chapter presents the results of the investigation of the fluid saturation effects on the elastic properties of carbonates at seismic and ultrasonic frequencies. The aims of this investigation are firstly to explore the applicability of Gassmann's model for predictions of the elastic moduli of water- and hydrocarbon-saturated Savonnieres limestone and secondly estimate the effects of partial water saturation on elastic properties of the rock. We present results of two sets of laboratory experiments. In the first set, we study elastic moduli and extensional attenuation behaviour in the rock fully saturated with distilled water or hydrocarbon (n-decane)

at seismic (0.1 Hz - 120 Hz) and ultrasonic (0.5 MHz) frequencies. In the second set of experiments we investigate dependences of the elastic and anelastic properties of rock on water saturation at two seismic frequencies of 1 Hz and 10 Hz. The seismic-frequency (SF) measurements were carried out on two samples of the Savonnieres limestone with identical mineralogy and similar petrophysical parameters using a low-frequency laboratory apparatus. To ensure the validity of the seismic-frequency results, the samples for our experiments were selected after their homogeneity was carefully checked with an X-ray microscope. The ultrasonic tests were performed using the pulse transmission ("time of flight") method with a center frequency of ultrasonic pulses of 0.5 MHz.

5.2 Sample description

Two samples of the Savonnieres oolitic limestone selected for this study were cut from a single block with dimensions of 40 cm × 40 cm × 40 cm, which also was used for the measurements in Lebedev et al. (2014). The rock texture is calcite-cemented oolitic grainstone with elliptical and spherical ooids up to 6 mm in diameter (Lebedev et al. 2014). The Savonnieres limestone is predominantly a macroporous rock with 30–40% porosity, consisting of 98% pure calcite (Fronteau et al. 2010), without clay minerals (Derluyn et al. 2011). The total porosity in our samples, which for convenience are designated as sample A and sample B, is 26% (sample A) and 30 % (sample B). The physical characteristics of both samples are summarised and presented in Table 5.1.

As was indicated by Madonna and Tisato (2013), the intrinsic heterogeneities of a rock sample may produce an error when the total sample strain differs from the local strain detected by a gauge. Considering that carbonate rocks usually demonstrate large heterogeneity which can violate the requirements imposed by the stress-strain technique, both samples were thoroughly tested with an X-ray microscope VersaXRM-500 (Zeiss-Xradia Ltd.) to ensure that the heterogeneities of the samples are essentially less than the length of strain gauges (type KSP-6-350-E4, Kyowa Ltd, 6-mm length). The X-ray scans obtained for each sample are presented in Figure 5.1. The homogeneity of the samples on a scale of the strain gauge length was verified using VersaXRM-500 Tomography Software.

Table 5.1 Petrophysical data for the Savonnieres limestone samples.

Sample	A Savonnieres Limestone	B Savonnieres Limestone
Porosity, %	26	30
Helium permeability, $\times 10^{-15}$ m^2 (mD)	60.2 (61)	60.2 (61)
Density, kg/m^2	1965	1886
Length, mm	72	60
Diameter, mm	38	38
Mineral bulk modulus, GPa	76.8	76.8

5.3 Experimental procedures

5.3.1 Experiments with fully n-decane/water-saturated Savonnieres limestone

The experiments aiming to investigate the elastic properties of the Savonnieres limestone under dry and fully water/n-decane -saturated conditions were organized in the following way. First, sample A was vacuum dried at a temperature of 60^0 C for one day, upon which it was jacketed with shrink tubing. Then ultrasonic and seismic-frequency measurements were carried out at a confining pressure of 15 MPa and a pore pressure of ~0.1 MPa. In the next step, the sample was saturated with deionized and degassed water (the amount of total dissolved solids (TDS) is less than 1 ppm) and the same measurements were carried out under fully saturated conditions. The confining and pore pressures were set to 17 MPa and 2 MPa, respectively, so the differential pressure (differential pressure is the difference between confining and pore pressures) was corresponding to the confining pressure of the dry cycle. Upon completion of these tests, sample A was again vacuum dried for two days. Then the sample was saturated with n-decane and the ultrasonic and seismic-frequency measurements were repeated at the same confining and pore pressures as for water-saturated condition.

Sample A

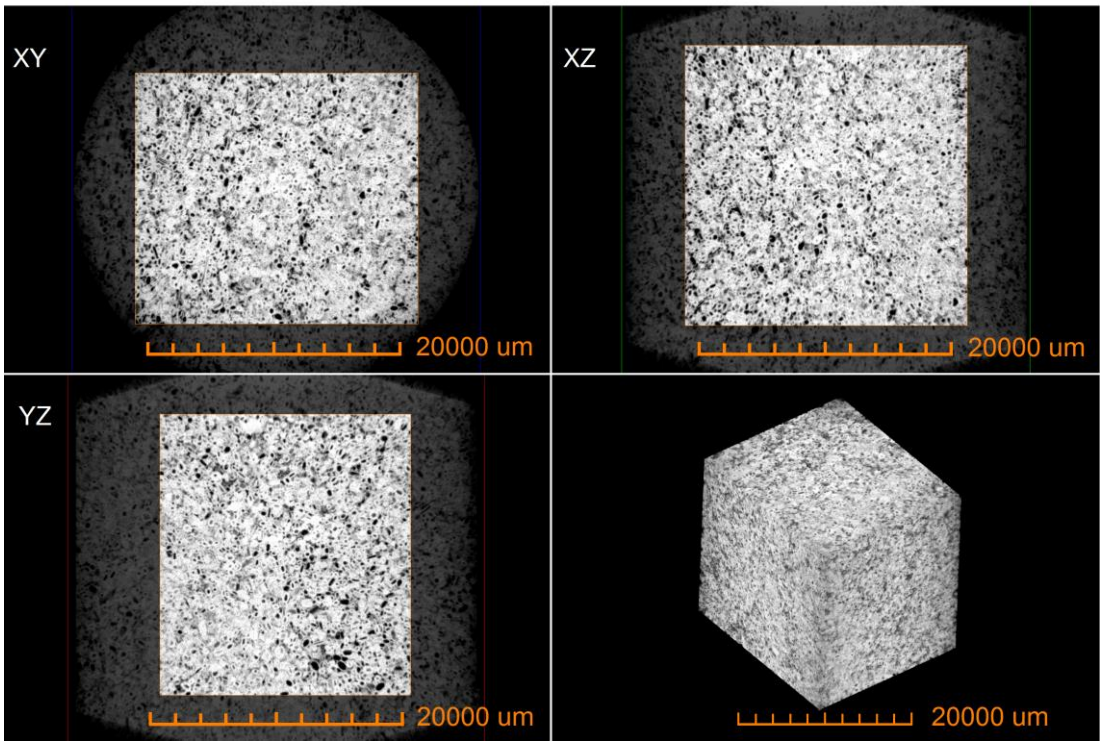

Sample B

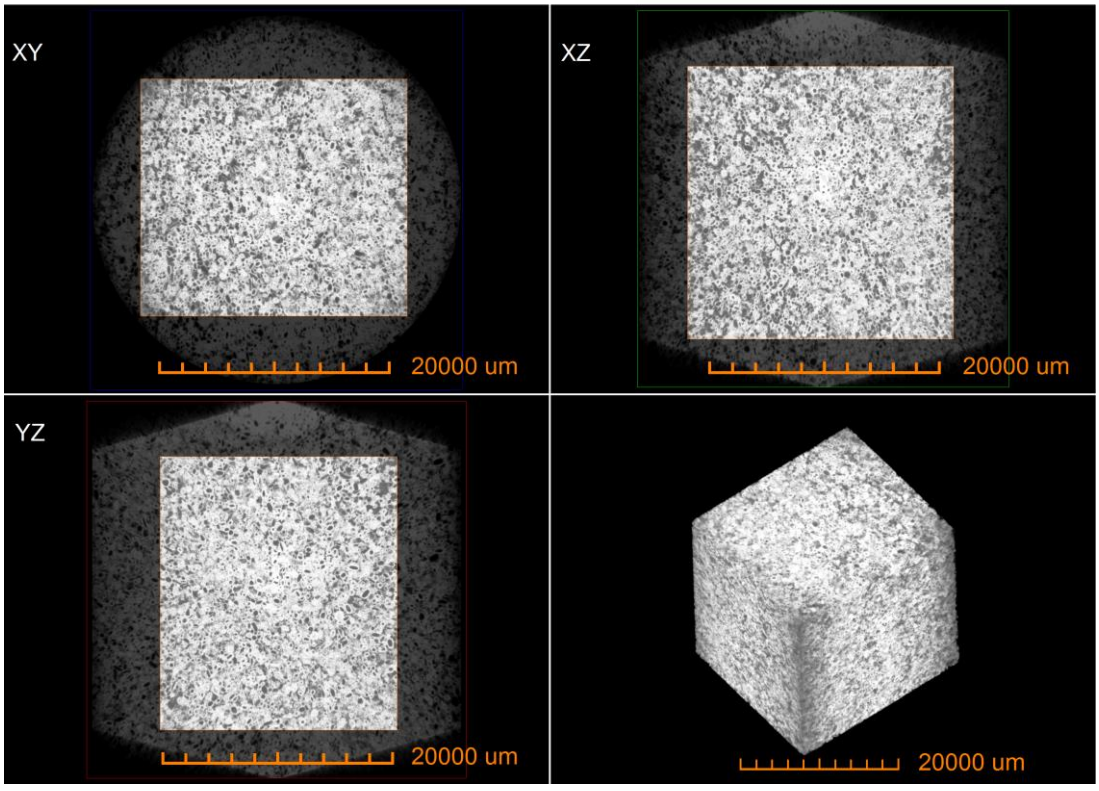

Figure 5.1 X-ray micro-CT images of Savonnieres limestone samples A and B.

5.3.2 Experiments with partially water-saturated Savonnieres limestone

In this set of tests, we studied the elastic and anelastic properties of the Savonnieres limestone as a function of water saturation. The experiments were conducted at two frequencies of 1 Hz and 10 Hz on sample B. Prior measurements, the sample was dried and jacketed in the same way as it was described for sample A. The procedure of the measurements was as follows. The elastic parameters and extensional attenuation of the dry sample were measured at a confining pressure of 10 MPa and at an ambient pore pressure. Then the sample was gradually saturated by injecting deionized and degassed water under the same confining pressure which was used for the dry measurements. Water was injected through the pore-fluid line to the bottom end of the sample using a syringe pump (model 260D, Teledyne Isco). The fluid line connected to the top end of the sample was kept open during the injection and closed after the injection is finished. After a 15 minute break (which allowed time for the water to be distributed inside the sample) the same measurements as for the dry cycle were repeated for each 1-ml increment. At the end, to ensure full saturation, a backpressure of 1 MPa was applied to the pore-fluid line outlet using a second syringe pump and at least 5 pore volumes of water were pumped through the sample, whereupon the backpressure level was reduced to ambient and the pore-fluid lines were closed by the valves located next to the sample. The flow rate of water during saturation did not exceed 0.03 cm^3/s (2 cm^3/min).

Detailed descriptions of the experimental setups used for seismic-frequency and ultrasonic measurements are given in Chapters 1 and 4, correspondingly.

5.4 Experimental results

5.4.1 Results on fully n-decane/water-saturated Savonnieres limestone

The experimental results obtained for both Savonnieres limestone samples are presented in Figures 5.2 – 5.11. The error bars for the moduli and attenuation estimates were computed in accordance with the uncertainty analysis procedure elaborated in Adam (2009) and Adam et al. (2009).

The seismic-frequency and ultrasonic experiments with dry and fully n-decane/water saturated sample A were conducted at frequencies of 0.1 Hz -120 Hz and 0.5 MHz, correspondingly, under a differential pressure of 15 MPa. The

confining and pore pressures for the sample in dry condition were 15 MPa and ~0.1 MPa, respectively. In the measurements under fluid-saturated condition, both confining and pore pressures were 2 MPa higher, so the differential pressure was unchanged.

The results obtained for the elastic moduli, extensional attenuation, P- and S-wave velocities in dry and fully n-decane/water saturated sample A are presented in Figures 5.2 – 5.6. In Figure 5.2, we compare the measured bulk moduli with the predictions of Gassmann's equation (Gassmann 1951)

$$K_{\text{sat}} = K_{\text{dry}} + \frac{\left(1 - \frac{K_{\text{dry}}}{K_{\text{min}}}\right)^2}{\frac{\phi}{K_{\text{fluid}}} + \frac{1-\phi}{K_{\text{min}}} - \frac{K_{\text{dry}}}{K_{\text{min}}^2}}, \tag{5.1}$$

where K_{dry} and K_{sat} are dry and fluid saturated bulk moduli, respectively, K_{min} is the bulk modulus of the minerals forming the rock, ϕ is the rock porosity. For equation 5.1 we use the following mineral (calcite) and fluid moduli: K_{min} = 76.8 GPa (Simmons and Wang 1971), K_{fluid} = 0.86 GPa for n-decane and 2.2 GPa for water (White 1986). The measured bulk and shear moduli of the n-decane saturated Savonnieres limestone are consistent with Gassmann's model (Figures 5.2 and 5.3). A change of the sample state from dry to water saturated increases the bulk modulus of the limestone in agreement with Gassmann's predictions, but decreases the shear modulus by ~6% (Figure 5.3) and slightly, within 2%, reduces the Young modulus (Figure 5.4). Compressional and shear wave velocities, presented in Figure 5.5, were computed using equations

$$V_p = \sqrt{(K + \frac{4}{3}\mu)/\rho}, \tag{5.2}$$

$$V_s = \sqrt{\mu/\rho}, \tag{5.3}$$

where the density of rock ρ was found as

$$\rho = (1-\phi)\rho_{\text{dry}} + \phi\rho_{\text{fluid}}. \tag{5.4}$$

Here ρ_{dry} is the density of dry rock (see Table 5.1), ρ_{fluid} = 1000 kg/m^3 for water and 730 kg/m^3 for n-decane (White 1986).

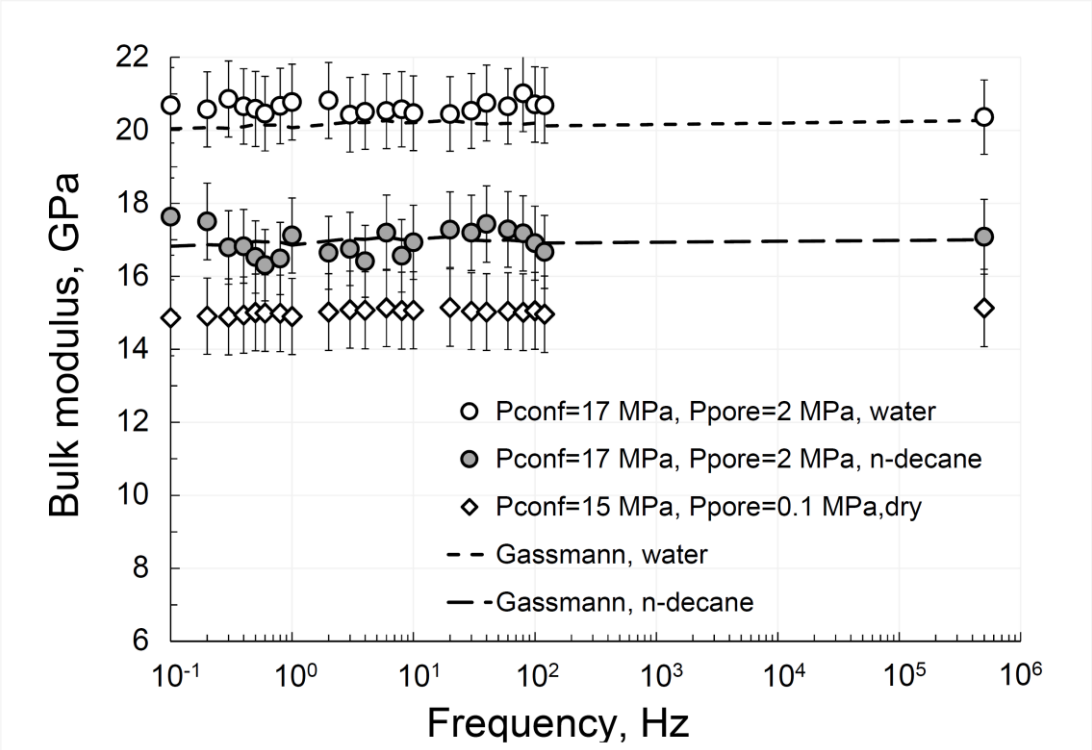

Figure 5.2 The bulk modulus measured for dry, n-decane- and water-saturated Savonnieres sample A at frequencies of 0.1 Hz to 120 Hz and 500 kHz. The measurements on the dry sample are conducted at a confining pressure of 15 MPa and a pore pressure of 0.1 MPa; the confining and pore pressures for n-decane/ water-saturated rock are 17 MPa and 2 MPa, correspondingly. Note that the Gassmann n-decane dashed line symbol appears as a solid line in the legend.

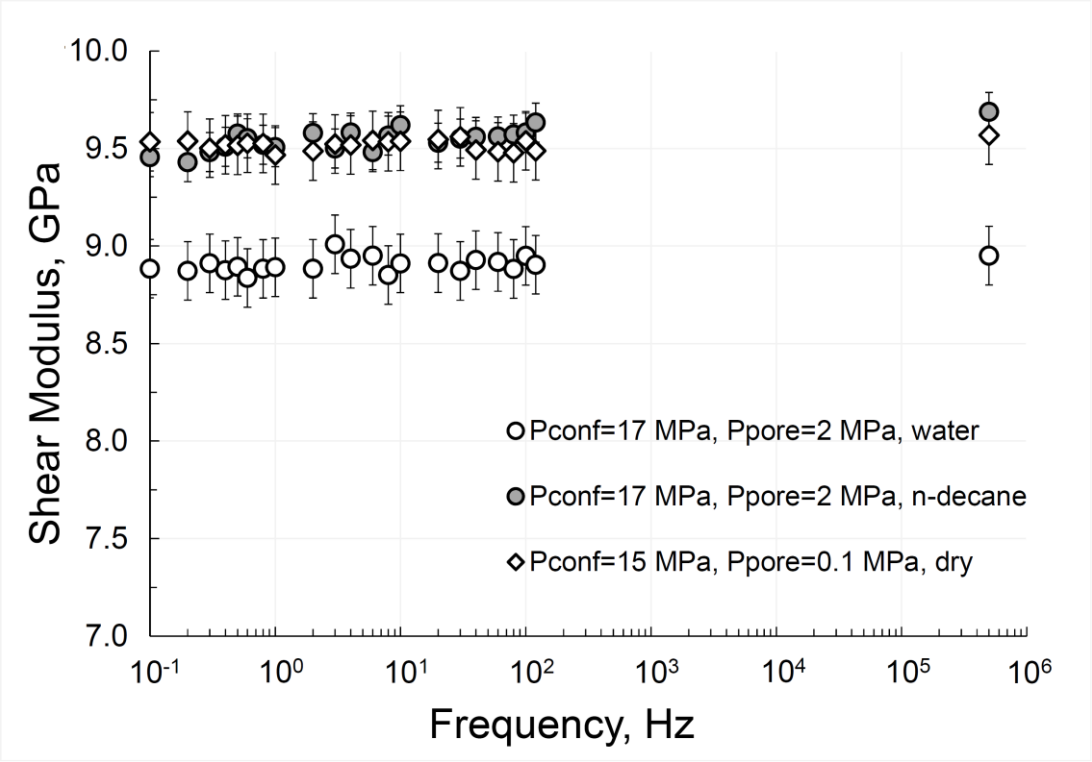

Figure 5.3 The shear modulus measured for dry, n-decane- and water-saturated Savonnieres sample A. The measurement frequencies, confining and pore pressures are the same as in Figure 5.2.

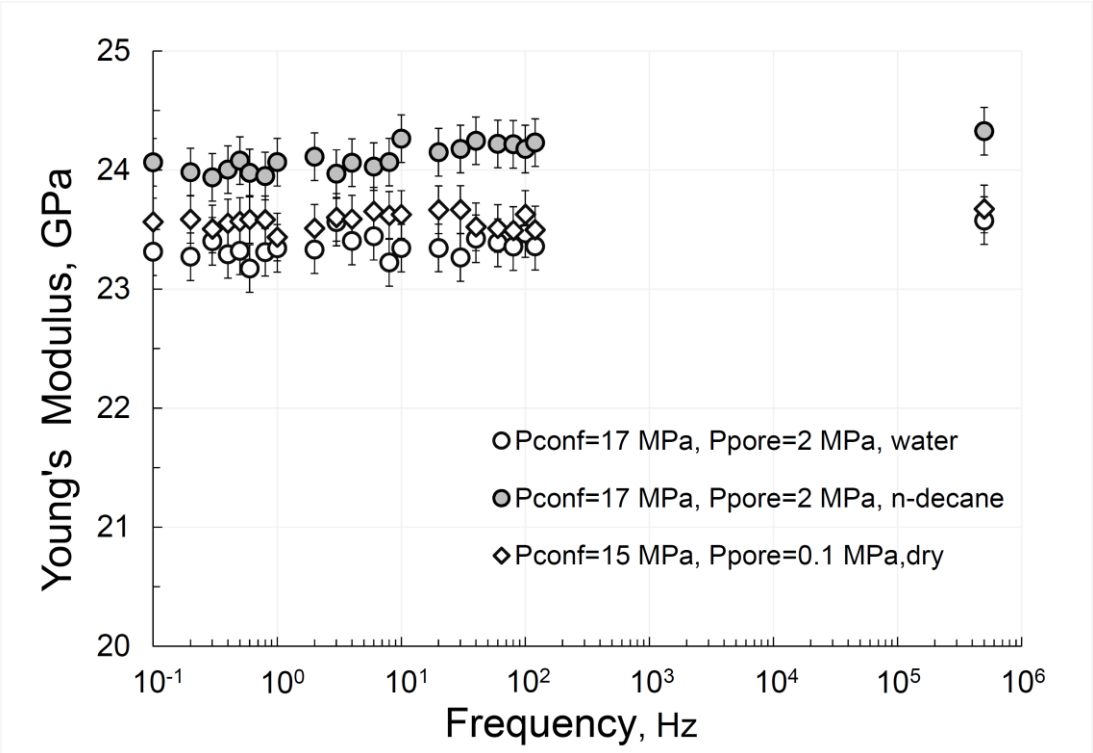

Figure 5.4 The Young's modulus measured for dry, n-decane- and water-saturated sample A. The experimental parameters are the same as in Figure 5.2.

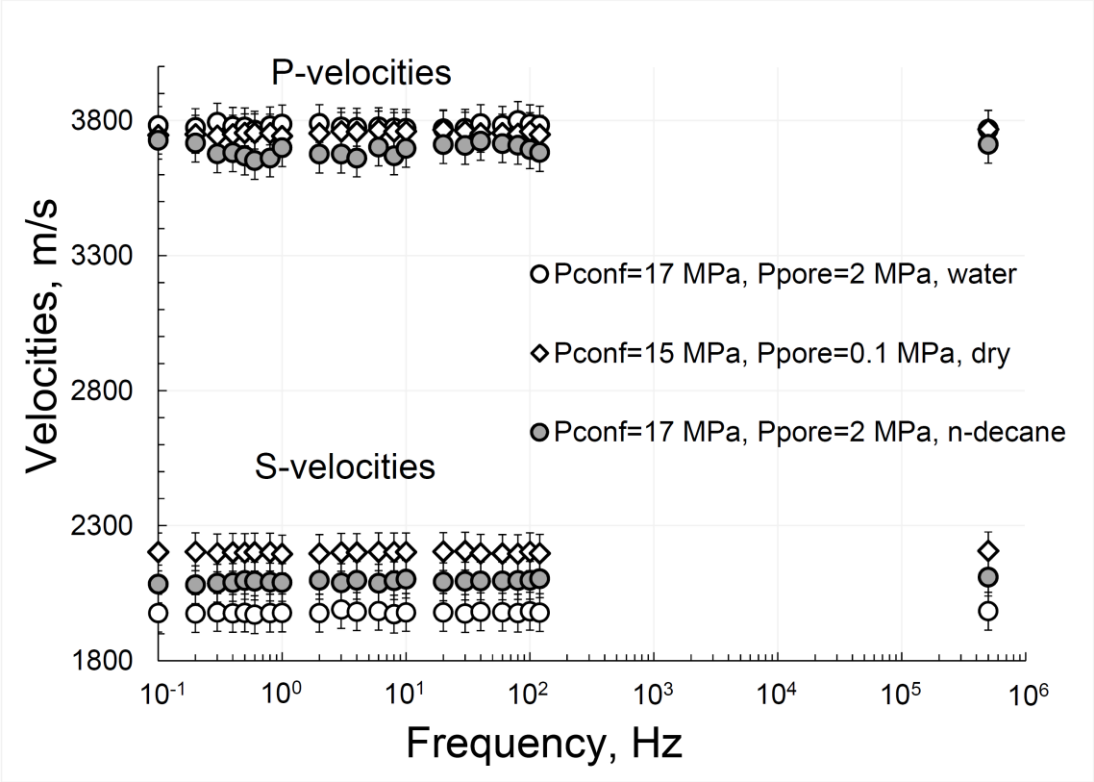

Figure 5.5 P- and S-velocities computed for dry, n-decane- and water saturated Savonnieres sample A.

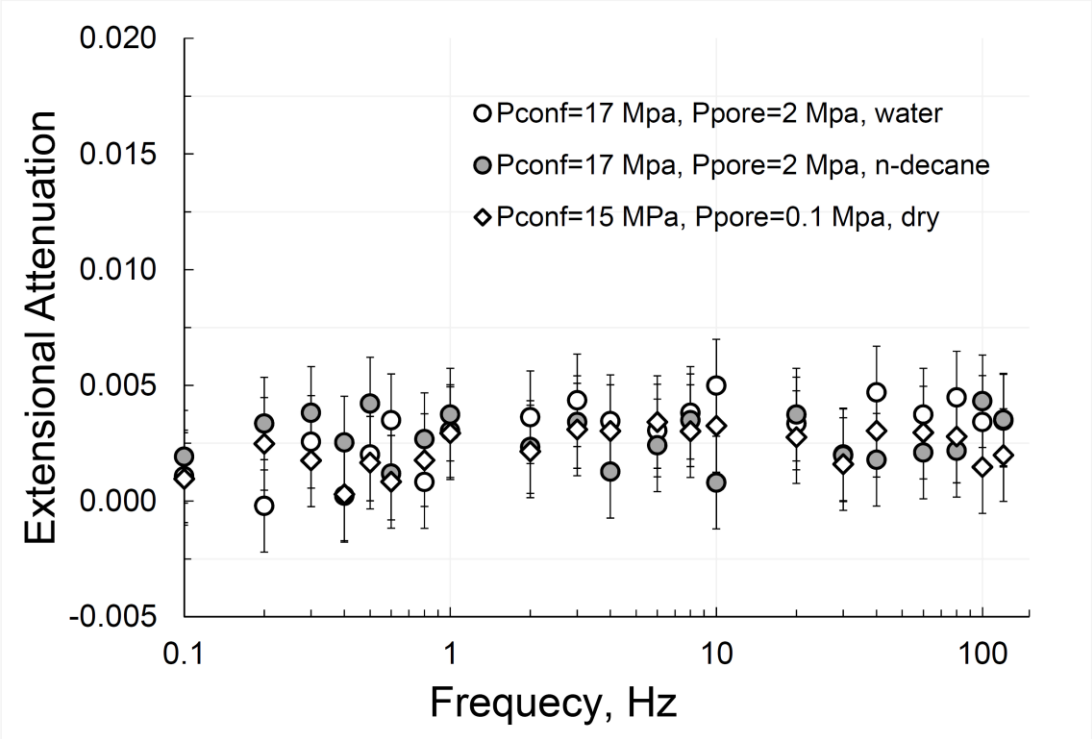

Figure 5.6 The extensional attenuation Q_E^{-1} in sample A obtained at a frequency range of 0.1 Hz to 100 Hz under dry, n-decane- and water saturated conditions. The measurement parameters are the same as in Figure 5.2.

As seen in Figure 5.5, the P-velocities measured in dry and water-saturated rock are virtually indistinguishable, inasmuch as the increase in bulk modulus due to saturation is completely compensated by the decrease in shear modulus and change in the density of rock as consistent with equation 5.2. The extensional attenuation measured in sample A under both n-decane- and water-saturated conditions is in close, within the limits of the experimental error, agreement with the results of the measurements on the dry sample (Figure 5.6).

5.4.2 Results on partially water-saturated Savonnieres limestone

The results of the experiments conducted on partially saturated sample B at frequencies of 1 Hz and 10 Hz are presented in Figures 5.7-5.11. The Young's modulus dependence on saturation, shown in Figure 5.7, displays a slight decrease in the rock Young's modulus during saturation which switches to a modest rising at full saturation. Figure 5.8 compares the measured and Gassmann-predicted bulk moduli as functions of saturation.

The Gassmann-predicted moduli were computed using equation 5.1, where the bulk modulus of fluid K_{fluid} was estimated as Wood's average (Wood, 1955):

$$K_{\text{fluid}} = \left(\frac{S}{K_{\text{water}}} + \frac{1-S}{K_{\text{air}}} \right)^{-1}. \tag{5.4}$$

In equation 5.4, K_{water} and K_{air} are the bulk moduli of water and air, correspondingly, S is the fraction of water in the pores of the rock; in our study S changes from 0 to 1. The values used for the fluid moduli are: K_{water} =2.2 GPa (White 1986) and K_{air} =131 kPa (Mavko et al. 2009).

The measured bulk modulus (Figure 5.8) demonstrates a slight declining trend with increasing saturation until it is replaced by a sharp rise by 27 % when all pore space in the sample is filled with water. The deviation of the measured dependence from the theoretical curve computed using the Gassmann-Wood approach is very close to the measurement accuracy.

The dependence of the shear modulus on water saturation, as can be seen in Figure 5.9, is lowering until at full saturation the modulus reduction reaches 6%. The shear modulus weakening accompanied by the change of rock density due to saturation, results in the decrease of the S-wave velocities by 10 % under fully water-

saturated condition (Figure 5.10a). The P-wave velocities lower when saturating by up to 8% and then sharply increase by more than 10% at full saturation (Figure 5.10b). The extensional attenuation (Figure 5.11) is insignificant in the dry and fully saturated sample, however it is distinctly higher in the partially saturated state.

5.5 Analysis of results

Our results obtained for the elastic moduli of n-decane saturated Savonnieres limestone are in good agreement with Gassmann's model and corroborate earlier findings (Adam et al. 2006; Lebedev et al. 2014) indicating that the solid matrix of carbonate is not affected by n-decane saturation.

We also found that the fabric weakening in water-saturated Savonnieres limestone, as documented in Lebedev et al. (2014), is mainly reflected in the reduction of the shear modulus, whereas the bulk modulus deviations from Gassmann's predictions are close to the measurement accuracy.

As shown in a number of studies, attenuation and elastic moduli of fluid-saturated carbonates are functions of a significant number of factors, such as heterogeneity and clay content (Jaspen et al., 2002; Adam et al., 2006), pH and polarity of a pore fluid (Adam et al. 2006, Vialle et al. 2011, Lebedev et al. 2014), porosity and carbonate pore types (Rafavich et al. 1984; Wang 1997; Eberli et al. 2002; Baechle et al. 2005; Baechle et al. 2008). Adam et al. (2006, 2009) and Agersborg et al. (2008) pointed out that heterogeneities, vugs or moldic pore structures can cause significant attenuation at ultrasonic frequencies due to scattering of the waves from pore-grain interfaces. Best at al. (1994), Sams at al. (1997), Assefa et al. (1999) and Agersborg et al. (2008) found that the results of sonic and ultrasonic measurements can be essentially altered by the squirt-flow effect.

The insignificant dispersions between the elastic moduli and velocities measured for saturated sample A at seismic and ultrasonic frequencies (Figures 5.2 – 5.5) indicates that squirt flow is absent or has a negligible effect on our measurements. Considering that the modulus dispersion and intrinsic attenuation in a material are directly connected via the causality principle commonly expressed in terms of Kramers-Kronig relations (Mavko et al. 2009), the lack of dispersion in the seismic band can be confirmed by the low level of attenuation observed in the water saturated rock (Figure 5.6).

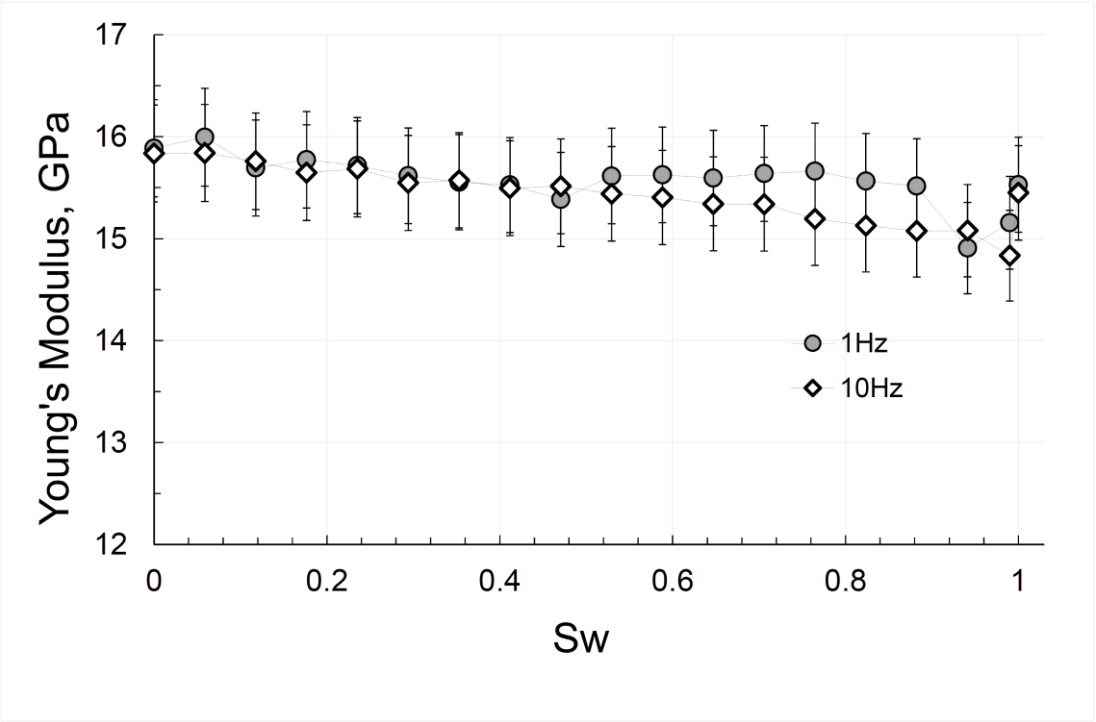

Figure 5.7 The dependences of the Young's modulus on water saturation (Sw) measured for Savonnieres sample B at two seismic frequencies of 1 Hz and 10 Hz. The measurements are conducted at a confining pressure of 10 MPa and at an ambient pore pressure.

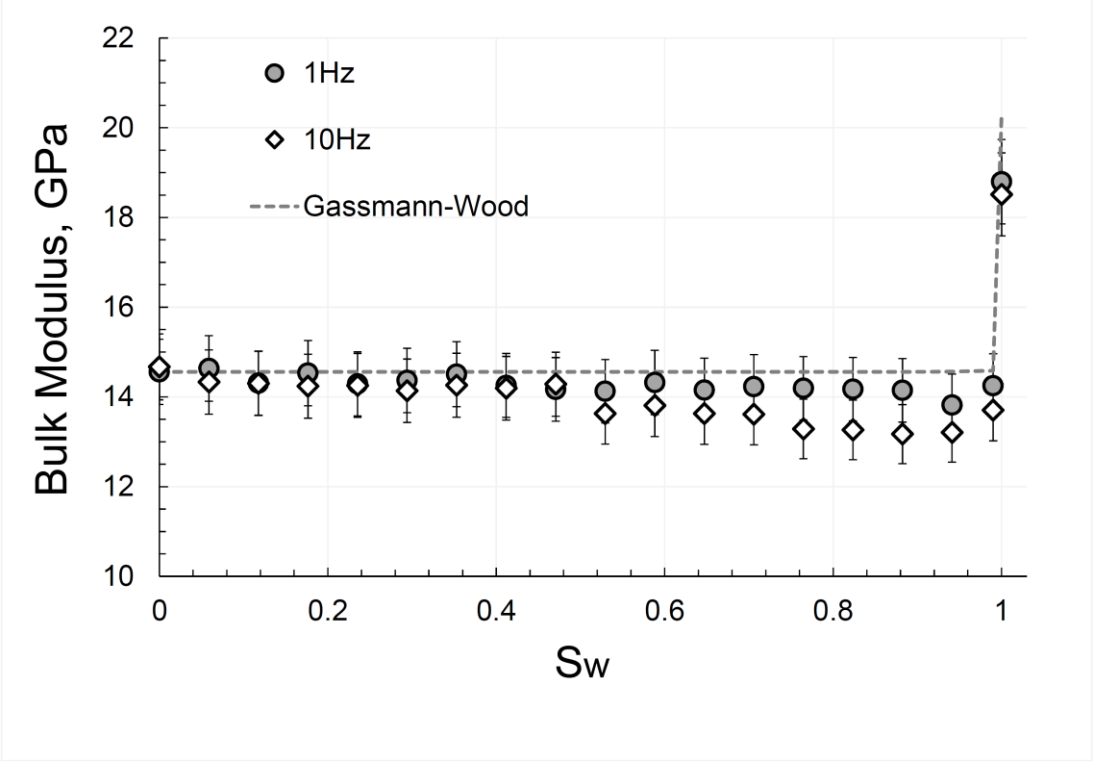

Figure 5.8 The dependences of the bulk moduli on water saturation (Sw) measured for Savonnieres limestone sample B. The experimental parameters are the same as in Figure 5.7.

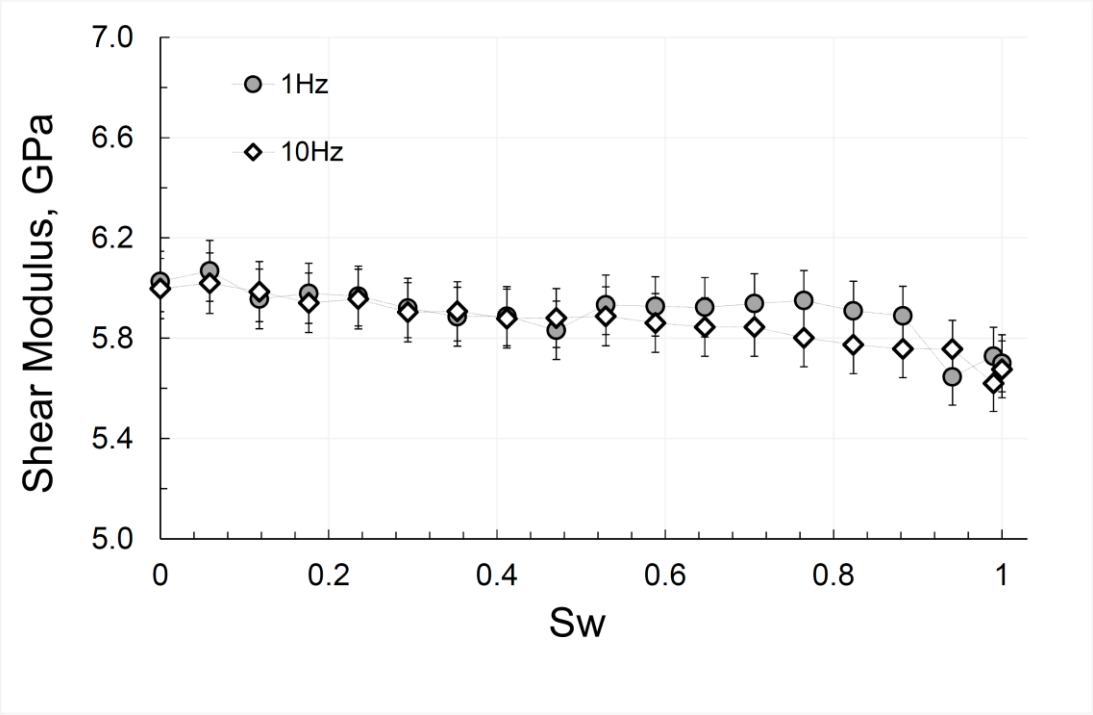

Figure 5.9 The shear modulus dependences on water saturation (Sw) obtained for Savonnieres limestone sample B. The measurement conditions and parameters are the same as in Figure 5.7.

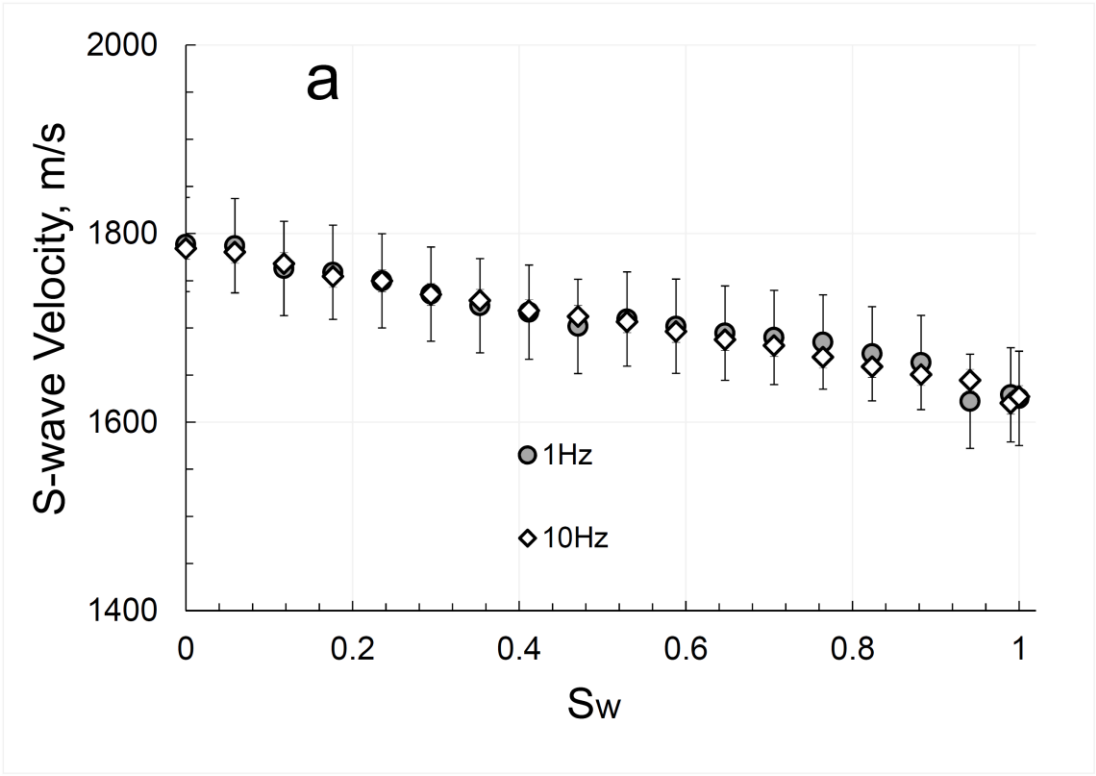

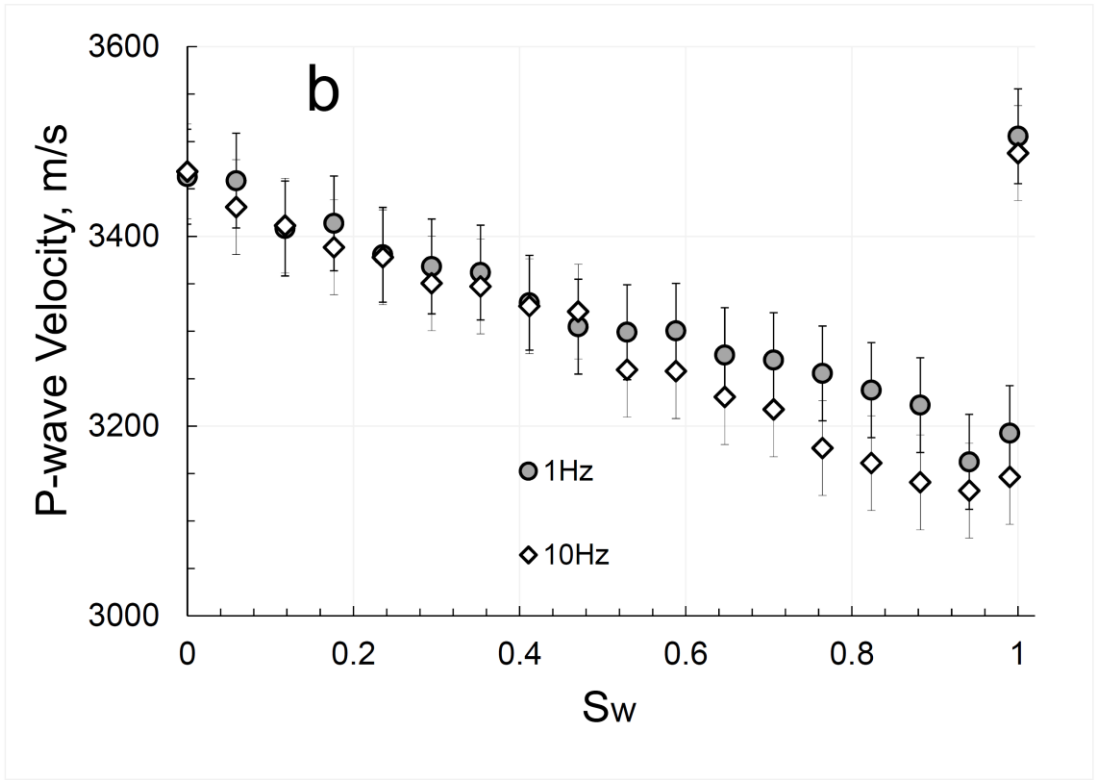

Figure 5.10 The S-wave (a) and P-wave (b) velocities as functions of water saturation (Sw) computed for Savonnieres limestone sample B.

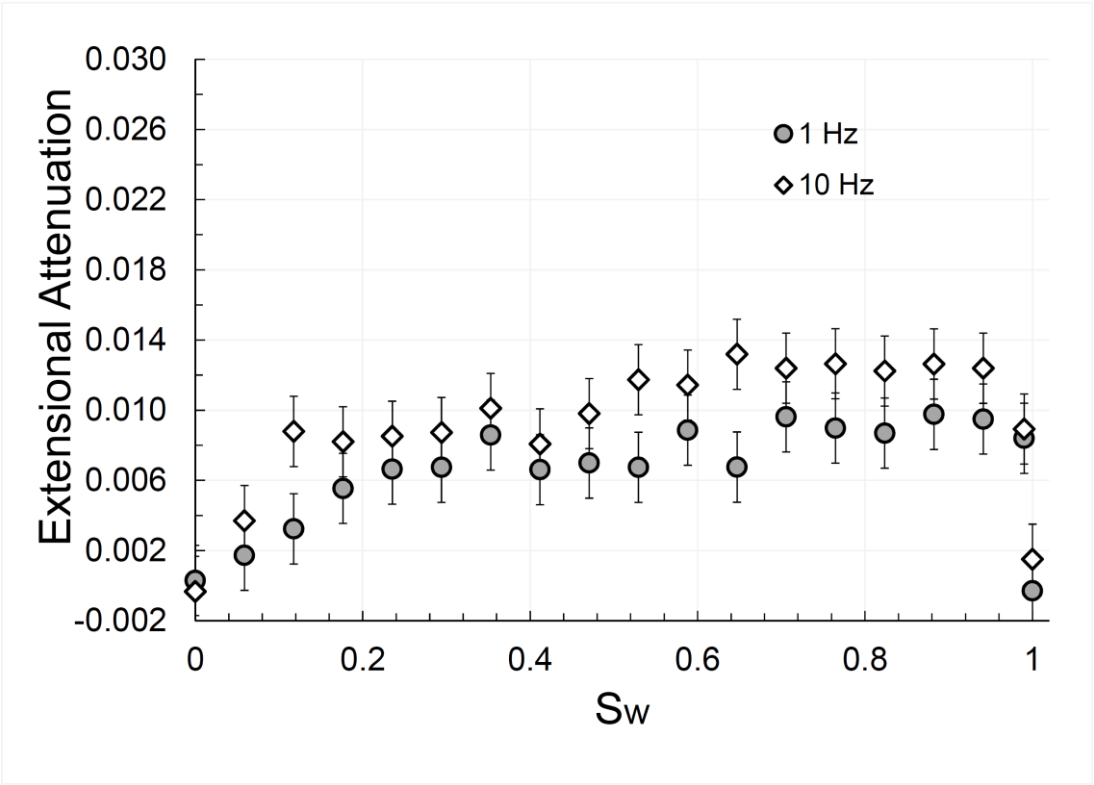

Figure 5.11 The dependencies of the extensional attenuation on water saturation (Sw) measured in Savonnieres limestone sample B at frequencies of 1Hz and 10 Hz. Pore and confining pressures are the same as in Figure 5.7.

As was demonstrated by Lebedev et al. (2014), introducing distilled water to the Savonnieres limestone causes dissolution processes in the palisadic cement between ooids, as well as in the peloidal nuclei and ooid cortices, while there was no dissolution observed in n-decane saturated limestone. The comparison of the results obtained in the seismic-frequency and ultrasonic experiments carried out under n-decane- and water saturated conditions, shows that the dissolution processes associated with polarity of fluid is likely the main mechanism responsible for the changes of the elastic parameters of the water-saturated samples measured in this study.

The behavior of the extensional attenuation in the partly water-saturated Savonnieres limestone observed at two frequencies of 1 Hz and 10 Hz (Figure 5.11) is rather an unusual result of our tests. Let us analyze this situation in more detail.

In the second set of our measurements, the liquid saturating the sample is not completely sealed in the pore space, except for the last measurement point corresponding to 100% saturation, and can move in and out of the pores when variable stress is applied to the sample. These movements may cause attenuation similar to those observed in Spencer (1981) and in Paffenholz and Burkhardt (1989). The characteristic frequency of the peak of this attenuation can be estimated as a frequency where the wavelength of the Biot's slow compressional wave equals the size of a water-saturated patch in the sample (Dutta and Seriff 1979):

$$f_c = \frac{1}{\pi}\frac{kK_{\text{water}}}{\phi\eta h^2}. \tag{5.5}$$

If the measurement frequencies are much lower than the characteristic frequency f_c, there is enough time for the pressure in the pore space filled with water to equilibrate with the pressure in the pore space occupied by air, and we get a drained regime, where the measured moduli are close to those of the dry sample and the attenuation caused by relative motion between water and rock is little.

The lowest possible value of the frequency f_c in our experiments can be obtained when the size of the water saturated patch reaches the diameter of the sample and is equal to

$$f_c \approx 98 \text{ Hz}. \tag{5.6}$$

The found characteristic frequency of the attenuation peak is only one and two orders of magnitude greater than the frequencies (1 Hz and 10 Hz) used in our tests, which

indicates that the conditions of our measurements are not purely drained and the energy loss due to water motion might be noticeable. This can explain the behavior of the attenuation curves (Figure 5.11) observed in sample B, which grow steadily with saturation increase, accompanied by the corresponding increase of the patch size h and by the lowering of the frequency f_c, and drop at the stage, when the sample is fully saturated, the pore-fluid lines are closed and any movement of liquid in the pores becomes impossible, i.e. when the experimental condition is transformed to undrained.

The dependences presented on Figure 5.11 display very low attenuation at 0 and 100% water saturation and the attenuation distribution smoothly varying between these two points. The low level of attenuation at zero and full aturation agrees with the experiments carried out under closed boundary conditions (see, e.g., Cadoret et al. 1998). As was shown in Knight and Nolen-Hoeksema (1990) and Cadoret et al. (1995), the shape of the attenuation distribution over saturation depends on a method of water saturation. Imbibition of water to a rock (the technique used in this study) provides relatively homogeneous saturation when drainage produces heterogeneous saturation strongly depending on the saturation history (Yin et al. 1992, Cadoret et al. 1995). For example, the attenuation measurements of Yin et al. (1984) conducted on high-permeability (568 mD) brine-saturated sandstone at frequencies of 1600 Hz to 1800 Hz demonstrate attenuation peaks at 97 % brine saturation in the imbibition tests and at 90 % brine saturation in the drainage experiment. The numerical experiments presented by Helle et al. (2003) showed that in a partially saturated rock with closed boundaries and uniform distribution of water, the behavior of attenuation peaks is strongly dependent on the permeability of the rock. They demonstrate that the decrease in permeability from 550 mD to 100 mD at a frequency of 100 kHz decreases the attenuation peak more than threefold and shifts it towards 60 % water saturation. Based on these results, we assume that the attenuation dependence on saturation obtained for sample B is determined by two factors: (i) the difference between the frequency of the harmonic stress applied to the sample and the characteristic frequency f_c presented by equation 5.5, and (ii) the relatively low permeability of the sample.

5.6 Conclusions

We present the results of two sets of laboratory measurements designed to assess the effects associated with fluid saturation on elastic and anelastic parameters of carbonates. The experiments were carried on two Savonnieres limestone samples with identical mineralogy and similar petrophysical parameters.

In the first set of the laboratory tests performed at seismic (0.1 Hz - 120 Hz) and ultrasonic (0.5 MHz) frequencies and at differential pressure of 15 MPa, the effects of full saturation with nonpolar (n-decane) and polar (distilled water) fluids were studied. The important finding of these experiments is the fact that the bulk modulus measured under either n-decane or water saturated conditions is consistent with Gassmann's theory. We also observed no change in the shear modulus of n-decane saturated limestone, whereas the shear modulus of water saturated limestone is reduced by 6%. It was also found that the extensional attenuation measured under n-decane or water saturated condition is virtually indistinguishable from the attenuation obtained in the dry measurement.

In the second set of the experiments conducted at two seismic frequencies of 1 Hz and 10 Hz and at a confining pressure of 10 MPa, we studied the dependences of elastic moduli and extensional attenuation on water saturation.

It was found that the measured bulk modulus decreases with the saturation increase and sharply rises by 27 % upon full saturation, while the shear modulus decreases until the modulus reduction reaches 6% at full saturation. Our analysis shows that for nonzero water saturation the measured bulk modulus is close to the predictions of the Gassmann-Wood model.

One of the findings of our measurements is that polarity of a pore fluid may exert unequal changes in the shear and bulk moduli of limestone, with the shear modulus experiencing relatively larger decrease than the bulk modulus.

Our analysis of the attenuation results obtained for partially water-saturated limestone demonstrates that attenuation is dependent on the relationship between the frequency of the harmonic stress applied to the rock and the characteristic frequency at which the half wavelength of the Biot's slow compressional wave equals the size of a water saturated patch.

Chapter 6

Seismic dispersion and attenuation in shales - laboratory measurements

6.1 Introduction

Shales, generally considered as fine-grained sedimentary rocks composed of mud, clay minerals and silt-sized particles of other minerals (Speight, 2014), represent approximately 70% of all clastic sedimentary rocks covering the Earth's surface (Thompson and Turk, 1993). It is well established that shales are transversely isotropic (or hexagonal) materials, which is a result of a preferred alignment of the clay particles in the bedding plane and to some extent of the intrinsic anisotropy of individual clay platelets (Sayers, 1994). The increasing interest in shale oil and gas exploration requires development of different laboratory techniques for characterization of the elastic anisotropy of shales. The accurate measurements of shale anisotropy are essential for understanding the influence of the stress distribution on the elastic properties of shales (Dewhurst and Siggins, 2006; Kuila et al., 2011) as well as for predicting the near-wellbore stress concentrations during hydraulic fracturing (Suarez-Rivera et al., 2006). Most common laboratory practices used for measuring elastic anisotropy of shales operate at ultrasonic frequencies (e. g., Jones and Wang, 1981, Hornby, 1998; Dewhurst and Siggins, 2006; Wong et al., 2008; Malehmir et al., 2013), where dispersion and attenuation may be dominated by very different mechanisms than at seismic frequencies. Suarez-Rivera et al. (2001) tested Pierre and Mancos shale samples in four frequency ranges: static, seismic (7 Hz), sonic (0.4 kHz-9 kHz) and ultrasonic (150 kHz-1 MHz). Strong velocity dispersion was observed in the range from 10 kHz to 1 MHz for Pierre shale, and 1

kHz to 1 MHz for Mancos shale. Duranti et al. (2005) also reported strong velocity dispersion between 1 kHz and 1 MHz found in the West African shale. Bauer et al. (2015) measured the Young's modulus of the water-saturated Mancos shale at seismic (1 Hz – 800 Hz) and ultrasonic (1 MHz) frequencies and showed that for the samples saturated at a relative humidity of 75% and higher the characteristic frequencies of the modulus dispersion are in the sonic frequency band. Thus, the laboratory measurements of the elastic anisotropy of shales at seismic frequencies are an issue of significant importance.

Chapter 6 presents first the stress-strain methodology of the laboratory low-frequency measurements for estimating the elastic anisotropy parameters of shale, and then describes the application of this methodology to the investigation of the influence of water saturation on the P-wave anisotropy of shale.

The stress-strain methodology was tested on three fully water-saturated Wellington shale samples cored at 0°, 45° and 90° angles with respect to the bedding plane. The effect of water saturation on the P-wave anisotropy was studied using two Mancos shale specimens drilled in vertical and parallel directions to bedding. The laboratory tests were carried out using low-frequency apparatus presented in Chapter 1 at a relatively low confining pressure to avoid a laceration of strain gauges due to the high compressibility of both shales.

6.2 Determination of elastic anisotropy in shales

In this study, we assume that sedimentary shales meet the requirements of a polar or transversal isotropic (TI) symmetry. Using the Voigt notation, Hook's law for a TI medium with the axis of symmetry directed along x_3 -axis (x_3-axis is normal to the bedding plane which is defined by x_1 and x_2 axes), can be expressed as (e.g., Mavko *et al.* (2009))

$$\boldsymbol{E} = \boldsymbol{S}\boldsymbol{\Sigma}, \tag{6.1}$$

where strain $\boldsymbol{E}$, stress $\boldsymbol{\Sigma}$ and compliance $\boldsymbol{S}$ tensors are

$$\boldsymbol{E}=\begin{pmatrix}\varepsilon_1\\ \varepsilon_2\\ \varepsilon_3\\ \varepsilon_4\\ \varepsilon_5\\ \varepsilon_6\end{pmatrix},\ \boldsymbol{S}=\begin{pmatrix}s_{11} & s_{12} & s_{13} & 0 & 0 & 0\\ s_{12} & s_{11} & s_{13} & 0 & 0 & 0\\ s_{13} & s_{13} & s_{33} & 0 & 0 & 0\\ 0 & 0 & 0 & s_{44} & 0 & 0\\ 0 & 0 & 0 & 0 & s_{44} & 0\\ 0 & 0 & 0 & 0 & 0 & s_{66}\end{pmatrix},\ \boldsymbol{\Sigma}=\begin{pmatrix}\sigma_1\\ \sigma_2\\ \sigma_3\\ \sigma_4\\ \sigma_5\\ \sigma_6\end{pmatrix},\ s_{66}=2(s_{11}-s_{12}). \qquad (6.2)$$

It is useful for interpretation of the results of laboratory measurements to present the compliance matrix $\boldsymbol{S}$ via the TI Young's and shear moduli and Poisson's ratios associated with an experiment (Jaeger et al. 2013):

$$\boldsymbol{S}=\begin{pmatrix}\frac{1}{E_{11}} & -\frac{\nu_{12}}{E_{11}} & -\frac{\nu_{31}}{E_{33}} & 0 & 0 & 0\\ -\frac{\nu_{12}}{E_{11}} & \frac{1}{E_{11}} & -\frac{\nu_{31}}{E_{33}} & 0 & 0 & 0\\ -\frac{\nu_{31}}{E_{33}} & -\frac{\nu_{31}}{E_{33}} & \frac{1}{E_{33}} & 0 & 0 & 0\\ 0 & 0 & 0 & \frac{1}{G_{13}} & 0 & 0\\ 0 & 0 & 0 & 0 & \frac{1}{G_{13}} & 0\\ 0 & 0 & 0 & 0 & 0 & \frac{1}{G_{12}}\end{pmatrix}, \qquad (6.3)$$

where E_{ii} is the TI Young's modulus in the x_i - direction, ν_{ij} is the Poisson's ratio related to the compression in the x_i -direction and expansion in the x_j -direction, G_{ij} is the shear modulus in the x_i-x_j plane.

If the uniaxial dynamic stress σ_3 is applied along x_3 -axis to the sample cored in the x_3 -direction (further on referred to as V-sample), then $\sigma_1=\sigma_2=\sigma_4=\sigma_5=\sigma_6=0$ $\varepsilon_1=\varepsilon_2\neq\varepsilon_3$, $\varepsilon_4=\varepsilon_5=\varepsilon_6=0$, and the measurements conducted on the V-sample give the following relationships:

$$s_{33}=\frac{1}{E_{33}}=\frac{\varepsilon_3}{\sigma_3},\ s_{13}=-\frac{\nu_{31}}{E_{33}}=\frac{\varepsilon_1}{\sigma_3},\ \nu_{31}=-\frac{\varepsilon_1}{\varepsilon_3}. \qquad (6.4)$$

Let us now consider the low-frequency tests conducted on samples cored along a direction of $\theta \neq 0°$ with respect to the bedding plane, the compliance matrix $\boldsymbol{S}$ has to be rotated into the direction of the core symmetry as

$$\boldsymbol{S}' = N\boldsymbol{S}N^T, \tag{6.5}$$

where N is the Bond rotation matrix (Winterstein, 1990):

$$N = \begin{pmatrix} a_{11}^2 & a_{12}^2 & a_{13}^2 & a_{12}a_{13} & a_{13}a_{11} & a_{11}a_{12} \\ a_{21}^2 & a_{22}^2 & a_{23}^2 & a_{22}a_{23} & a_{23}a_{21} & a_{21}a_{22} \\ a_{31}^2 & a_{32}^2 & a_{33}^2 & a_{32}a_{33} & a_{33}a_{31} & a_{31}a_{32} \\ 2a_{21}a_{31} & 2a_{22}a_{32} & 2a_{23}a_{33} & a_{22}a_{33}+a_{23}a_{32} & a_{21}a_{33}+a_{23}a_{31} & a_{22}a_{31}+a_{21}a_{32} \\ 2a_{31}a_{11} & 2a_{32}a_{12} & 2a_{33}a_{13} & a_{12}a_{33}+a_{13}a_{32} & a_{13}a_{31}+a_{11}a_{33} & a_{11}a_{32}+a_{12}a_{31} \\ 2a_{11}a_{21} & 2a_{12}a_{22} & 2a_{13}a_{23} & a_{12}a_{23}+a_{13}a_{22} & a_{13}a_{21}+a_{11}a_{23} & a_{11}a_{22}+a_{12}a_{21} \end{pmatrix}, \tag{6.6}$$

a_{ij} are the elements of a rotation or symmetry orientation matrix A.

If we introduce a new coordinate system with the axes $x_1' = x_1$, x_2' and x_3', where x_3' is directed along the axis of the core symmetry and forms angle θ with respect to x_3, then for rotation about the x_1-axis by angle θ, A can be presented as

$$A = \begin{pmatrix} 1 & 0 & 0 \\ 0 & c & -s \\ 0 & s & c \end{pmatrix}, \tag{6.7}$$

where $c = \cos\theta$ and $s = \sin\theta$. For this rotation, the matrix N takes the form:

$$N = \begin{pmatrix} 1 & 0 & 0 & 0 & 0 & 0 \\ 0 & c^2 & s^2 & -cs & 0 & 0 \\ 0 & s^2 & c^2 & cs & 0 & 0 \\ 0 & 2cs & -2cs & c^2-s^2 & 0 & 0 \\ 0 & 0 & 0 & 0 & c & s \\ 0 & 0 & 0 & 0 & -s & c \end{pmatrix}, \tag{6.8}$$

where $c = \cos\theta$ and $s = \sin\theta$.

For $\theta = 90°$, we have

$$N = \begin{pmatrix} 1 & 0 & 0 & 0 & 0 & 0 \\ 0 & 0 & 1 & 0 & 0 & 0 \\ 0 & 1 & 0 & 0 & 0 & 0 \\ 0 & 0 & 0 & -1 & 0 & 0 \\ 0 & 0 & 0 & 0 & 0 & 1 \\ 0 & 0 & 0 & 0 & -1 & 0 \end{pmatrix}. \tag{6.9}$$

Thus, for the measurements on the horizontal sample (further on referred to as H-sample) the Hook's law can be written as:

$$\begin{pmatrix} \varepsilon_1 \\ \varepsilon_2 \\ \varepsilon_3 \\ 0 \\ 0 \\ 0 \end{pmatrix} = \begin{pmatrix} s_{11} & s_{13} & s_{12} & 0 & 0 & 0 \\ s_{13} & s_{33} & s_{13} & 0 & 0 & 0 \\ s_{12} & s_{13} & s_{11} & 0 & 0 & 0 \\ 0 & 0 & 0 & s_{44} & 0 & 0 \\ 0 & 0 & 0 & 0 & 2(s_{11}-s_{12}) & 0 \\ 0 & 0 & 0 & 0 & 0 & s_{44} \end{pmatrix} \begin{pmatrix} 0 \\ 0 \\ \sigma_3 \\ 0 \\ 0 \\ 0 \end{pmatrix}. \tag{6.10}$$

From equation 6.10 we get

$$s_{11} = \frac{1}{E_{11}} = \frac{\varepsilon_3}{\sigma_3},\ s_{12} = -\frac{\nu_{12}}{E_{11}} = \frac{\varepsilon_1}{\sigma_3},\ \nu_{12} = -\frac{\varepsilon_1}{\varepsilon_3}. \tag{6.11}$$

The component s_{44} can be found from the tests conducted on the sample cored along a direction of $\theta = 45°$ with respect to the bedding.

The Bond rotation matrix for $\theta = 45°$ is

$$N = \frac{1}{2}\begin{pmatrix} 2 & 0 & 0 & 0 & 0 & 0 \\ 0 & 1 & 1 & -1 & 0 & 0 \\ 0 & 1 & 1 & 1 & 0 & 0 \\ 0 & 2 & -2 & 0 & 0 & 0 \\ 0 & 0 & 0 & 0 & \sqrt{2} & \sqrt{2} \\ 0 & 0 & 0 & 0 & -\sqrt{2} & \sqrt{2} \end{pmatrix}. \tag{6.12}$$

Substituting expression 6.12 into equation 6.5 gives the relationship for element s_{44}:

$$s_{44} = \frac{4\varepsilon_3}{\sigma_3} - s_{11} - s_{33} - 2s_{13}. \tag{6.13}$$

Thus, using three plugs sampled in directions of 0°, 45° and 90° with respect to the bedding plane, all five independent components of the elastic compliance matrix can be determined:

$$s_{33} = \frac{e_3}{\sigma_3} = \frac{1}{E_{33}} = \frac{1}{E_V},\ s_{13} = \frac{e_1}{\sigma_3} = -\frac{\nu_{31}}{E_{33}} = -\frac{\nu_V}{E_V},\ \nu_{31} \equiv \nu_V = -\frac{e_1}{e_3},\ \text{–V-sample} \tag{6.14a}$$

$$s_{11}=\frac{e_1}{\sigma_1}=\frac{1}{E_{11}}=\frac{1}{E_H},\ s_{12}=\frac{e_2}{\sigma_1}=-\frac{\nu_{12}}{E_{11}}=-\frac{\nu_H}{E_H},\ \nu_{12}\equiv\nu_H=-\frac{e_2}{e_1},\ \text{–H-sample} \quad (6.14b)$$

$$s_{44}=s_{55}=\frac{4\varepsilon_3}{\sigma_3}-s_{11}-s_{33}-2s_{13}=\frac{4\varepsilon_3}{\sigma_3}-\frac{1}{E_{11}}-\frac{1}{E_{33}}+2\frac{\nu_{31}}{E_{33}}=\frac{4\varepsilon_3}{\sigma_3}-\frac{1}{E_H}-\frac{1}{E_V}+2\frac{\nu_V}{E_V},$$

– 45°-sample (6.14c)

where we used notation $E_H\equiv E_{11},\ E_V\equiv E_{33},\ \nu_V\equiv\nu_{31}$ and $\nu_H\equiv\nu_{12}$.

The relationships between the elements of the compliance and stiffness matrices can be found using the inverse compliance matrix:

$$C=\begin{pmatrix} c_{11} & c_{12} & c_{13} & 0 & 0 & 0 \\ c_{12} & c_{11} & c_{13} & 0 & 0 & 0 \\ c_{13} & c_{13} & c_{33} & 0 & 0 & 0 \\ 0 & 0 & 0 & c_{44} & 0 & 0 \\ 0 & 0 & 0 & 0 & c_{44} & 0 \\ 0 & 0 & 0 & 0 & 0 & (c_{11}-c_{12})/2 \end{pmatrix}$$

$$=\Delta^{-1}\begin{pmatrix} s_{11}s_{33}-s_{13}^2 & s_{13}^2-s_{12}s_{33} & (s_{12}-s_{11})s_{13} & 0 & 0 & 0 \\ s_{13}^2-s_{12}s_{33} & s_{11}s_{33}-s_{13}^2 & (s_{12}-s_{11})s_{13} & 0 & 0 & 0 \\ (s_{12}-s_{11})s_{13} & (s_{12}-s_{11})s_{13} & s_{11}^2-s_{12}^2 & 0 & 0 & 0 \\ 0 & 0 & 0 & \Delta/s_{44} & 0 & 0 \\ 0 & 0 & 0 & 0 & \Delta/s_{44} & 0 \\ 0 & 0 & 0 & 0 & 0 & \Delta/s_{66} \end{pmatrix}, \quad (6.15)$$

$\Delta=(s_{11}-s_{12})(s_{11}s_{33}+s_{12}s_{33}-2s_{13}^2)$.

Using equation 6.15, the non-zero components of the elastic stiffness matrix (inverse to the compliance matrix $\boldsymbol{S}$) can be found as follows

$$c_{11}=c_{22}=\frac{s_{11}s_{33}-s_{13}^2}{\Delta}=\frac{1}{\Delta}\cdot\frac{E_HE_V-\nu_V^2E_H^2}{E_H^2E_V^2}, \quad (6.16a)$$

$$c_{12}=c_{21}=\frac{s_{13}^2-s_{12}s_{33}}{\Delta}=\frac{1}{\Delta}\cdot\frac{E_H\nu_V^2+E_V\nu_H}{E_HE_V^2}, \quad (6.16b)$$

$$c_{13}=c_{23}=c_{31}=c_{32}=\frac{(s_{12}-s_{11})s_{13}}{\Delta}=\frac{1}{\Delta}\cdot\frac{\nu_V(\nu_H+1)}{E_HE_V}, \quad (6.16c)$$

$$c_{33}=\frac{s_{11}^2-s_{12}^2}{\Delta}=\frac{1}{\Delta}\cdot\frac{1-\nu_H^2}{E_H^2}, \quad (6.16d)$$

$$c_{44}=c_{55}=G_{13}=\frac{1}{s_{44}}, \quad (6.16e)$$

$$c_{66} = G_{12} = \frac{c_{11} - c_{12}}{2} = \frac{E_H}{2(1+\nu_H)}. \quad (6.16f)$$

$$\Delta=(s_{11} - s_{12})(s_{11}s_{33} + s_{12}s_{33} - 2s_{13}^2) = \frac{1}{E_H^2 E_V^2}(1+\nu_H)(E_V - \nu_H E_V - 2\nu_V^2 E_H). \quad (6.16g)$$

The TI phase velocities for the quasi P-wave (V_{QP}), quasi S-wave (V_{QS}) and pure S-wave (V_{SH}) polarized orthogonal to the quasi P-wave are given by (Mavko et al. 2009)

$$V_{QP} = (c_{11}\sin^2\theta + c_{33}\cos^2\theta + c_{44} + \sqrt{M})^{1/2}(2\rho)^{-1/2}, \quad (6.17a)$$

$$V_{QS} = (c_{11}\sin^2\theta + c_{33}\cos^2\theta + c_{44} - \sqrt{M})^{1/2}(2\rho)^{-1/2}, \quad (6.17b)$$

$$V_{SH} = (c_{66}\sin^2\theta + c_{44}\cos^2\theta)^{1/2}(\rho)^{-1/2}, \quad (6.17c)$$

$$M = [(c_{11} - c_{44})\sin^2\theta - (c_{33} - c_{44})\cos^2\theta]^2 + (c_{13} + c_{44})\sin^2 2\theta, \quad (6.17d)$$

where θ = 0°, 90° and 45° for V-. H- and 45°-sample, correspondingly.

The phase velocities for V-sample are:

$$V_{QP} = \sqrt{\frac{c_{33}}{\rho}},\ V_{QS} = V_{SH} = \sqrt{\frac{c_{44}}{\rho}} = \sqrt{\frac{G_{23}}{\rho}}, \quad (6.18)$$

and for H-sample:

$$V_{QP} = \sqrt{\frac{c_{11}}{\rho}},\ V_{QS} = \sqrt{\frac{c_{44}}{\rho}} = \sqrt{\frac{G_{23}}{\rho}},\ V_{SH} = \sqrt{\frac{c_{66}}{\rho}} = \sqrt{\frac{c_{11} - c_{12}}{2\rho}} = \sqrt{\frac{E_{11}}{2(1+\nu_{12})\rho}}, \quad (6.19)$$

The P-wave anisotropy of shale can be assessed using Thomsen's parameters ε and δ (Thomsen, 1986)

$$\varepsilon = \frac{c_{11} - c_{33}}{2c_{33}} = \frac{1}{2}\cdot\frac{\left(\frac{E_H}{E_V} - \frac{E_H^2}{E_V^2}\nu_V^2\right) - \left(1 - \nu_H^2\right)}{1 - \nu_H^2}, \quad (6.15)$$

$$\delta = \frac{(c_{13} + c_{44})^2 - (c_{33} - c_{44})^2}{2c_{33}(c_{33} - c_{44})}. \quad (6.16)$$

The relative difference between the *SH*-wave velocities in the horizontal and vertical directions can be estimated with Thomsen's parameter γ (Thomsen, 1986):

$$\gamma = \frac{c_{66} - c_{44}}{2c_{44}}. \quad (6.17)$$

6.3 Elastic anisotropy in the Wellington shale

6.3.1 Description of samples

The tests were carried out on three fully water-saturated Wellington shale samples cut in directions of 0°, 45° and 90° with respect to the bedding plane. The physical and petrographic parameters of the samples are presented in Tables 6.1 and 6.2. The photographs of the samples and SEM images of a typical thin section of the shale are presented in Figures 6.1 and 6.2, correspondingly. The gas permeability of the shale was estimated at < 1 μD, the porosity was found within the range from 8.9% to 9.1%.

Table 6.1 The physical parameters of the Wellington shale samples.

Sample	**Length, mm**	**Diameter, mm**	**Density, kg/m^3**
V-sample	73	38	2499
H-sample	45	38	2550
45°-sample	77	38	2487

Table 6.2 The mineral composition of Wellington shale.

Mineral	**%**
Quartz	22
Albite/ Anorthite	2
Orthoclase/ Microcline/ Anorthoclase	1
Pyrite	1
Anatase	<1
Calcite	31
Dolomite/ Ankerite	3
Kaolinite	9
Chlorite/ Vermiculite	<1
Mica/ Illite	5
Smectite	6
Illite-Smectite	19

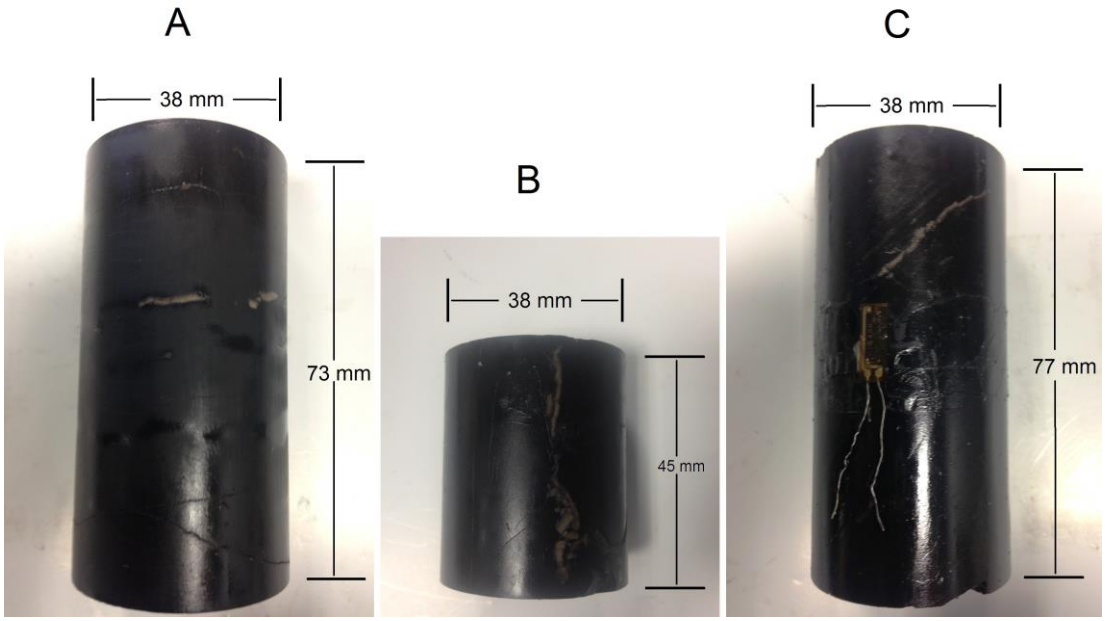

Figure 6.1 The V-, H- and 45°- samples of the Wellington shale.

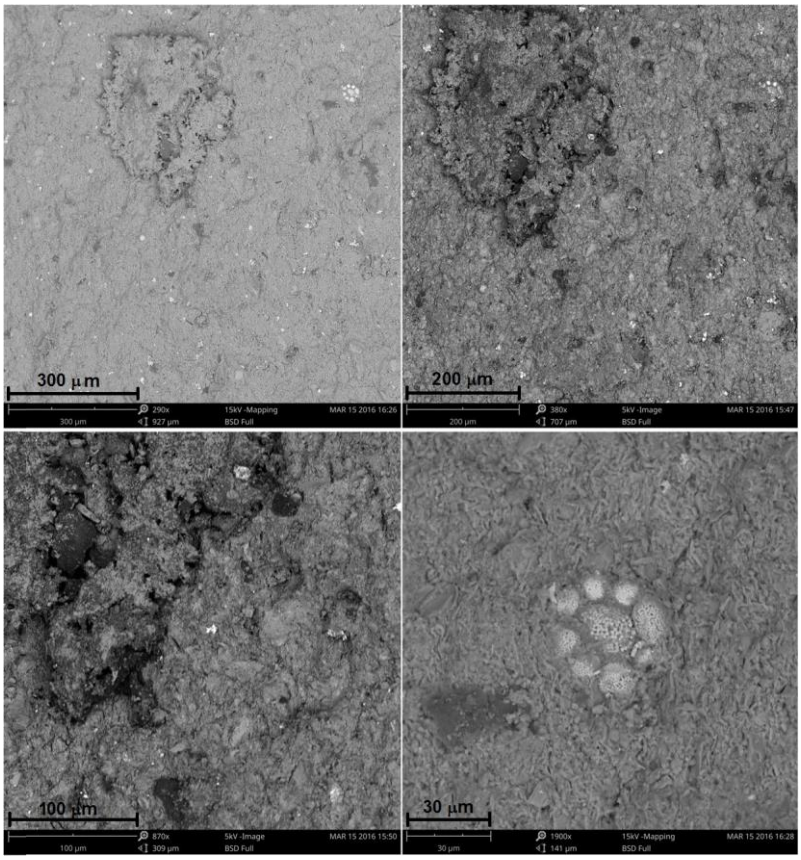

Figure 6.2 Microscopic images of a thin section of Wellington shale at two scales.

6.3.2 Results and Discussion

The laboratory measurements were conducted in the range of frequencies from 0.1 Hz to 100 Hz at a confining pressure of 6 MPa. The results of the measurements are presented in Figures 6.3–6.8. The dependences of the TI Young's moduli and Poisson's ratios on the frequency of stress oscillations are shown in Figures 6.3 and 6.4, correspondingly. Six components c_{11}, c_{12}, c_{13}, c_{33}, c_{44} and c_{66} of the elastic stiffness tensor and Thomsen's anisotropy parameters are given in Figures 6.5 and 6.6. Figure 6.7 presents four velocities $\sqrt{c_{11}/\rho}$, $\sqrt{c_{33}/\rho}$, $\sqrt{c_{44}/\rho}$ and $\sqrt{c_{66}/\rho}$ versus frequency. Inasmuch as the velocities $\sqrt{c_{11}/\rho}$ and $\sqrt{c_{66}/\rho}$ correspond to the quasi P-wave V_{QP} and pure S-wave V_{SH} velocities in the horizontal shale sample, the density ρ used for computing these velocities is the density of H-sample, whereas for the velocity $\sqrt{c_{33}/\rho}$ representing quasi S-wave velocity V_{QS} in the vertical specimen, ρ is the density of V-sample (Table 6.1). The extensional attenuation measured in the samples is given in Figure 6.8. The uncertainty of the attenuation measurements is ± 0.003.

Let us consider the results obtained for extensional attenuation in more detail. In our consideration, we assume that the samples are fully water saturated, and that the characteristic size of water-saturated patches is equal to the length of the samples. The characteristic frequency f_c of attenuation peaks in partially water saturated rock can be estimated using equation 2.1

$$f_c = \frac{1}{\pi}\frac{kK_f}{\phi\eta h^2},$$

where η = 8.9·10^{-4} Pa·s is the water viscosity, ϕ =0.09 is the porosity of the shale, K_f = 2.2 GPa is the bulk modulus of water, k is the shale permeability, h =0.07 m is the characteristic size of the water patch. Since the permeability for the Wellington shale does not exceed 1 μD, we obtain $f_c \approx 0.0016$ Hz. Therefore, the lower limit of the seismic frequencies used in our experiments might be three orders higher than the characteristic frequency f_c of the attenuation peak and, as a result, all our measurements are conducted in the non-dispersive frequency range.

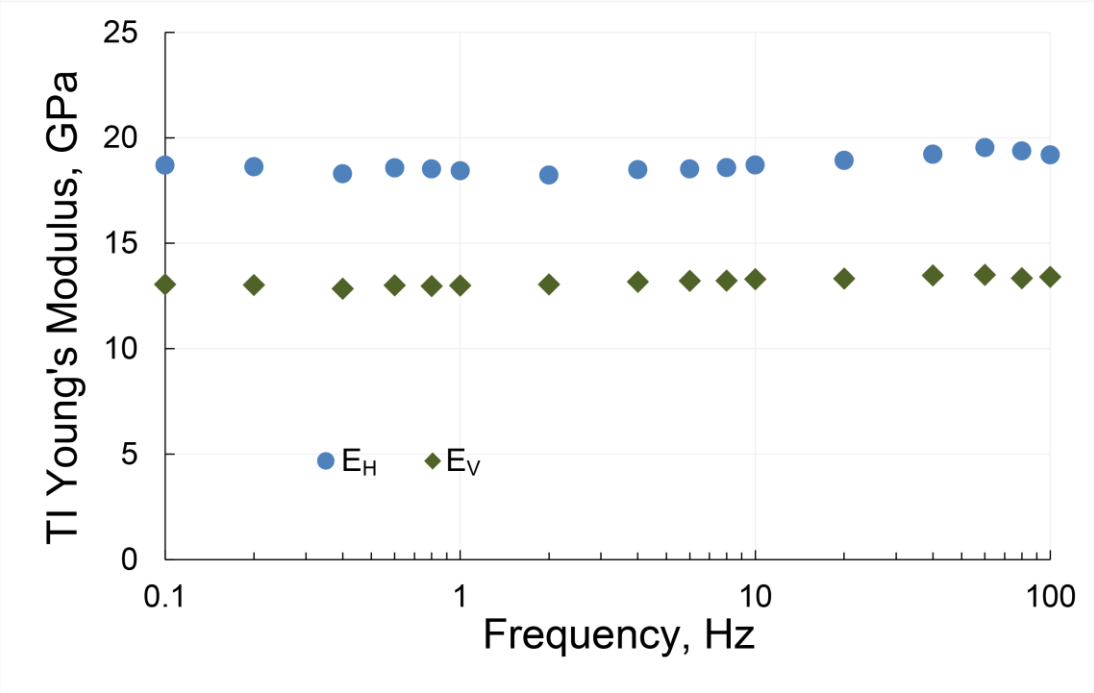

Figure 6.3 The TI Young's moduli E_H and E_V measured on the horizontal and vertical shale samples at a confining pressure of 6 MPa.

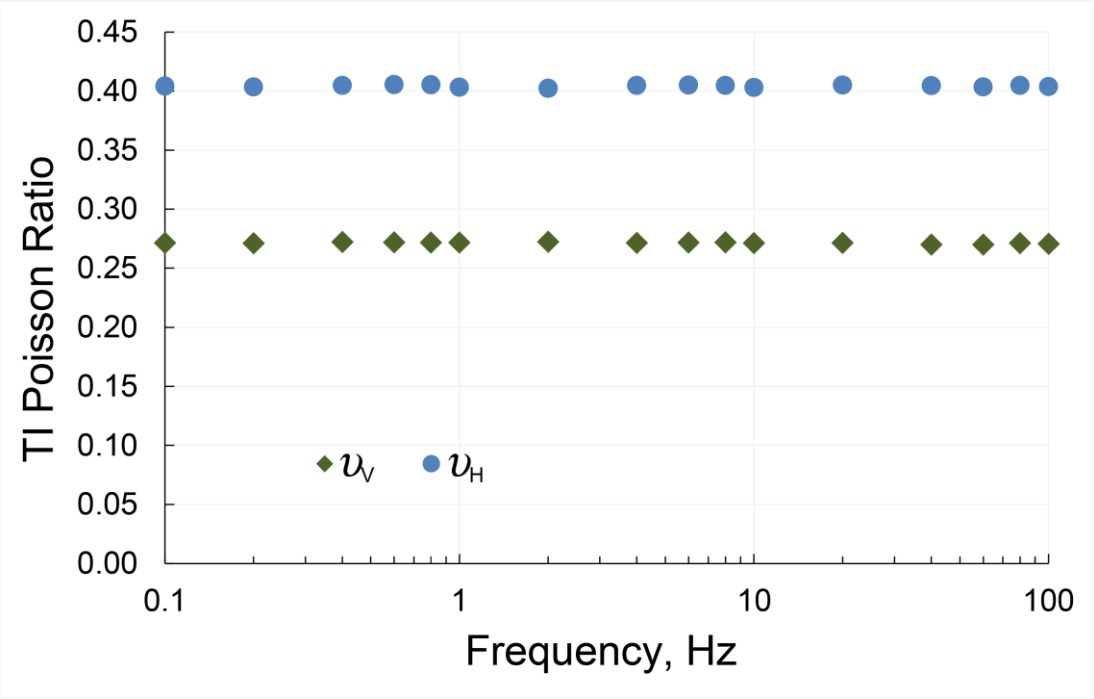

Figure 6.4 The TI Poisson's ratios ν_V and ν_H measured on the vertical and horizontal samples at a confining pressure of 6 MPa.

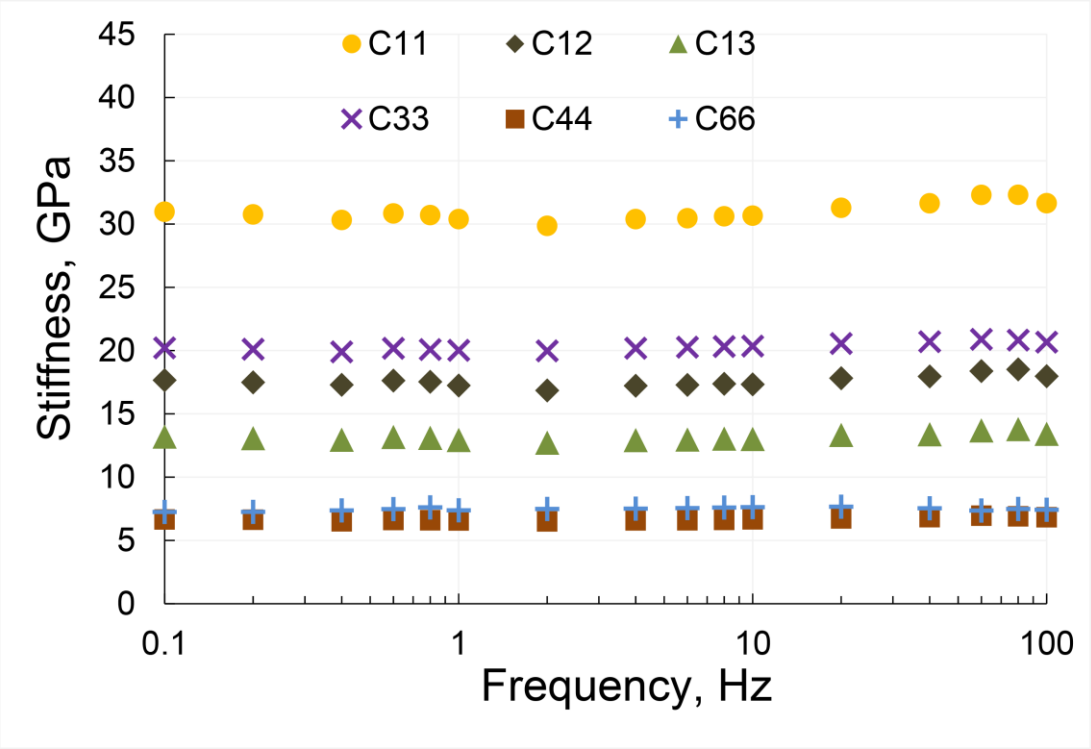

Figure 6.5 The components c_{11}, c_{12}, c_{13}, c_{33}, c_{44} and c_{66} of the elastic stiffness tensor computed for the Wellington shale samples.

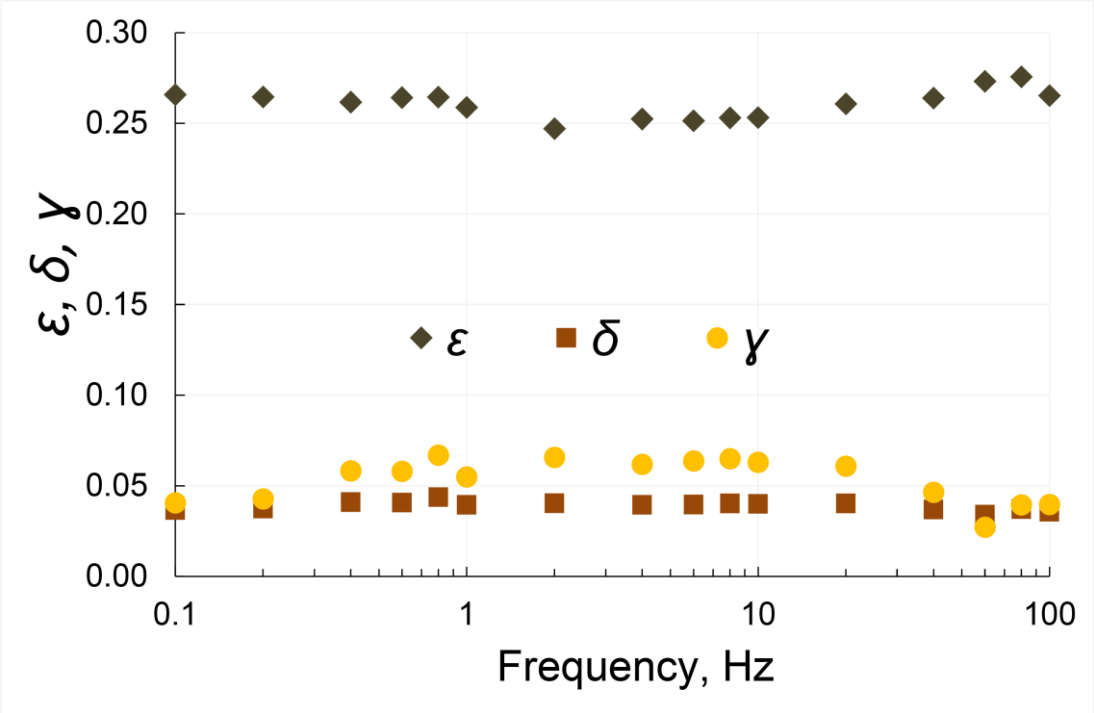

Figure 6.6 Thomsen's anisotropic parameters ε, δ and γ calculated for the Wellington shale.

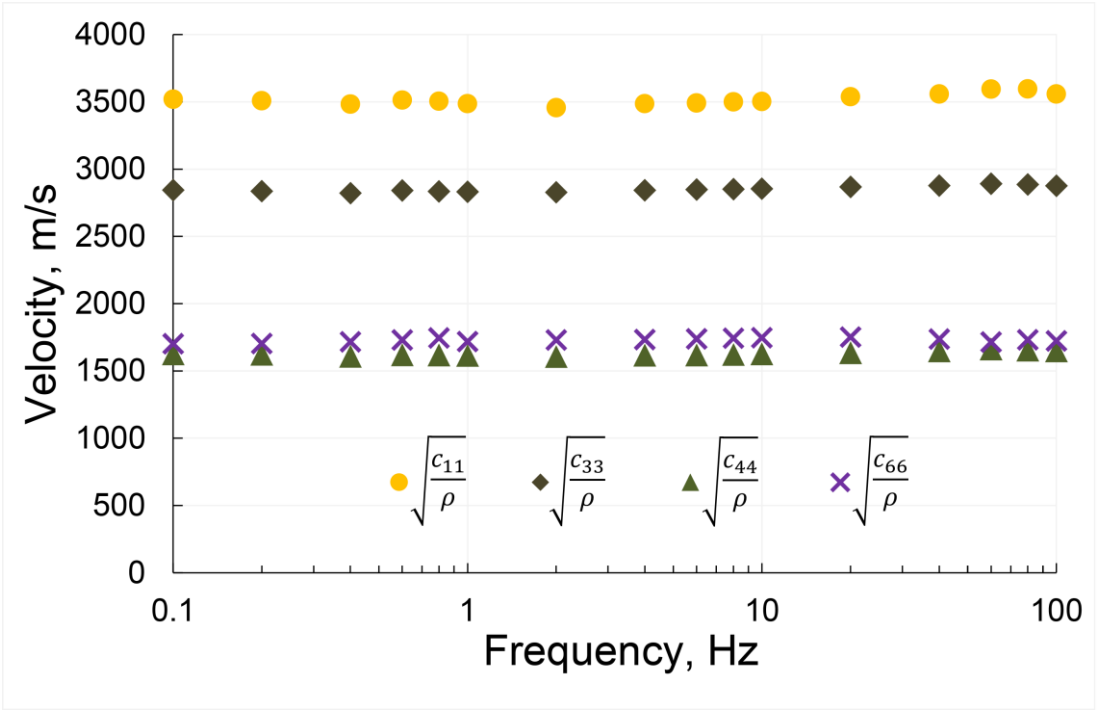

Figure 6.7 The computed velocities $\sqrt{\frac{c_{11}}{\rho}}$, $\sqrt{\frac{c_{33}}{\rho}}$, $\sqrt{\frac{c_{44}}{\rho}}$ and $\sqrt{\frac{c_{66}}{\rho}}$.

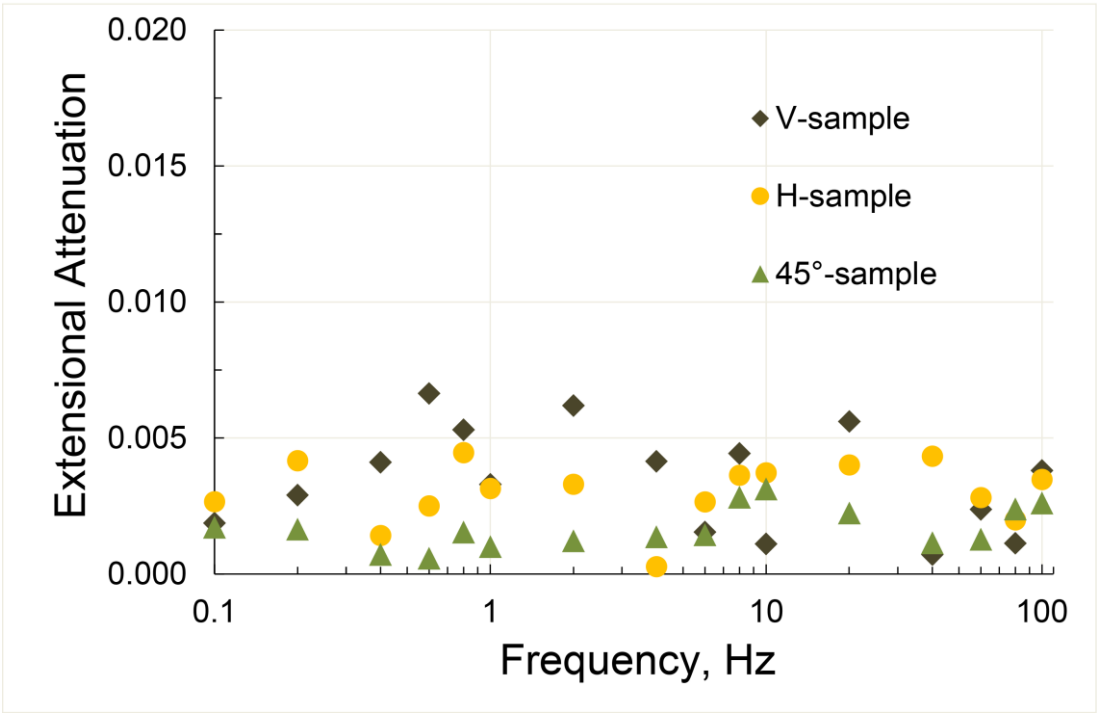

Figure 6.8 The extensional attenuation measured in the V-, H- and 45°- samples.

6.4 The impact of water saturation on the elastic anisotropy in the Mancos shale

6.4.1 Background

The Mancos Shale is one of the most prolific formations of the Western United States with the thickness ranging from 300 to 1500 meters that is genetically related to several Cretaceous Western Interior Seaway formations (Walker et al., 2015). The petroleum system and lithology of the Mancos Shale were investigated in numerous studies (see, e.g., Cole et al. (1997), Hampson et al. (1999) and Kirschbaum (2003)). There are several published studies devoted to laboratory measurements of the elastic properties carried out on the Mancos Shale samples. Suarez-Rivera et al. (2001) tested Mancos shale in four frequency ranges: static, seismic (~7 Hz), sonic (0.4 kHz – 9 kHz) and ultrasonic (150 kHz – 1 MHz). Over these ranges, the Mancos shale demonstrated a smooth and monotonic increase in compressional and shear wave velocities with frequency. Strong velocity dispersion was observed in the range from 1 kHz to 1 MHz with a transition frequency of ~ 10 kHz. The ultrasonic velocities were approximately 45% higher than the seismic velocity. Sarker and Batzle (2010) measured no significant dispersion from low (0.2 – 1000 Hz) to ultrasonic (800 kHz) frequencies for room-dry and n-decane saturated Mancos shale samples. Significant P-wave anisotropy was observed, in particular, for the dry sample. The anisotropy was significantly reduced as a result of saturation, primarily due to increasing the stiffness in the direction normal to bedding. Bauer et al. (2015) measured water-saturated Mancos shale at seismic (1 Hz – 800 Hz) and ultrasonic (1 MHz) frequencies and found an increase in dispersion of the dynamic Young's modulus with increasing water saturation accompanied by a gradual softening of the samples.

The purpose of the measurements conducted on Mancos shale is to quantify the saturation sensitivity of the shale in the seismic frequency range and investigate the influence of water saturation on the P-wave anisotropy of the shale.

6.4.2 Description of samples and experimental procedure

The physical parameters of both V- and H- samples (Figure 6.9) are as follows: length - 70 mm, diameter – 38 mm, density – 2500 kg/m^3 (at a relative humidity of 40 %). The gas permeability of the samples was estimated at < 1 μD. The XRD analysis of the samples is presented in Table 6.3. Using the data of samples' weights at different values of relative humidity (Table 6.4), the porosity of the samples was found equal to 5.7%.

The low-frequency tests were conducted at frequencies ranging between 0.1 Hz and 100 Hz under a confining pressure of 10 MPa. At each frequency the stress-strain readings of 100 oscillations were averaged to improve the signal-to-noise ratio of the signals obtained from strain gauges. The samples were saturated at relative humidities of 9, 32.5, 40, 52.5, 71 and 97.5%. In order to ensure a uniform saturation of the samples, the weights of the samples were monitored during the time of saturation, which was 50 days for each value of humidity.

Table 6.3 The mineral content of Mancos shale.

Mineral	%
Quartz	39.3
Illite	33.0
Chamosite	9.1
Apatite	10.8
Pyrite	7.8

Table 6.4 The masses of Mancos shale samples at different values of relative humidity.

Relative Humidity, %	Mass (V-sample), g	Mass (H-sample), g
9	197.44	197.13
32.5	198.14	197.81
40	198.43	198.05
52.5	199.02	198.66
71	200.25	199.86
97.5	202.00	201.64

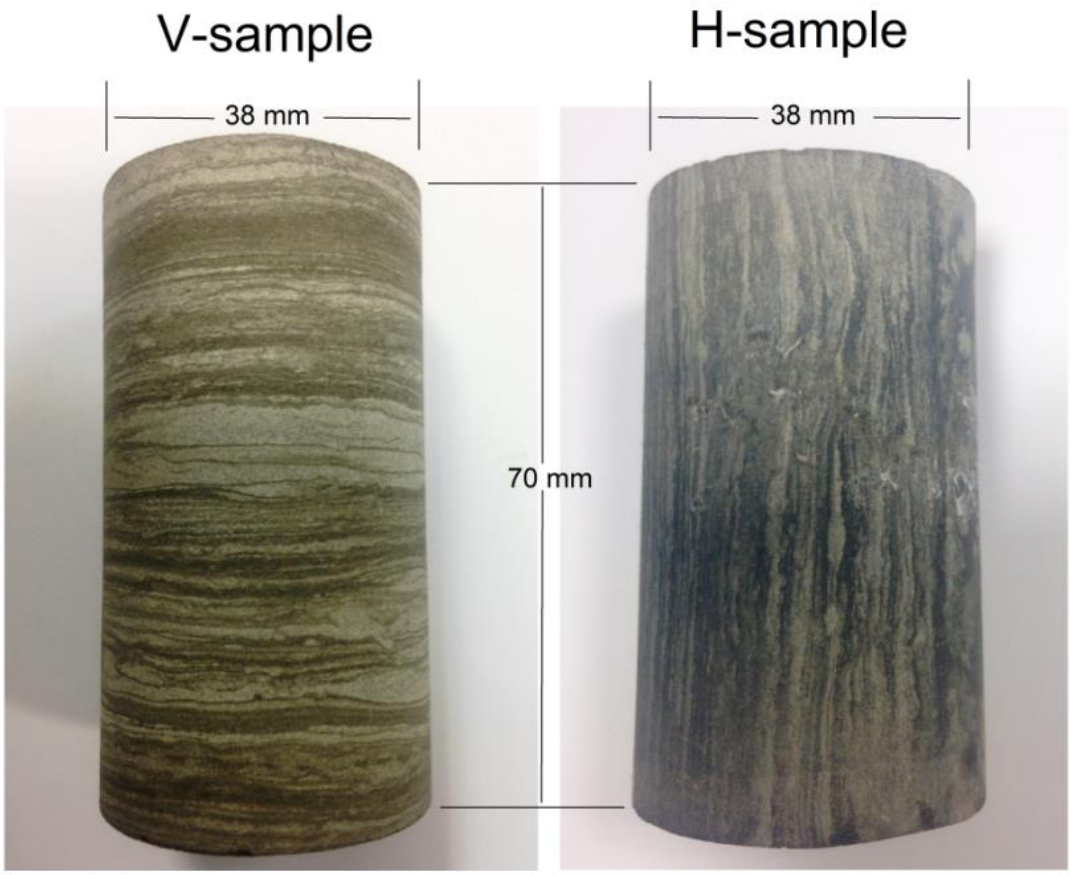

Figure 6.9 The vertical and horizontal samples of Mancos shale.

6.4.3 Results and discussion

The results of the measurements are presented in Figures 6.10 – 6.16. Figures 6.10 and 6.11 present the extensional attenuation versus frequency measured for V- and H-sample at different saturations. The dependences of the TI Young's moduli and Poisson ratios on the frequency of stress oscillations are shown in Figures 6.12 – 6.15. The P-wave anisotropy was estimated with Thomsen's parameter ε using equation 6.15 and presented in Figure 6.16.

As can be seen from Figures 6.10 and 6.11 the extensional attenuation measured in both V- and H-samples is insignificant at all saturations except the one corresponding to 97.5% of relative humidity. The dependences of attenuation obtained for the shale saturated at 97.5% humidity demonstrate two prominent peaks at 8 Hz (V-sample) and 40 Hz (H-sample). The characteristic frequency f_c of these peaks, which is described by equation 2.1, can be considered as a transition frequency separating the drained and undrained regimes. If the measurement frequencies are much lower than f_c, there is enough time for the pressure in the pore space filled with water to equilibrate with the pressure in the pore space occupied by air, and we get the drained regime where the measured moduli are close to those of the sample with empty pores and the attenuation caused by relative motion between water and rock is minimal. If the measurement frequencies are higher than f_c, we get the undrained regime where the pore pressure in saturated and unsaturated patches become different. In this case the Young's modulus of the sample is growing with saturation.

In our measurements at the lower frequencies, we observe a gradual softening of the samples with increasing saturation accompanied by the monotonic reduction of the Young's modulus (Figures 6.12 and 6.13) and growth of the P-wave anisotropy (Figure 6.16). At the higher frequencies corresponding to the undrained regime, the softening effect in the samples saturated at 97.5% humidity is partly counterbalanced by the dispersion of the Young's modulus, which also leads to the decrease of anisotropy.

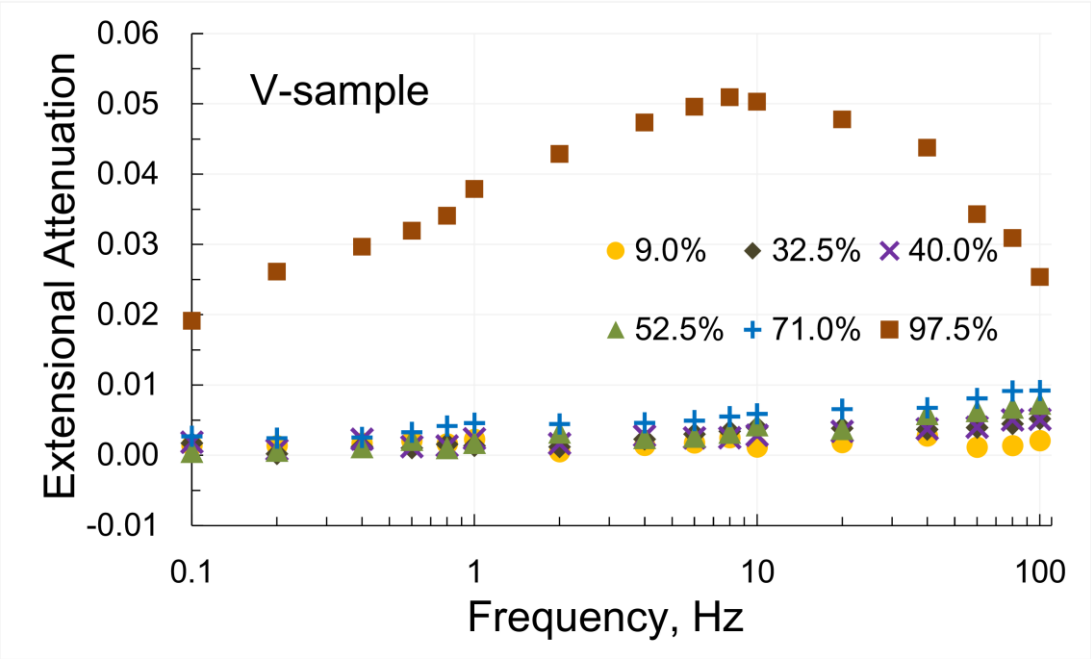

Figure 6.10 The extensional attenuation measured in the vertical sample at a confining pressure of 10 MPa.

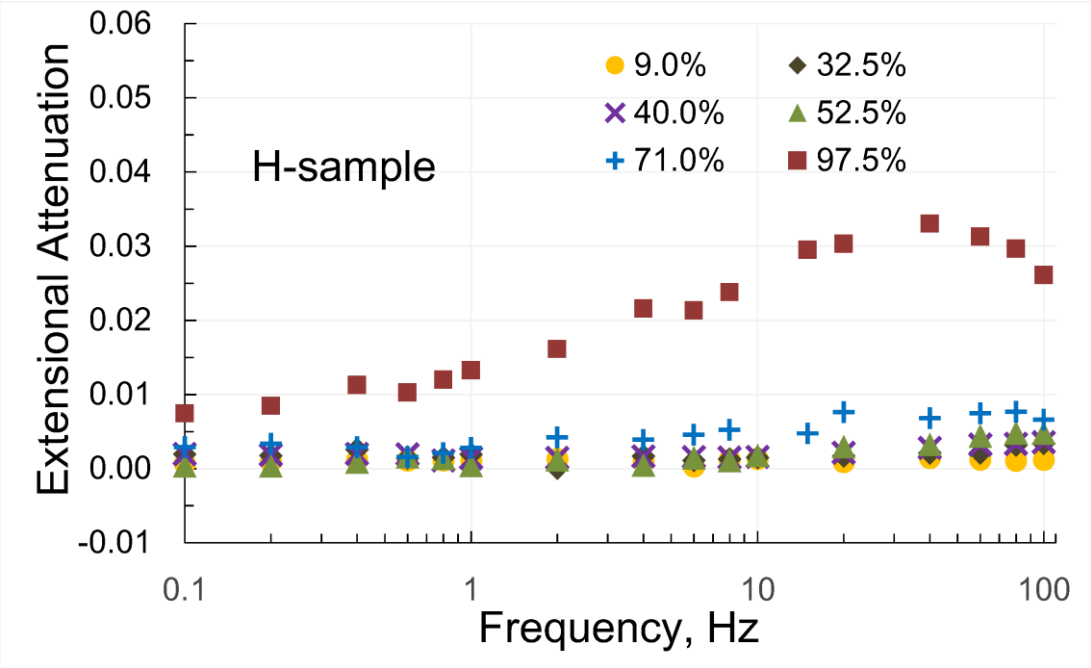

Figure 6.11 The extensional attenuation measured in the horizontal sample at a confining pressure of 10 MPa.

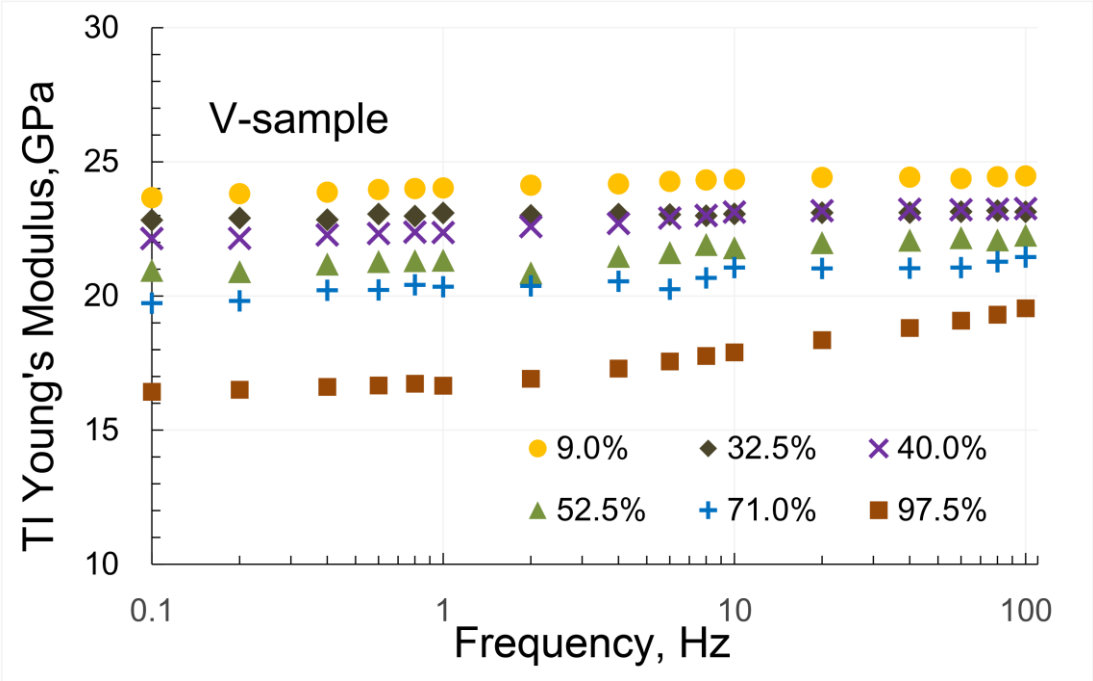

Figure 6.12 The TI Young's modulus E_V measured on the vertical shale sample at a confining pressure of 10 MPa.

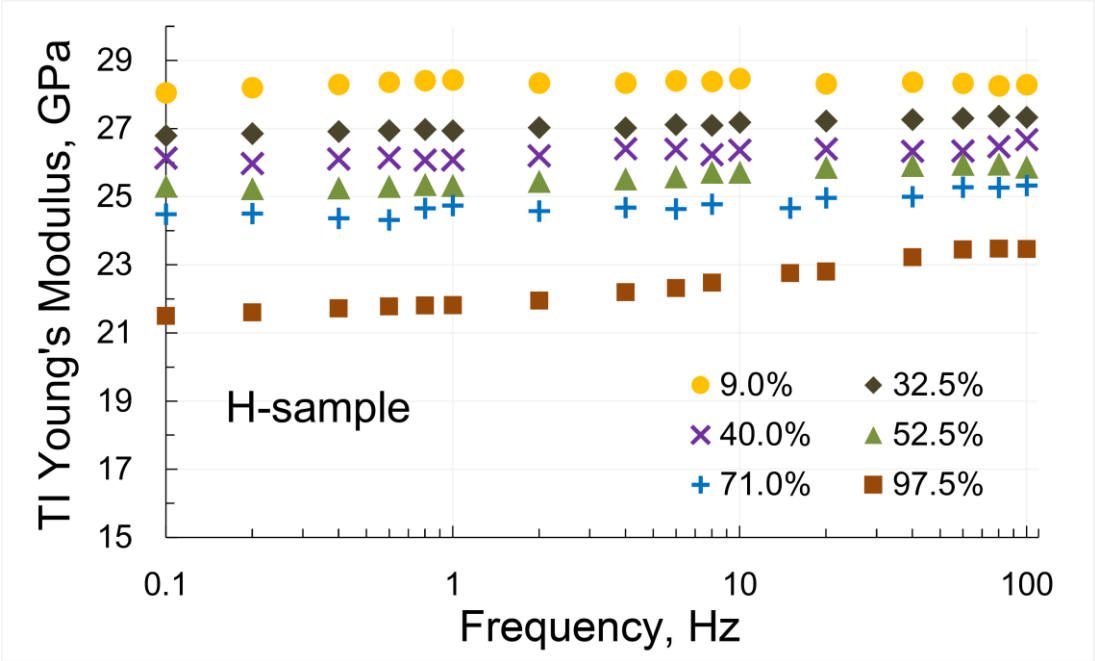

Figure 6.13 The TI Young's modulus E_H measured on the horizontal shale sample at a confining pressure of 10 MPa.

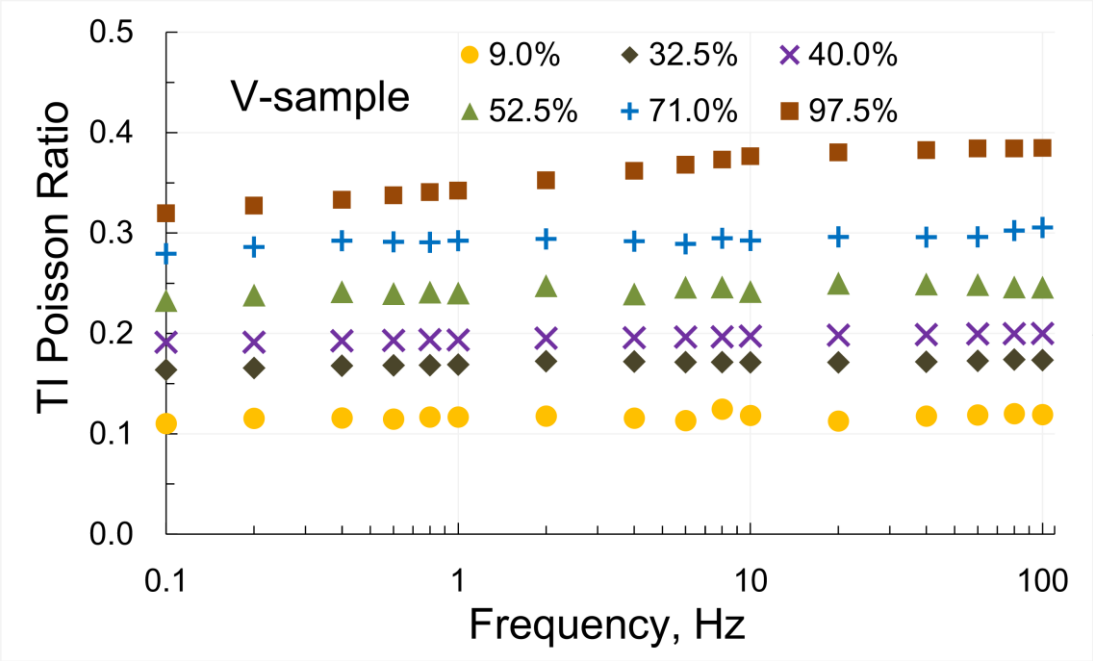

Figure 6.14 The TI Poisson ratio ν_V measured on the vertical sample at a confining pressure of 10 MPa.

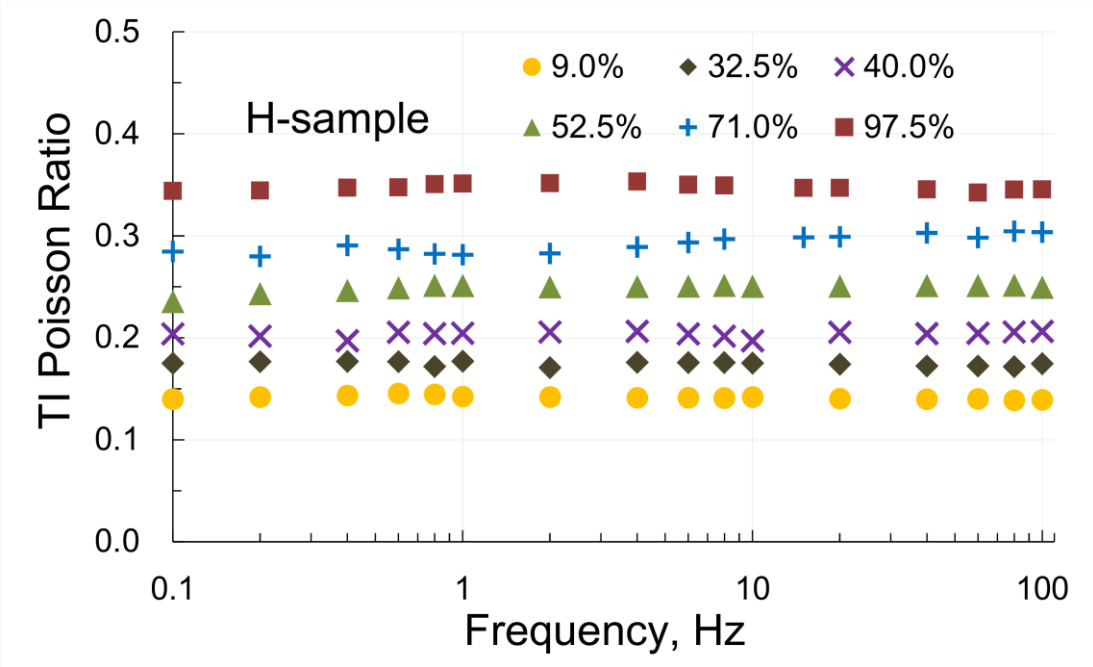

Figure 6.15 The TI Poisson ratio ν_H measured on the horizontal sample at a confining pressure of 10 MPa.

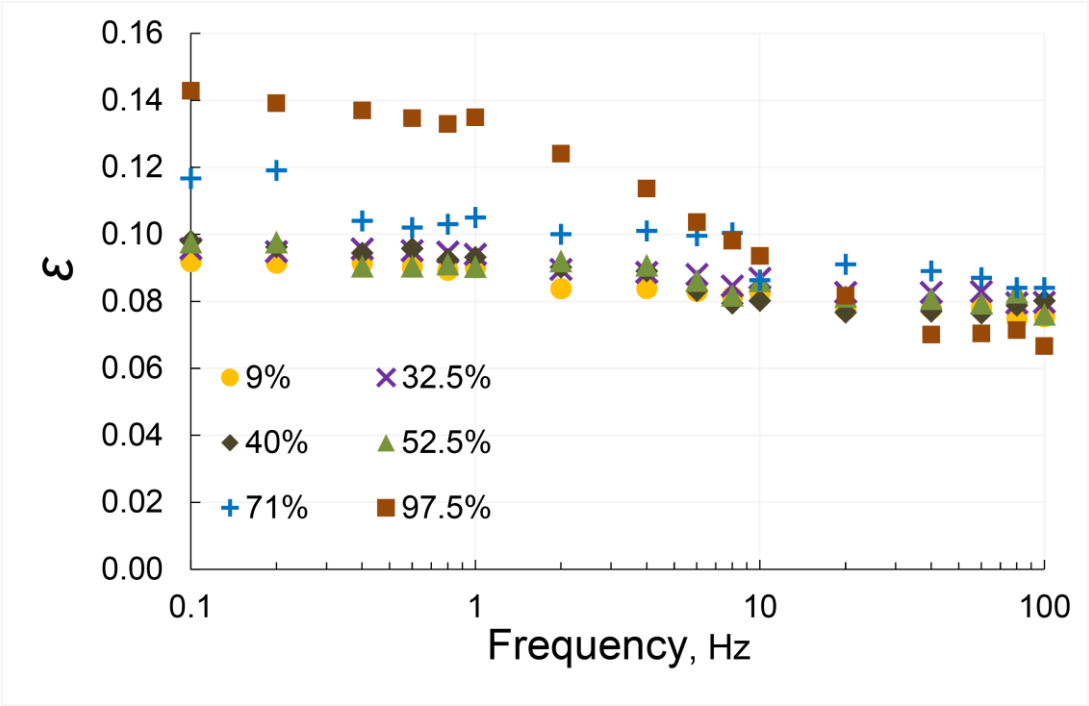

Figure 6.16 The P-wave anisotropy estimated via Thomsen parameter ε for the samples saturated with water at relative humidities of 9% to 97.5%.

6.5 Conclusions

The laboratory stress-strain measurements of shale anisotropy offer an important advantage over traditional ultrasonic methods. The low-frequency methodology of estimating the anisotropy parameters presented in the first part of Chapter 6 allows to avoid the difficulty in the interpretation of seismic data using the results obtained at ultrasonic frequencies. The experimental tests conducted on Wellington shale demonstrate that using three samples cored at 0°, 45° and 90° with respect to the bedding plane of a shale formation, it is possible to estimate all five independent elastic constants, which are necessary for characterization of a TI medium, as well as seismic velocities and Thomsen's anisotropy parameters. Our analysis also demonstrates that a peak of attenuation in fully water-saturated shale samples of the standard size used in laboratory tests can be at a frequency of a few orders lower than the lower frequency limit of the seismic-frequency measurements.

The developed methodology of low-frequency laboratory measurements on shales was used to study the elastic and anelastic properties of two vertical and horizontal Mancos shale samples saturated with water at relative humidities of 9, 32.5, 40, 52.5, 71 and 97.5%. The laboratory tests were conducted in the frequency range of 0.1 Hz to 100 Hz at a confining pressure of 10 MPa.

The experimental data show an increased softening of the samples which manifests itself as the Young's modulus reduction with increasing saturation. When both vertical and horizontal samples were saturated at a relative humidity of 97.5 %, the softening at the higher frequencies was partly compensated by the modulus dispersion.

Our measurements also demonstrate that the modulus dispersion, which occurs when the samples are saturated at a relative humidity of 97.5 %, can significantly decrease the P-wave anisotropy.

Chapter 7

Thesis conclusions

The main objective of this project is to develop and validate an experimental approach based on a stress-strain technique which could be used for LF laboratory investigations of the elastic and anelastic properties of the sedimentary rocks such as sandstones, carbonates and shales. This general task was specified in the following research topics. First, we designed and tested a new FO apparatus based on the strain-stress relationship which operates at frequencies of 0 to 100 Hz and measures the complex Young's moduli and Poisson ratio of rock samples at confining or uniaxial pressures from 0 to 70 MPa (Chapter 1). The new apparatus was employed to investigate the elastic properties of water-saturated sandstones with low intrinsic permeability (Chapter 2). At the next stage, we used the experimental results of Chapters 1 and 2, and the results of the measurements on glycerol-saturated Berea sandstone to develop a procedure based on the Kramers-Kronig relation for verification of the data obtained in FO measurements (Chapter 3). Then, our research was focused on the experimental study of the following aspects of the behavior of sedimentary rocks: we examined the effects of supercritical CO_2 injection on the elastic and anelastic properties of Donnybrook sandstone and compared the obtained data with ultrasonic measurements (Chapter 4), and we investigated the impact of saturation with nonpolar (n-decane) and polar (distilled water) liquids on oolitic limestone (Chapter 5). Finally, we developed a methodology of the FO measurements of the transversely isotropic materials, which was applied to study the anisotropy parameters of water-saturated Wellington and Mancos shale (Chapter 6).

The first FO laboratory systems capable of measuring the complete set of elastic moduli (Young's, bulk and shear) were developed in 1990s (Spencer et al., 1994, Batzle et al., 1999). Since both systems are mounted inside a pressure vessel

filled with gas as a confining pressure medium, the dimensions of the systems are limited and their mass is insufficient to avoid spurious resonances in the mechanical parts (Batzle et al., 2006). In Chapter 1, we presented a FO laboratory setup based on the strain-stress method which was constructed in the Rock Physics Laboratory at the Department of Exploration Geophysics of Curtin University University (Mikhaltsevitch et al., 2011a, 2011b, 2012; Lebedev et al., 2012). The main distinctive features of the proposed design consist in using (i) liquid instead of gas as a confining pressure medium, (ii) a triaxial core holder comprising only a specimen to be tested which allows (iii) to significantly increase the mass of the setup in order to avoid the resonances in the mechanical assembly. The performance characteristics of the setup have been experimentally tested on Berea sandstone, Eagle Ford shale and polymethyl methacrylate (PMMA).

In the LF measurements discussed in Chapter 2, we found a significant dispersion of the bulk and Young's moduli in water/brine saturated low-permeability sandstones, accompanied by strong attenuation. It was demonstrated that the observed dispersion cannot result from the global flow mechanism and that a contribution of the mesoscopic heterogeneities to the dispersion is beyond the instrument's sensitivity. We concluded that the dispersion and attenuation observed in our experiments can be caused by the squirt flow. The results presented in Chapter 2 indicate that for low-permeability rocks the lower frequency limit of acoustic wave dispersion can be within the seismic bandwidth.

Inasmuch as the spurious mechanical resonances present a serious issue for the LF laboratory systems based on the FO approach, in Chapter 3 we developed a simple technique based on the Kramers-Kronig relation to validate the experimental data. The technique was applied to verify the measurements discussed in Chapters 1 and 2, and the results of the LF experiments conducted on glycerol-saturated Berea sandstone, which are described in Chapter 3. We demonstrated that the quantitative relationship between the extensional attenuation and the Young's modulus is consistent with the causality principle presented by the Kramers-Kronig relationship.

In Chapter 4 we discussed the results of the LF and ultrasonic measurements carried out on water saturated Donnybrook sandstone flooded with supercritical CO_2 ($scCO_2$). We found that the elastic moduli of the sandstone with $scCO_2$ measured at seismic and ultrasonic frequencies are close to the elastic moduli measured on the

dry rock. It was also shown that the Gassmann fluid substitution theory is applicable for estimating the elastic moduli of $scCO_2$-injected sandstones.

In Chapter 5, we considered the applicability of Gassmann's theory for predictions of the elastic moduli of water- and hydrocarbon-saturated Savonnieres limestone and the influence of partial water saturation on elastic properties of the rock. It was demonstrated that the bulk modulus of the limestone fully saturated either with n-decane or water is consistent with Gassmann's fluid substitution model. No changes were observed in the shear modulus of n-decane-saturated limestone, whereas the shear modulus of water-saturated limestone was noticeably reduced. The experiments with partial water-saturation demonstrated that the bulk modulus decreases with saturation to a lesser extent than the Young's and shear moduli. The extensional attenuation in the dry and fully water-saturated samples is insignificant, but it changes greatly when saturation is between 0 and 20% or 95% and 100%.

In Chapter 6, we presented an experimental technique to measure five independent compliance components required for characterizing a transversely isotropic medium, such as shale, and estimate Thomsen's anisotropy parameters. The technique was successfully used to characterise the elastic anisotropy of Wellington shale and to estimate the impact of partial water saturation on the stiffness tensor components c_{11} and c_{33}, and on the P-wave anisotropy of Mancos shale.

REFERENCES

Adam, L., 2009, Elastic and viscoelastic laboratory properties in carbonates: Doctor of Phylosophy, Colorado School of Mines.

Adam, L., and M. Batzle, 2007, Moduli dispersion and attenuation in limestones in the laboratory, SEG Technical Program Expanded Abstracts 2007, 1634-1638.

Adam, L., and M. Batzle, 2008, Elastic properties of carbonates from laboratory measurements at seismic and ultrasonic frequencies: The Leading Edge, **27**, 1026-1032.

Adam, L., M. Batzle, and I. Brevik, 2006, Gassmann's fluid substitution and shear modulus variability in carbonates at laboratory seismic and ultrasonic frequencies: GEOPHYSICS, **71**, F173–F183.

Adam, L., M. Batzle, K. T. Lewallen, and K. van Wijk, 2009, Seismic wave attenuation in carbonates: Journal of Geophysical Research, **114**, B06208.

Adam, L., and T. Otheim, 2013, Elastic laboratory measurements and modeling of saturated basalts: Journal of Geophysical Research: Solid Earth, **118**, 840-851.

Adelinet, M., J. Fortin, Y. Gueguen, A. Schubnel, and L. Geoffroy, 2010, Frequency and fluid effects on elastic properties of basalt: Experimental investigations: Geophysical Research Letters, **37**, L02303.

Agersborg, R., T. A. Johansen, M. Jakobsen, J. Sothcott, and A. Best, 2008, Effects of fluids and dual-pore systems on pressure-dependent velocities and attenuations in carbonates: GEOPHYSICS, **73**, N35-N47.

Ahr, W. M., 2008, Geology of carbonate reservoirs: the identification, description, and characterization of hydrocarbon reservoirs in carbonate rocks: Wiley.

Alemu, B. L., E. Aker, M. Soldal, Ø. Johnsen, and P. Aagard, 2013, Effect of sub-core scale heterogeneities on acoustic and electrical properties of a reservoir rock: a CO_2 flooding experiment of brine saturated sandstone in a computed tomography scanner: Geophysical Prospecting, **61**, 235-250.

Angel, R. J., R. M. Hazen, T. C. McCormick, C. T. Prewitt, and J. R. Smyth, 1988, Comparative compressibility of end-member feldspars: Physics and Chemistry of Minerals, **15**, 313-318.

Assefa, S., C. McCann, and J. Sothcott, 1999, Attenuation of P- and S-waves in limestones: Geophysical Prospecting, **47**, 359–392.

Assefa, S., C. McCann, and J. Sothcott, 2003, Velocities of compressional and shear waves in limestones: Geophysical Prospecting, **51**, 1–13.

Baechle, G. T., G. P. Eberli, R. J. Weger, and J. L. Massaferro, 2009, Changes in dynamic shear moduli of carbonate rocks with fluid substitution: GEOPHYSICS, **74**, E135–E147.

Baechle, G. T., R. J. Weger, G. P. Eberli, J. L. Massaferro, and Y.-F. Sun, 2005, Changes of shear moduli in limestone rocks. Implications for Gassmann applicability: The Leading Edge, **24**, 507-510.

Batzle, M., D.-H. Han, and J. Castagna, 1999, Fluids and frequency dependent seismic velocity of rocks, SEG Technical Program Expanded Abstracts 1999, 5-8.

Batzle, M., and Z. Wang, 1992, Seismic properties of pore fluids: GEOPHYSICS, **57**, 1396-1408.

Batzle, M. L., D.-H. Han, and R. Hofmann, 2006, Fluid mobility and frequency-dependent seismic velocity - Direct measurements: GEOPHYSICS, **71**, N1–N9.

Behura, J., M. Batzle, R. Hofmann, and J. Dorgan, 2007, Heavy oils: Their shear story: GEOPHYSICS, **72**, E175-E183.

Bauer, A., D. Szewczyk, J. Hedegaard, and R. M. Holt, 2015, Seismic dispersion in Mancos shale, 3rd International Workshop on Rock Physics, 4.

Beggerow, G., 1980, High-pressure properties of matter, *in* K. Schäfer, ed., Landolt-Börnstein - Group IV Physical Chemistry: Springer, 4, 427.

Berryman, J. G., 1999, Origin of Gassmann's equations: GEOPHYSICS, **64**, 1627–1629.

Best, A. I., and C. McCann, 1995, Seismic attenuation and pore-fluid viscosity in clay-rich reservoir sandstones: GEOPHYSICS, **60**, 1386-1397.

Best, A. I., C. McCann, and J. Sothcott, 1994, The relationships between the velocities, attenuations and petrophysical properties of reservoir sedimentary rocks: Geophysical Prospecting, **42**, 151–178.

Biot, M. A., 1956, Theory of propagation of elastic waves in a fluid-saturated porous solid. I. Low-frequency range: The Journal of the Acoustical Society of America, **28**, 168–178.

Biot, M. A., 1956, Theory of propagation of elastic waves in a fluid saturated porous solid. II. Higher frequency range: Journal of the Acoustical Society of America, **28**, 179-191.

Birch, F., and D. Bancroft, 1938, The Effect of Pressure on the Rigidity of Rocks. I: The Journal of Geology, **46**, 59-87.

Birch, F., and D. Bancroft, 1938, The Effect of Pressure on the Rigidity of Rocks. II: The Journal of Geology, **46**, 113-141.

Birch, F., and D. Bancroft, 1938, Elasticity and internal friction in a long column of granite: Bulletin of the Seismological Society of America, **28**, 243-254.

Booij, H. C., and G. P. J. M. Thoone, 1982, Generalization of Kramers-Kronig transforms and some approximations of relations between viscoelastic quantities: Rheologica Acta, **21**, 15 – 24.

Bourbié, T., O. Coussy, and B. Zinszner, 1987, Acoustics of porous media: Gulf Publishing Company.

Bruckshaw, J. M., and P. C. Mahanta, 1961, The variation of the elastic constants of rocks with frequency: Geophysical Prospecting, **9**, 65-76.

Cadoret, T., D. Marion, and B. Zinszner, 1995, Influence of frequency and fluid distribution on elastic wave velocities in partially saturated limestones: Journal of Geophysical Research, **100**, 9789-9803.

Cadoret, T., G. Mavko, and B. Zinszner, 1998, Fluid distribution effect on sonic attenuation in partially saturated limestones: GEOPHYSICS, **63**, 154-160.

Cheng, N. S., 2008, Formula for the viscosity of a glycerol-water mixture: Industrial and Engineering Chemistry Research, **47**, 3285-3288.

Christensen, R. M., 1982, Theory of viscoelasticity : an introduction: Academic Press.

Cole, R. D., and R. G. Young, 1991, Facies characterization and architecture of a muddy shelf-sandstone complex: Mancos B interval of Upper Cretaceous Mancos Shale, northwest Colorado-northeast Utah, *in* A. D. Miall and N. Tyler, eds., The three-dimensional facies architecture of terrigenous clastic sediments and its applications for hydrocarbon discovery and recovery: Society of Economic Paleontologists and Mineralogists (SEPM), 3, 277-287.

D'Anna, G., and W. Benoit, 1990, Apparatus for dynamic and static measurements of mechanical properties of solids and of fluxlattice in typeII superconductors at low frequency (10^{-5}–10 Hz) and temperature (4.7–500 K): Review of Scientific Instruments, **61**, 3821-3826.

De Paula, O., M. Pervukhina, D. Makarynska, and B. Gurevich, 2012, Modeling squirt dispersion and attenuation in fluid-saturated rocks using pressure dependency of dry ultrasonic velocities: GEOPHYSICS, **77**, WA157 – WA168.

Derluyn, H., M. Griffa, D. Mannes, I. Jerjen, J. Dewanckele, P. Vontobel, D. Derome, V. Cnudde, E. Lehmann, and J. Carmeliet, 2011, Quantitative analysis of saline transport and crystallization damage in porous limestone visualized by neutron and X-ray imaging, *in* I. Ioannou and M. Theodoridou, eds., Proceedings SWBSS 2011 : Salt Weathering on Buildings and Stone Sculptures: EasyConferences, 47–54.

Dewhurst, D. N., and A. F. Siggins, 2006, Impact of fabric, microcracks and stress field on shale anisotropy: Geophysical Journal International, **165**, 135-148.

Dunn, K.-J., 1986, Acoustic attenuation in fluid-saturated porous cylinders at low frequencies: Journal of Acoustical Society of America, **79**, 1709 – 1721.

Duranti, L., R. Ewy, and R. Hofmann, 2005, Dispersive and attenuative nature of shales: Multiscale and multifrequency observations, SEG Technical Program Expanded Abstracts 2005, 1577-1580.

Dutta, N. C., and A. J. Seriff, 1979, On White's model of attenuation in rocks with partial gas saturation: GEOPHYSICS, **44**.

Dvorkin, J., and G. Mavko, 2006, Modeling attenuation in reservoir and nonreservoir rock: The Leading Edge, **25**, 194 – 197.

Dvorkin, J., G. Mavko, and A. Nur, 1995, Squirt flow in fully saturated rocks: GEOPHYSICS, **60**, 97–107.

Dvorkin, J., T. Taner, N. Derzhi, and G. Mavko, 2006, Attenuation at patchy saturation – a model, Extended Abstracts: 65th EAGE Conference & Exhibition: EAGE. E23.

Eberli, G. P., G. T. Baechle, F. S. Anselmetti, and M. L. Incze, 2003, Factors controlling elastic properties in carbonate sediments and rocks: The Leading Edge, **22**, 654–660.

Ellis, D. V., and J. M. Singer, 2007, Exploration Seismology: Springer Science.

Forster, A., B. Norden, K. Zinck-Jurgensen, P. Frykman, J. Kulenkampff, E. Spangenberg, J. Erzinger, M. Zimmer, J. Kopp, G. Borm, C. Juhlin, C. Cosma, and S. Hurter, 2006, Baseline characterization of the CO_2SINK geological storage site at Ketzin, Germany: Environmental Geosciences, **13**, 145 – 161.

Fronteau, G., C. Schneider-Thomachot, E. Chopin, V. Barbin, D. Mouze, and A. Pascal, 2010, Black-crust growth and interaction with underlying limestone microfacies, *in* R. Prykryl and A. Torok, eds., Natural Stone Resources for Historical Monuments: Geological Society of London, Special Publications, 333, 25-34.

Gassmann, F., 1951, Über die elastizität poröser medien: Vierteljahrsschrift der Naturforschenden Gesellschaft in Zürich, **96**, 1–23.

Gelinsky, S., S. A. Shapiro, T. M. Müller, and B. Gurevich, 1998, Dynamic poroelasticity of thinly layered structures: International Journal of Solids and Structures, **35**, 4739–4751.

Glubokovskikh, S., M. Lebedev, V. Mikhaltsevitch, and B. Gurevich, 2016, Generalized squirt theory for an arbitrary viscoelastic pore fill and partial saturation, SEG Technical Program Expanded Abstracts 2016 3513-3517.

Gordon, R. B., and L. A. Davis, 1968, Velocity and attenuation of seismic waves in imperfectly elastic rock: Journal of Geophysical Research, **73**, 3917–3935.

Gurevich, B., and S. L. Lopatnikov, 1995, Velocity and attenuation of elastic waves in finely layered porous rocks: Geophysical Journal International, **121**, 933-947.

Gurevich, B., D. Makarynska, O. De Paula, and M. Pervukhina, 2010, A simple model for squirt-flow dispersion and attenuation in fluid-saturated granular rocks: GEOPHYSICS, **75**, N109-N120.

Gurevich, B., A. P. Sadovnichaja, S. L. Lopatnikov, and S. A. Shapiro, 1998, Scattering of a compressional wave in a poroelastic medium by an ellipsoidal inclusion: Geophysical Journal International, **133**, 91-103.

Hampson, G. J., J. A. Howell, and S. S. Flint, 1999, A sedimentological and sequence stratigraphic re-interpretation of the Upper Cretaceous Prairie Canyon Member (“Mancos B”) and associated strata, Book Cliffs area, Utah, USA: Journal of Sedimentary Research, **69**, 414-433.

Hangx, S., A. Van der Linden, F. Marceils, and A. Bauer, 2013, The effect of CO_2 on the mechanical properties of the Captain Sandstone: Geological storage of CO_2 at the Goldeneye field (UK): International Journal of Greenhouse Gas Control, **19**, 609-619.

Helle, H. B., N. H. Pham, and J. M. Carcione, 2003, Velocity and attenuation in partially saturated rocks: poroelastic numerical experiments: Geophysical Prospecting, **51**, 551-566.

Hobbs, B. E., and H. C. Heard, 1986, Mineral and rock deformation: Laboratory Studies - The Paterson Volume: American Geophysical Union, e-book.

Hoefner, M. L., and H. S. Fogler, 1988, Pore evolution and channel during flow and reaction in porous media: AIChE Journal, **34**, 45-54.

Hornby, B. E., 1998, Experimental laboratory determination of the dynamic elastic properties of wet, drained shales: Journal of Geophysical Research: Solid Earth, **103**, 29945–29964.

Hughes, D. S., and H. J. Jones, 1950, Variation of elastic moduli of igneous rocks with pressure and temperature: Bulletin of the Geological Society of America, **61**, 843-856.

Hughes, D. S., and H. J. Jones, 1951, Elastic wave velocities in sedimentary rocks: Transactions of the American Geophysical Union, **32**, 173-178.

Ide, J. M., 1935, Some dynamic methods for determination of Young's modulus: Review of Scientific Instruments, **6**, 296-298.

Ide, J. M., 1936, An experimental study of the elastic properties of rocks: GEOPHYSICS, **1**, 347-352.

Jackson, I., 1986, The laboratory study of seismic wave attenuation, *in* B. E. Hobbs and H. C. Heard, eds., Mineral and rock deformation: Laboratory studies: American Geophysical Union, 11-24.

Jackson, I., and M. S. Paterson, 1987, Shear modulus and internal friction of calcite rocks at seismic frequencies: pressure, frequency and grain size dependence: Physics of the Earth and Planetary Interiors, **45**, 349-367.

Japsen, P., C. Høier, K. Rasmussen, I. Fabricius, G. Mavko, and J. Pedersen, 2002, Effect of fluid substitution on ultrasonic velocities in chalk plugs, South Arne field, North Sea, SEG Technical Program Expanded Abstracts 2002, 1881-1884.

Jones, L. E. A., and H. F. Wang, 1981, Ultrasonic velocities in Cretaceous shales from the Williston basin: GEOPHYSICS, **46**, 288-297.

Jones, T. D., 1986, Pore fluids and frequency-dependent wave propagation in rocks: GEOPHYSICS, **51**, 1939–1953.

Kirschbaum, M. A., 2003, Geologic assessment of undiscovered oil and gas resources of the Mancos/Mowry total petroleum system, Uinta-Piceance Basin Province, Utah and Colorado, Petroleum systems and geologic assessment of oil and gas in the Uinta-Piceance Province, Utah and Colorado: U.S. Geological Survey Digital Data Series DDS-69-B, 46 p.

Knight, R., and R. Nolen-Hoeksema, 1990, A laboratory study of the dependence of elastic wave velocities on pore scale fluid distribution: Geophysical Research Letters, **17**, 1529-1532.

Kuila, U., D. N. Dewhurst, A. F. Siggins, and M. D. Raven, 2011, Stress anisotropy in low porosity shale: Tectonophysics, **503**, 34-44.

Le Guen, Y., F. Renard, R. Hellmann, E. Brosse, M. Collombet, D. Tisserand, and J.-P. Gratier, 2007, Enhanced deformation of limestone and sandstone in the presence of high P_{CO2} fluids: Journal of Geophysical Research-Solid Earth, **112**, B05421.

Lebedev, M., M. Pervukhina, V. Mikhaltsevitch, T. Dance, O. Bilenko, and B. Gurevich, 2013, An experimental study of acoustic responses on the injection of supercritical CO_2 into sandstones from the Otway Basin: GEOPHYSICS, **78**, D293-D306.

Lebedev, M., M. E. J. Wilson, and V. Mikhaltsevitch, 2014, An experimental study of solid matrix weakening in water-saturated Savonnieres limestone: Geophysical Prospecting, **62**, 1253-1265.

Lei, X., and Z. Xue, 2009, Ultrasonic velocity and attenuation during CO_2 injection into water-saturated porous sandstone: Measurements using difference seismic tomography: Physics of the Earth and Planetary Interiors, **176**, 224-234.

Lemmon, E., M. McLinden, and D. Friend, 2011, Thermophysical properties of fluid systems.

Madonna, C., and N. Tisato, 2013, A new Seismic Wave Attenuation Module to experimentally measure low-frequency attenuation in extensional mode: Geophysical Prospecting, **61**, 302-314.

Malehmir, A., M. Andersson, M. Lebedev, M. Urosevic, and V. Mikhaltsevitch, 2013, Experimental estimation of velocities and anisotropy of a series of Swedish crystalline rocks and ores: Geophysical Prospecting, **61**, 153-167.

Marion, D., and D. Jizba, 1997, Acoustic properties of carbonate rocks: Use in quantitative interpretation of sonic and seismic measurements, *in* I. Palaz and K. J. Marfurt, eds., Carbonate Seismology, 75-94.

Mavko, G., 1979, Frictional attenuation: an inherent amplitude dependence: Journal of Geophysical Research: Journal of Geophysical Research: Solid Earth, **84**, 4769-4776.

Mavko, G., T. Mukerji, and J. Dvorkin, 2009, The rock physics handbook : tools for seismic analysis of porous media: Cambridge University Press.

Mavko, G., 1979, Frictional attenuation: an inherent amplitude dependence: Journal of Geophysical Research: Solid Earth, **84**, 4769-4776.

Mavko, G., and A. Nur, 1979, Wave attenuation in partially saturated rocks: GEOPHYSICS, **44**, 61-178.

Mikhaltsevitch, V., M. Lebedev, and B. Gurevich, 2011a, A low-frequency apparatus for characterizing the mechanical properties of rocks, 73rd EAGE Conference and Exhibition Incorporating SPE EUROPEC 2011: EAGE, P155.

Mikhaltsevitch, V., M. Lebedev, and B. Gurevich, 2011b, A low-frequency laboratory apparatus for measuring elastic and anelastic properties of rocks, SEG Technical Program Expanded Abstracts 2011, 2256-2260.

Mikhaltsevitch, V., M. Lebedev, and B. Gurevich, 2012, Low-frequency measurements of the mechanical parameters of sandstone with low permeability, ASEG Extended Abstracts 2012: 22nd Geophysical Conference, 1-4.

Lebedev M., V. Mikhaltsevitch, M. Lwin, B. Gurevich, 2012, An apparatus for and a method of characterising mechanical properties of a sample. Patent AU2011318229 granted in Australia on 22 January 2015.

Misaghi, A., S. Negahban, M. Landrø, and A. Javaherian, 2010, A comparison of rock physics models for fluid substitution in carbonate rocks: Exploration Geophysics, **41**, 146–154.

Müller, T. M., and B. Gurevich, 2005, A first-order statistical smoothing approximation for the coherent wave field in random porous media: Journal of the Acoustical Society of America, **117**, 1796 – 1805.

Müller, T. M., B. Gurevich, and M. Lebedev, 2010, Seismic wave attenuation and dispersion due to wave-induced flow in porous rocks - a review: GEOPHYSICS, **75**, A147-A164.

Murphy, W. F., 1982, Effects of partial water saturation on attenuation in Massilon sandstone and Vycor porous glass: Journal of the Acoustical Society of America, **71**, 1458–1468.

Murphy, W. F., 1984, Frame modulus reduction in sedimentary rocks: The effect of adsorption on grain contacts: Geophysical Research Letters, **1**, 805-808.

Murphy, W. M., K. W. Winkler, and R. L. Kleinberg, 1986, Acoustic relaxation in sedimentary rocks: Dependence on grain contacts and fluid saturation: GEOPHYSICS, **51**, 758-768.

Nakagawa, S., T. J. Kneafsey, T. M. Daley, B. M. Freifeld, and E. V. Rees, 2013, Laboratory seismic monitoring of supercritical CO_2 flooding in sandstone cores using the split Hopkinson resonant bar technique with concurrent X-ray computed tomography imaging: Geophysical Prospecting, **61**, 254-269.

Nelson, P. H., 2009, Pore-throat sizes in sandstones, tight sandstones, and shales: American Association of Petroleum Geologists Bulletin, **93**, 329-340.

Norris, A. N., 1993, Low-frequency dispersion and attenuation in partially saturated rocks: Journal of the Acoustical Society of America, **94**, 359-370.

Nover, G., J. Von Der Gönna, S. Heikamp, and J. Köster, 2013, Changes of petrophysical properties of sandstones due to interaction with supercritical carbon dioxide - a laboratory study: European Journal of Mineralogy, **25**, 317-329.

O'Connell, R. J., and B. Budiansky, 1977, Viscoelastic properties of fluid-saturated cracked solids: Journal of Geophysical Research, **82**, 5719-5735.

O'Donnel, M., E. T. Jaynes, and J. G. Miller, 1978, General relationships between ultrasonic attenuation and dispersion: Journal of the Acoustical Society of America, **63**, 1935–1937.

O'Donnel, M., E. T. Jaynes, and J. G. Miller, 1981, Kramers - Kronig relationship between ultrasonic attenuation and phase velocity: Journal of the Acoustical Society of America, **69**, 696-701.

Oikawa, Y., T. Takehara, and T. Tosha, 2008, Effect of CO_2 injection on mechanical properties of Berea Sandstone, 42nd US Rock Mechanics Symposium /2nd US-Canada Rock Mechanics Symposium.

Paffenholz, J., and H. Burkhardt, 1989, Absorption and modulus measurements in the seismic frequency and strain range on partially saturated sedimentary rocks: Journal of Geophysical Research, **94**, 9493–9507.

Palaz, I., and K. J. Marfurt, 1997, Carbonate seismology: Society of Exploration Geophysicists.

Palmer, I. D., and M. L. Traviolia, 1980, Attenuation by squirt flow in undersaturated gas sands: GEOPHYSICS, **45**, 1780-1792.

Peselnick, L., and W. F. Outerbridge, 1961, Internal friction in shear and shear modulus of Solenhofen limestone over a frequency range of 10^7 cycles per second: Journal of Geophysical Research, **66**, 581-588.

Peselnick, L., and I. Zietz, 1959, Internal friction of fine-grained limestones at ultrasonic frequencies: GEOPHYSICS, **24**, 285-296.

Pimienta, L., J. Fortin, and Y. Gueguen, 2015, Experimental study of Young's modulus dispersion and attenuation in fully saturated sandstones: GEOPHYSICS, **80**, L57-L72.

Pimienta, L., J. Fortin, and Y. Gueguen, 2016, Effect of fluids and frequencies on Poisson's ratio of sandstone samples: GEOPHYSICS, **81**, D183-D195.

Pride, S. R., 2005, Relationships between Seismic and Hydrological Properties, *in* Y. Rubin and S. S. Hubbard, eds., Hydrogeophysics: Springer Netherlands, 253-290.

Pride, S. R., J. G. Berryman, and J. M. Harris, 2004, Seismic attenuation due to wave-induced flow: Journal of Geophysical Research, **109**, B01201.

Pride, S. R., J. H. Harris, D. L. Johnson, A. Mateeva, K. T. Nihei, R. L. Nowack, J. W. Rector, H. Spetzler, R. Wu, T. Yamomoto, J. G. Berryman, and M. Fehler, 2003, Acquisition/processing-Permeability dependence of seismic amplitudes: The Leading Edge, **22**, 518-525.

Rafavich, F., C. H. S. C. Kendall, and T. P. Todd, 1984, The relationship between acoustic properties and the petrographic character of carbonate rocks: GEOPHYSICS, **49**, 1622-1636.

Rituparna, S., and B. Mike, 2010, Anisotropic elastic moduli of the Mancos B Shale-An experimental study, SEG Technical Program Expanded Abstracts 2010, 2600-2605.

Rochelle, C. A., I. Czernichowski-Lauriol, and A. E. Milodowski, 2004, The impact of chemical reactions on CO_2 storage in geological formations: a brief review: Geological Society, London, Special Publications, **233**, 87-106.

Røgen, B., I. L. Fabricius, P. Japsen, C. Høier, G. Mavko, and J. B. Pedersen, 2005, Ultrasonic velocities of North Sea chalk samples: Influence of porosity, fluid content and texture: Geophysical Prospecting, **53**, 481-496.

Ross, G. D., A. C. Todd, J. A. Tweedie, and A. G. S. Will, 1982, Dissolution effects of CO2-brine systems on the permeability of UK and North Sea calcareous sandstones, SPE/DOE Symposium on Enhanced Oil Recovery.

Sams, M. S., J. P. Neep, M. H. Worthington, and M. S. King, 1997, The measurement of velocity dispersion and frequency-dependent intrinsic attenuation in sedimentary rocks: GEOPHYSICS, **62**, 1456-1464.

Sarker, R., and M. Batzle, 2010, Anisotropic elastic moduli of the Mancos B Shale – An experimental study, SEG Technical Program Expanded Abstracts 2010.

Sayers, C. M., 1994, The elastic anisotropy of shales: Journal of Geophysical Research, **99**, 767-774.

Sayers, C. M., 2013, The effect of anisotropy on the Young's moduli and Poisson's ratios of shales: Geophysical Prospecting, **61**, 416 - 426.

Sharma, R., M. Prasad, G. Surve, and G. C. Katiyar, 2006, On the applicability of Gassmann model in carbonates, SEG Technical Program Expanded Abstracts 2006, 1866-1870.

Sheriff, R. E., and L. P. Geldart, 1995, Exploration Seismology: Cambridge University Press.

Shi, J.-Q., Z. Xue, and S. Durucan, 2007, Seismic monitoring and modelling of supercritical CO_2 injection into a water-saturated sandstone: Interpretation of P-wave velocity data: International Journal of Greenhouse Gas Control, **1**, 473-480.

Siggins, A. F., 2006, Velocity-effective stress response of CO_2-saturated sandstones: Exploration Geophysics, **37**, 60-66.

Siggins, A. F., M. Lwin, and P. Wisman, 2010, Laboratory calibration of the seismo-acoustic response of CO_2 saturated sandstones: International Journal of Greenhouse Gas Control, **4**, 920-927.

Simmons, G., and H. Wang, 1971, Single crystal elastic constants and calculated aggregate properties: a handbook: M.I.T. Press.

Speight, J. G., 2014, Handbook of offshore oil and gas operations: Elsevier science & technology.

Spencer, J. W., 1981, Stress relaxation at low frequencies in fluid-saturated rocks: Attenuation and modulus dispersion: Journal of Geophysical Research, **86**, 1803-1812.

Spencer, J. W., 2013, Viscoelasticity of Ells River bitumen sand and 4D monitoring of thermal enhanced oil recovery processes: GEOPHYSICS, **78**, D419-D428.

Spencer, J. W., M. E. Cates, and D. D. Thompson, 1994, Frame moduli of unconsolidated sands and sandstones: GEOPHYSICS, **59**, 1352-1361.

Spencer, J. W., and J. Shine, 2016, Seismic wave attenuation and modulus dispersion in sandstones: GEOPHYSICS, **81**, D219-D239.

Suarez-Rivera, R., S. J. Green, J. McLennan, and M. Bai, 2006, Effect of layered heterogeneity on fracture initiation in tight gas shales. , Annual Technical Conference and Exhibition: Society of Petroleum Engineers. 103327-MS.

Suarez-Rivera, R., S. Willson, S. Nakagawa, and O. Magnar-Ness, 2001, Frequency scaling for evaluation of shale and mudstone properties from acoustic velocities. , AGU 2001 Fall Meeting.

Subramaniyan, S., B. Quintal, N. Tisato, E. H. Saenger, and C. Madonna, 2014, An overview of laboratory apparatuses to measure seismic attenuation in reservoir rocks: Geophysical Prospecting, **62**, 1211–1223.

Szewczyk, D., A. Bauer, and R. M. Holt, 2016, A new laboratory apparatus for the measurement of seismic dispersion under deviatoric stress conditions: Geophysical Prospecting, **64**, 789-798.

Takei, Y., K. Fujisawa, and C. McCarthy, 2011, Experimental study of attenuation and dispersion over a broad frequency range: 1. The apparatus: Journal of Geophysical Research, **116**, B09204.

Tenner, T. J., R. A. Lange, and R. T. Downs, 2007, The albite fusion curve re-examined: New experiments and the high-pressure density and compressibility of high albite and $NaAlSi_3O_8$ liquid: American Mineralogist, **92**, 1573 - 1585.

Thompson, G. R., and J. Turk, 1997, Introduction to physical geology: Saunders College Publishing.

Thomsen, L., 1986, Weak elastic anisotropy: GEOPHYSICS, **51**, 1954-1966.

Timoshenko, S., and J. N. Goodier, 1951, Theory of elasticity: McGraw-Hill.

Tisato, N., and C. Madonna, 2012, Attenuation at low seismic frequencies in partially saturated rocks: Measurements and description of a new apparatus: Journal of Applied Geophysics, **86**, 44-53.

Usher, M. J., 1962, Elastic behaviour of rocks at low frequencies: Geophysical Prospecting, **10**, 119-127.

Vanorio, T., M. Prasad, and A. Nur, 2003, Elastic properties of dry clay mineral aggregates, suspensions and sandstones: Geophysical Journal International, **155**, 319 – 326.

Vanorio, T., C. Scotallero, and G. Mavko, 2008, The effect of chemical and physical processes on the acoustic properties of carbonate rocks, **27**, 1040-1048.

Vialle, S., and T. Vanorio, 2011, Laboratory measurements of elastic properties of carbonate rocks during injection of reactive CO_2-saturated water: Geophysical Research Letters, **38**, L01302.

Wang, Z., 1997, Seismic properties of carbonate rocks, *in* I. Palaz and K. J. Marfurt, eds., Carbonate seismology Society of Exploration Geophysicists, 29-52.

Wang, Z., W. K. Hirsche, and G. Sedgwick, 1991, Seismic velocities in carbonate rocks: The Journal of Canadian Petroleum Technology, **30**, 112-122.

Wang, Z., and A. Nur, 1989, Effect of CO_2 flooding on wave velocities in rocks and hydrocarbons: Society of Petroleum Engineers Reservoir Engineering, **4**, 429–439.

Wang, Z., R. Wang, and D. R. Schmitt, 2015, The elastic moduli velocities of artificial carbonate rocks with known pore structure at different saturation conditions, CSPG Geoconvention 2015: New Horizons, Abstracts.

Weidner, D. J., 1987, Elastic properties of rocks and minerals, *in* C. G. Sammis and T. L. Henyey, eds., Methods of Experimental Physics: Academic Press, 24: Geophysics, Part A: Laboratory Measurements, 1-30.

White, J. E., 1975, Computed seismic speeds and attenuation in rocks with partial gas saturation: GEOPHYSICS, **40**, 224– 232.

White, J. E., 1983, Underground sound: Applications of seismic waves: Elsevier.

White, J. E., 1986, Biot-Gardner theory of extensional waves in porous rods: GEOPHYSICS, **51**, 742-745.

White, J. E., N. G. Mikhaylova, and F. M. Lyakhovitsky, 1975, Low frequency seismic waves in fluid-saturated layered rocks: Izvestija Academy of Sciences USSR, Physics of the Solid Earth, **11**, 654-659.

Winkler, K., A. Nur, and M. Gladwin, 1979, Friction and seismic attenuation in rocks: Nature, **277**, 528-531.

Winterstein, D. F., 1990, Velocity anisotropy terminology for geophysicists: GEOPHYSICS, **55**, 1070-1088.

Wong, R. C. K., D. R. Schmitt, D. Collis, and R. Gautam, 2008, Inherent transversely isotropic elastic parameters of over-consolidated shale measured by ultrasonic waves and their comparison with static and acoustic in situ log measurements: Journal of Geophysics and Engineering, **5**, 103-117.

Wood, A. B., 1955, A textbook of sound: being an account of the physics of vibrations with special reference to recent theoretical and technical developments: Macmillan.

Wyllie, M. R. J., A. R. Gregory, and L. W. Gardner, 1956, Elastic wave velocities in heterogeneous and porous media: GEOPHYSICS, **21**, 41-70.

Xue, Z., and X. Lei, 2006, Laboratory study of CO_2 migration in water-saturated anisotropic sandstone, based on P-wave velocity imaging: Exploration Geophysics, **37**, 10-18.

Xue, Z., and T. Ohsumi, 2004, Seismic wave monitoring of CO_2 migration in water-saturated porous sandstone: Exploration Geophysics, **35**, 25-32.

Yin, C.-S., M. L. Batzle, and B. J. Smith, 1992, Effects of partial liquid/gas saturation on extensional wave attenuation in Berea sandstone: Geophysical Research Letters, **19**, 1399-1402.

Zemke, K., A. Liebscher, and M. Wandrey, 2010, Petrophysical analysis to investigate the effects of carbon dioxide storage in a subsurface saline aquifer at Ketzin, Germany (CO_2SINK). : International Journal of Greenhouse Gas Control, **4**, 990-999.

Zhang, J., I. Martinez, F. Guyot, and R. J. Reeder, 1998, Effects of Mg-Fe^{2++} substitution in calcite-structure carbonates: American Mineralogist, **83**, 280 – 287.

Zhang, J., and R. J. Reeder, 1999, Comparative compressibilities of calcite-structure carbonates: Deviations from empirical relations: American Mineralogist, **84**, 861-870.

Every reasonable effort has been made to acknowledge the owners of copyright material. I would be pleased to hear from any copyright owner who has been omitted or incorrectly acknowledged.

Copyright Clearance Center

Confirmation Number: 11663163
Order Date: 08/15/2017

Customer Information

Customer: Vassili Mikhaltsevitch
Account Number: 3001184760
Organization: Vassili Mikhaltsevitch
Email: V.Mikhaltsevitch@curtin.edu.au
Phone: +61 (8)92664976
Payment Method: Invoice

This is not an invoice

Order Details

The leading edge

Billing Status: **N/A**

Order detail ID:	70641670
ISSN:	1938-3789
Publication Type:	e-Journal
Volume:	
Issue:	
Start page:	
Publisher:	Society of Exploration Geophysicists
Author/Editor:	Society of Exploration Geophysicists

Permission Status: Granted
Permission type: Republish or display content
Type of use: Thesis/Dissertation
Order License Id: 4170301067567

Requestor type	Author of requested content
Format	Electronic
Portion	chapter/article
Title or numeric reference of the portion(s)	A laboratory study of low-frequency wave dispersion and attenuation in water-saturated sandstones
Title of the article or chapter the portion is from	N/A
Editor of portion(s)	Ludmila Adam, Kasper van Wijk
Author of portion(s)	V.Mikhaltsevitch, M.Lebedev, B.Gurevich
Volume of serial or monograph	Volume 33
Issue, if republishing an article from a serial	Issue 6
Page range of portion	
Publication date of portion	June 2014
Rights for	Main product
Duration of use	Life of current edition
Creation of copies for the disabled	no
With minor editing privileges	no
For distribution to	U.K. and Commonwealth (excluding Canada)
In the following language(s)	Original language of publication
With incidental promotional use	no
Lifetime unit quantity of new product	Up to 499
	education

Made available in the following markets	
The requesting person / organization	V.Mikhaltsevitch/ Curtin University
Order reference number	
Author / Editor	Vassili Mikhaltsevitch
The standard identifier of New Work	N/A
The proposed price	0
Title of New Work	INVESTIGATIONS OF ELASTIC PROPERTIES OF ISOTROPIC AND ANISOTROPIC ROCKS AT SEISMIC FREQUENCIES USING FORCED-OSCILLATION EXPERIMENTS
Publisher of New Work	Curtin University
Expected publication date	Jan 2018
Estimated size (pages)	6

Note: This item was invoiced separately through our **RightsLink service.** More info **$ 0.00**

Total order items: 1 **Order Total: $0.00**

Copyright Clearance Center

Confirmation Number: 11663169
Order Date: 08/15/2017

Customer Information

Customer: Vassili Mikhaltsevitch
Account Number: 3001184760
Organization: Vassili Mikhaltsevitch
Email: V.Mikhaltsevitch@curtin.edu.au
Phone: +61 (8)92664976
Payment Method: Invoice

This is not an invoice

Order Details

Geophysical research letters

Billing Status: **N/A**

Order detail ID: 70641691
ISSN: 1944-8007
Publication Type: Journal
Volume:
Issue:
Start page:
Publisher: American Geophysical Union
Author/Editor: American Geophysical Union

Permission Status: Granted
Permission type: Republish or display content
Type of use: Book
Order License Id: 4170310164033

Requestor type	Author of requested content
Format	Electronic
Portion	chapter/article
Number of pages in chapter/article	6
Title or numeric reference of the portion(s)	Validation of the laboratory measurements at seismic frequencies using the Kramers-Kronig relationship
Title of the article or chapter the portion is from	N/A
Editor of portion(s)	N/A
Author of portion(s)	V.Mikhaltsevitch, M.Lebedev, B.Gurevich
Volume of serial or monograph	Volume 43
Issue, if republishing an article from a serial	Issue 10
Page range of portion	4986–4991
Publication date of portion	28 May 2016
Rights for	Main product
Duration of use	Life of current edition
Creation of copies for the disabled	no
With minor editing privileges	no
For distribution to	U.K. and Commonwealth (excluding Canada)
In the following language(s)	Original language of publication
With incidental promotional use	no
	Up to 499

Lifetime unit quantity of new product	
Made available in the following markets	education
The requesting person / organization	V.Mikhaltsevitch/ Curtin University
Order reference number	
Author / Editor	Vassili Mikhaltsevitch
The standard identifier of New Work	N/A
The proposed price	0
Title of New Work	INVESTIGATIONS OF ELASTIC PROPERTIES OF ISOTROPIC AND ANISOTROPIC ROCKS AT SEISMIC FREQUENCIES USING FORCED-OSCILLATION EXPERIMENTS
Publisher of New Work	Curtin University
Expected publication date	Jan 2018
Estimated size (pages)	170

Note: This item was invoiced separately through our **RightsLink service.** More info **$ 0.00**

Total order items: 1 **Order Total: $0.00**

Copyright Clearance Center

Confirmation Number: 11663151
Order Date: 08/15/2017

Customer Information

Customer: Vassili Mikhaltsevitch
Account Number: 3001184760
Organization: Vassili Mikhaltsevitch
Email: V.Mikhaltsevitch@curtin.edu.au
Phone: +61 (8)92664976
Payment Method: Invoice

This is not an invoice

Order Details

Geophysical prospecting

Billing Status: **N/A**

Order detail ID:	70641647
ISSN:	1365-2478
Publication Type:	e-Journal
Volume:	
Issue:	
Start page:	
Publisher:	BLACKWELL PUBLISHING
Author/Editor:	European Association of Geoscientists and Engineers.Geophysical Division

Permission Status: Granted
Permission type: Republish or display content
Type of use: Book
Order License Id: 4170300033879

Requestor type	Author of requested content
Format	Electronic
Portion	chapter/article
Number of pages in chapter/article	12
Title or numeric reference of the portion(s)	Measurements of the elastic and anelastic properties of sandstone flooded with supercritical CO2
Title of the article or chapter the portion is from	N/A
Editor of portion(s)	N/A
Author of portion(s)	V.Mikhaltsevitch, M.Lebedev, B.Gurevich
Volume of serial or monograph	Volume 62
Issue, if republishing an article from a serial	Issue 6
Page range of portion	1266-1277
Publication date of portion	18 Sep 2014
Rights for	Main product
Duration of use	Life of current edition
Creation of copies for the disabled	no
With minor editing privileges	no
For distribution to	U.K. and Commonwealth (excluding Canada)
In the following language(s)	Original language of publication
With incidental promotional use	no
	Up to 499

Lifetime unit quantity of new product	
Made available in the following markets	education
The requesting person / organization	V.Mikhaltsevitch/ Curtin University
Order reference number	
Author / Editor	Vassili Mikhaltsevitch
The standard identifier of New Work	N/A
The proposed price	0
Title of New Work	INVESTIGATIONS OF ELASTIC PROPERTIES OF ISOTROPIC AND ANISOTROPIC ROCKS AT SEISMIC FREQUENCIES USING FORCED-OSCILLATION EXPERIMENTS
Publisher of New Work	Curtin University
Expected publication date	Jan 2018
Estimated size (pages)	170

Note: This item was invoiced separately through our **RightsLink service.** More info **$ 0.00**

Total order items: 1 **Order Total: $0.00**

Copyright Clearance Center

Confirmation Number: 11663158
Order Date: 08/15/2017

Customer Information

Customer: Vassili Mikhaltsevitch
Account Number: 3001184760
Organization: Vassili Mikhaltsevitch
Email: V.Mikhaltsevitch@curtin.edu.au
Phone: +61 (8)92664976
Payment Method: Invoice

This is not an invoice

Order Details

Geophysical prospecting

Billing Status: **N/A**

Order detail ID:	70641661
ISSN:	1365-2478
Publication Type:	e-Journal
Volume:	
Issue:	
Start page:	
Publisher:	BLACKWELL PUBLISHING
Author/Editor:	European Association of Geoscientists and Engineers.Geophysical Division

Permission Status: Granted
Permission type: Republish or display content
Type of use: Book
Order License Id: 4170300541971

Requestor type	Author of requested content
Format	Electronic
Portion	chapter/article
Number of pages in chapter/article	11
Title or numeric reference of the portion(s)	Laboratory measurements of the effect of fluid saturation on elastic properties of carbonates at seismic frequencies
Title of the article or chapter the portion is from	N/A
Editor of portion(s)	N/A
Author of portion(s)	V.Mikhaltsevitch, M.Lebedev, B.Gurevich
Volume of serial or monograph	Volume 64
Issue, if republishing an article from a serial	Issue 4
Page range of portion	799–809
Publication date of portion	28 Jun 2016
Rights for	Main product
Duration of use	Life of current edition
Creation of copies for the disabled	no
With minor editing privileges	no
For distribution to	U.K. and Commonwealth (excluding Canada)
In the following language(s)	Original language of publication
With incidental promotional use	no
	Up to 499

Lifetime unit quantity of new product	
Made available in the following markets	education
The requesting person / organization	V.Mikhaltsevitch/ Curtin University
Order reference number	
Author / Editor	Vassili Mikhaltsevitch
The standard identifier of New Work	N/A
The proposed price	0
Title of New Work	INVESTIGATIONS OF ELASTIC PROPERTIES OF ISOTROPIC AND ANISOTROPIC ROCKS AT SEISMIC FREQUENCIES USING FORCED-OSCILLATION EXPERIMENTS
Publisher of New Work	Curtin University
Expected publication date	Jan 2018
Estimated size (pages)	170

Note: This item was invoiced separately through our **RightsLink service.** More info **$ 0.00**

Total order items: 1 **Order Total: $0.00**

Copyright Clearance Center

Confirmation Number: 11663088
Order Date: 08/15/2017

Customer Information

Customer: Vassili Mikhaltsevitch
Account Number: 3001184760
Organization: Vassili Mikhaltsevitch
Email: V.Mikhaltsevitch@curtin.edu.au
Phone: +61 (8)92664976
Payment Method: Invoice

This is not an invoice

Order Details

SEG technical program expanded abstracts

Billing Status: **N/A**

Order detail ID:	70641250
ISSN:	1949-4645
Publication Type:	Journal
Volume:	
Issue:	
Start page:	
Publisher:	Society of Exploration Geophysicists
Author/Editor:	International SEG Meeting ; Society of Exploration Geophysicists

Permission Status: Granted
Permission type: Republish or display content
Type of use: Thesis/Dissertation
Order License Id: 4170221181780

Requestor type	Author of requested content
Format	Electronic
Portion	chapter/article
Title or numeric reference of the portion(s)	Expanded Abstracts: A laboratory study of the elastic anisotropy in the Mancos Shale at seismic frequencies; Elastic anisotropy of the Wellington shale at seismic frequencies: Laboratory measurements
Title of the article or chapter the portion is from	A laboratory study of the elastic anisotropy in the Mancos Shale at seismic frequencies; Elastic anisotropy of the Wellington shale at seismic frequencies: Laboratory measurements
Editor of portion(s)	Charles Sicking, John Ferguson
Author of portion(s)	V. Mikhaltsevitch, M. Lebedev, B. Gurevich
Volume of serial or monograph	SEG Technical Program Expanded Abstracts 2016
Page range of portion	
Publication date of portion	October 18, 2016
Rights for	Main product
Duration of use	Current edition and up to 5 years
Creation of copies for the disabled	no
With minor editing privileges	no
For distribution to	U.K. and Commonwealth (excluding Canada)

In the following language(s)	Original language of publication
With incidental promotional use	no
Lifetime unit quantity of new product	Up to 499
Made available in the following markets	education
The requesting person / organization	V.Mikhaltsevitch/ Curtin University
Order reference number	
Author / Editor	Vassili Mikhaltsevitch
The standard identifier of New Work	N/A
The proposed price	0
Title of New Work	INVESTIGATIONS OF ELASTIC PROPERTIES OF ISOTROPIC AND ANISOTROPIC ROCKS AT SEISMIC FREQUENCIES USING FORCED-OSCILLATION EXPERIMENTS
Publisher of New Work	Curtin University
Expected publication date	Jan 2018
Estimated size (pages)	170

Note: This item was invoiced separately through our **RightsLink service.** More info **$ 0.00**

Total order items: 1 **Order Total: $0.00**